FUSION OSCILLATIONS IN LIGHT HEAVY-IONS AND THE PARAMETRISATION OF NUCLEON-NUCLEON S-MATRIX

Thesis submitted in accordance with the requirements of the University of Liverpool for the degree of Doctor of Philosophy

by

ADNAN KABIR

August 1988

FUSION OSCILLATIONS IN LIGHT HEAVY-IONS AND THE PARAMETRISATION OF THE NUCLEON-NUCLEON S-MATRIX

ADNAN KABIR

ABSTRACT

We present a model that explains the mechanism responsible for the oscillatory structure observed in the fusion excitation function of nonsymmetric ions. An optical model potential containing a parity dependent term was used to reproduce these oscillations. It is shown that it is possible to reproduce the excitation function while simultaneously obtaining a satisfactory fit to the elastic angular distribution. In particular the anomalous large angle scattering is consistent with the parity dependence required to fit the fusion oscillations. For the systems in which the two nuclei differ by one or few nucleons, the parity dependence describes the elastic transfer of a valence particle between two identical cores.

For the symmetric ions, the previous model for describing the fusion oscillations in spinless bosons is used to calculate the fusion excitation function of symmetric non-zero spin systems. It is shown that oscillations are likely to appear in excitation function of two symmetric light ions with spin-$\frac{1}{2}$.

In the second part of the thesis, the various methods, suggested in recent years, of parametrising the 2x2 submatrix that describes the elastic component in coupled channel nucleon-nucleon scattering at energies above the pion threshold are discussed. The submatrix requires one less parameter when only one inelastic channel is present. In this case some of the parametrisations are not completely satisfactory. We present an alternative form of parametrising the submatrix and a comparison of these methods is made by applying them to four coupled channel potential wells.

For the 3x3 symmetric and unitary matrix, formulae for the amplitude or phase of each off-diagonal element in terms of the the diagonal amplitudes, together with the inverse relations, are presented. The formulae contain some interesting cyclic relationships and were used to check numerical calculations in the case of three coupled channel potential wells.

DECLARATION

I hereby declare that all the work described in this thesis is the result of my own research activities unless reference is given to others. None of this work has previously been submitted to this or any other University and it was all carried out in the Department of Applied Mathematics and Theoretical Physics during the period October 1985 to August 1988

C O N T E N T S

PREFACE

The work presented in this thesis was carried out at the Department of Applied Mathematics and Theoretical Physics during the period October 1985 to August 1988 under the supervision of Dr M.W. Kermode.

Some of the work presented in this thesis have been published in the following articles:

A.Kabir and M.W.Kermode

J. of Phys. **G13** (1987) 501;

J. of Phys. **A20** (1987) 5199;

J. of Phys. **A20** (1987) 6633;

A.Kabir, M.W.Kermode and N.Rowley

Nucl. Phys. **A481** (1988) 94.

I would like express my gratitude to Dr Mark. W. Kermode for his guidance and advice throughout the period of this research. The work presented in the first section of this thesis was carried out in collaboration with Dr Neil Rowley of Daresbury Laboratory. I am grateful for the useful conversations I had with him. I have learnt a lot from these two people and I enjoyed working with them.

During the period this work was carried out, many people outside the department have made my stay lively, I thank all of them. I would like to thank my parents, all my brothers and sisters. In particular, my thanks to Mansur, Sakinatu and Abba for everything including keeping me "at home". I would also like to thank my colleagues and friends. I am grateful to the Head of DAMTP for financial contribution to the conferences I attended.

Finally, I acknowledge the financial support from the Federal Government of Nigeria (Federal Ministry of Education).

May Allah (SWT) put his "barka" in this work.

CHAPTER 1

INTRODUCTION

Over the last few years considerable experimental and theoretical interest has been focused on the fusion cross section of light heavy ion reactions at energies above the Coulomb barrier for systems involving 1p-shell and 2s-1d shell nuclei. The interest was largely motivated by the discovery of oscillations in the fusion cross section as a function of the incident energy. The oscillations were observed in many spin-zero symmetric nuclei, such as $^{12}C + ^{12}C$ [Spe 76a], $^{14}C + ^{14}C$ [Fre 81], $^{16}O + ^{16}O$ [Kov 79] and $^{20}Ne + ^{20}Ne$ [Pof 83], but, to date, no oscillations have been observed in symmetric non-zero spin systems. For the nonsymmetric systems, oscillations were observed in various combinations of light heavy-ions. In particular, pronounced oscillatory structure was observed in $^{12}C + ^{16}O$ [Spe 76], $^{12}C + ^{24,26}Mg$ [Dan 82], $\alpha + ^{40,44}Ca$ [Ebe 79], $^{10}B + ^{13}C$ and $^{11}B + ^{12}C$ [Maj 82]. However, the oscillations are absent in some other systems, such as: $^{13}C + ^{16}O$ [Pap 86], $^{12}C + ^{15}N$, and $^{12}C + ^{18}O$ [Kav 79]. For heavier systems, like the $^{16}O + ^{24}Mg$, $^{16}O + ^{40}Ca$ [Tab 78], $^{24}Mg + ^{24}Mg$ [Jac 81], $^{28}Si + ^{28}Si$ [Cen 81], no oscillation was observed. In systems that do possess oscillations, significant differences in the magnitude and phase of the oscillations were observed between those that differ by one or two nucleons. For example, the magnitude of the oscillations for $^{11}B + ^{12}C$ is much greater than for $^{12}C + ^{12}C$. However, for the $^{12}C + ^{13}C$ [Kav 79] system, which differsby one and two nucleons from the above systems, very little structure was observed in the excitation function and the oscillations appeared to be out of phase with the oscillations in the $^{11}B + ^{12}C$ system. For the compound nuclei formed, marked differences are readily observed when two systems are

compared. For example, the systems $^{14}N + ^{14}N$ [DeY 82] and $^{12}C + ^{16}O$ form the same ^{28}Si compound nuclei, but the structure in the excitation function of these ions is completely different. Oscillations appeared in $^{12}C + ^{16}O$ but none was observed in $^{14}N + ^{14}N$ and the maximum fusion cross section obtained in the latter system is smaller than the maximum in the former system.

The elastic scattering of most of these systems also reveals some interesting oscillatory structures at energies above the Coulomb barrier. In most cases pronounced oscillations, that look more like resonances of width ranging from many KeV to a few MeV were observed in the elastic excitation functions. Also, in the angular distribution, pronounced oscillatory structures were observed at large angles in the symmetric and some nonsymmetric systems. Some of these structures were also observed in α-particle scattering on heavy ions, such as $\alpha + ^{40}Ca$ system [Eck 75]. Furthermore, in some systems, e.g. $^{28}Si + ^{28}Si$ and $^{12}C + ^{16}O$ [Mal 72], the angular distribution at large angles resembles the angular distribution of $|P_\ell(\theta)|^2$ remarkably well.

These structures in the elastic scattering have been explained satisfactorily using various theoretical models. For example, the pronounced large angle structures were explained in terms of symmetrisation of the system for identical ions, elastic exchange of a valence particle for almost identical ions [Von 73] and surface transference effects of the interacting potential in systems like $\alpha + ^{40}Ca$ [Bri 77]. Similarly, models like the sharp cut-off model have been used to explain some of the features of the elastic scattering process, for example in the $^{28}Si + ^{28}Si$ and $^{16}O + ^{16}O$ [Gob 73] systems. Also, because of the sharp resonances in the elastic excitation function, molecular effects have been proposed (see [Ebe 82]).

On the other hand, the theoretical explanation of the fusion oscillations has largely been unsuccessful. Classical models, such as the Glas and Mosel model [Gla 74] and the Bass model [Bas 77], did not attempt to explain any of these oscillations. The few models that explained the oscillations were concerned with a particular system, for example the oscillations in $^{16}O + ^{16}O$ system were explained by Tanimura [Tan 80] using a coupled channel approach and by Kondo et al [Kon 80] using the band-crossing model.

Recently, Poffe et al [Pof 83] have presented a satisfactory explanation of the mechanism responsible for the oscillatory structure in symmetric spin-zero bosons. These authors showed that, like the elastic scattering process, the oscillations appear because of the symmetrisation of the system. They demonstrated that the structures are essentially due to the sharpness of the cut-off of transmission coefficients as a function of angular momentum of the system.

For the nonsymmetric systems, Kabir et al [Kab 88] have presented a satisfactory explanation of the mechanism responsible for the oscillatory structure in the fusion excitation function of the $^{12}C + ^{16}O$ system. The oscillations were explained qualitatively by using an optical model potential containing a parity dependence which accounts for the elastic transfer of α^{an}-particle between the two carbon cores. We showed that the fusion excitation function can be reproduced while fitting simultaneously the elastic angular distribution. In particular the anomalous large angle scattering is consistent with the parity dependence required to fit the fusion oscillations. In this thesis, the model used for the $^{12}C + ^{16}O$ system will be presented and applied to other nonsymmetric systems that possess oscillatory structure in the fusion excitation function.

The explanation for the fusion oscillations in the symmetric and nonsymmetric ions is the main theme of the first part of this thesis (i.e Section I) and is presented in three chapters (chaps. 2 to 4). The first (chap. 2), develops the model and a simple numerical calculation of the excitation function for symmetric and nonsymmetric systems is made, so as to illustrate the various shapes of the fusion cross section as a function of energy. In chapter 3, the model is applied to spin-zero systems using an optical potential containing a parity dependent term. Finally in the last chapter of this section (chap. 4), the model is modified to included the spin structure of the systems and is applied to the $^{14}N + ^{14}N$, $^{11}B + ^{12}C$ and $^{12}C + ^{13}C$ systems.

In the second part of this thesis (Section II), we present various ways of parametrising the nucleon-nucleon scattering matrix at energies above the pion threshold. At energies below the pion threshold, if the scattering involves the coupling of two states then the channel S matrix is a 2x2 symmetric and unitary matrix. For example in the scattering of neutrons on protons in the presence of a tensor potential, where the states with $\ell = 0$ ($^3S_1$) and $\ell = 2$ ($^3D_1$) are coupled. This matrix requires three parameters to specify, and it can be parametrised either according to the "bar phase convention" of Stapp et al [Sta 57] (SYM) or the "eigen phase convention" [Bla 52]. As the energy increases beyond the threshold of pion production, this matrix is no longer unitary but it is symmetric. It is now a submatrix that describes the elastic component of the scattering. The size of the channel matrix depends on the number of channels opened. For example when one extra channel is opened, the channel S matrix is a 3x3 unitary and symmetric matrix.

For a four channel scattering process, Bryan [Bry 81] presented an extension to the bar phase shift analysis (the SYM) above the threshold of pion production. The channel $\mathbf{S}$ matrix is then a 4x4 unitary and symmetric matrix, and the elastic component of the scattering is described by a 2x2 submatrix of the $\mathbf{S}$ matrix, $\mathbf{S}_e$. The submatrix $\mathbf{S}_e$ is a modification of the SYM form, and includes the introduction of another matrix. This matrix, $\mathbf{N}$, accounts for the coupling between the elastic channels and the other inelastic channels involved in the scattering. The submatrix $\mathbf{S}_e$ can be parametrised by six real parameters for four or more open channels, by five parameters for three open channels only (see [Spr 82]) and reverts to the SYM form when there is no inelastic scattering. The $\mathbf{N}$ matrix requires three real parameters when there are four or more open channels and two real parameters for only three channels open. This matrix, which is real and symmetric, has been parametrised in various ways by Bryan [Bra 81 & 84], Klarsfeld [Kla 83], Melhem and Kermode [Mel 83], Sprung [Spr 85] and more recently by Kabir and Kermode [Kab 87a].

These various ways of parametrising the matrix $\mathbf{N}$ are given in chapter 5. It is shown [Kab 87a] that some of these parametrisations, which are designed for four or more open channels, are not completely satisfactory when only three channels are open. Also, at the threshold energies and at particular energies some of the parameters cannot be determined. A modified method of parametrising the $\mathbf{N}$ matrix that overcomes these problems for all possible values that the elements of the $\mathbf{N}$ matrix may take was presented [Kab 87a]. Also, we apply and compare these parametrisations to four coupled channel square potential wells.

In chapter 6, the 3x3 symmetric and unitary scattering matrix is considered. This matrix is particularly special because it requires

six independent real parameters which can be constructed from appropriate combinations of the three real amplitudes and the three real phases of the three diagonal or three off-diagonal elements. We showed [Kab 87b] that if the matrix is written in a form similar to that presented by Waldenstrom [Wal 74], interesting relationships between the parameters of the matrix are obtained. In particular, formulae for the amplitude or phase of each off-diagonal element in terms of the the diagonal amplitudes, together with the inverse relations, are obtained. These formulae have interesting cyclic relationships. The formulae were used to check numerical calculations in the case of three coupled channel potential wells, and the possible ways of parametrising this matrix were presented. The energy dependence of the parameters and the possible values they can take are investigated using the numerical calculations.

CHAPTER 2

FUSION OF SPINLESS NUCLEI (THEORY)

This chapter is on the fusion reaction of spinless light heavy ions that possess oscillatory structure in the fusion excitation function. These ions are grouped in two classes, the symmetric and nonsymmetric systems. The mechanism responsible for the oscillatory structure in the symmetric systems has been explained by Poffe et al [Pof 83]. Recently, Kabir et al [Kab 88] have explained the mechanism responsible for the oscillatory structure in the fusion excitation function of $^{12}C + ^{16}O$ system. In this chapter we present the model used for the $^{12}C + ^{16}O$ system. This model will then be applied to other nonsymmetric systems.

The model is similar to the one applied to the symmetric ions, i.e. it will be shown that the oscillatory structure can only be explained if the elastic scattering process is taken into account. Therefore, before we present the model, a brief review of the elastic scattering process will be given in the first section of this chapter. In the second section, the model for fusion reaction will be presented and in the last section a discussion on the two processes using an optical model will be made.

2.1 THE ELASTIC SCATTERING

At lower energies a pair of colliding nuclei will not come close enough, during collision, to experience the nuclear force, they are only within the range of Coulomb force. The quantal scattering amplitude is therefore the Coulomb scattering amplitude,

$$f(\theta) = f_c(\theta) = -(\eta/2k\sin^2\tfrac{1}{2}\theta)\exp(2i\sigma_0 - 2i\eta\log\sin\tfrac{1}{2}\theta) \qquad (2.1)$$

where $\eta = Z_1 Z_2 e^2/\hbar v$, is the Sommerfeld parameter and v is the relative velocity of the system in the centre of mass. The Coulomb phase shift is $\sigma_0 = \arg\Gamma(1+i\eta)$ and the differential cross section becomes

$$d\sigma/d\Omega = |f(\theta)|^2. \qquad (2.2)$$

However, if the energy of the nuclei is large then the interacting nuclei may come close enough and the effect of the nuclear force would be felt by the projectile. The scattering amplitude in partial wave expansion, for spinless particles, becomes

$$f(\theta) = \frac{1}{2ik}\sum_{l=0}^{\infty}(2l + 1)\, P_l(\cos\theta)(S_l - 1) \qquad (2.3)$$

where S_l is the scattering matrix. Because of the Coulomb interaction, the scattering matrix is usually written in terms of a nuclear and Coulomb parts, as $S_l = S^N_l \exp(2i\sigma_l)$ where σ_l are the Coulomb phases and S^N_l is the nuclear part of S_l. The scattering amplitude becomes

$$f(\theta) = f_c(\theta) - \frac{1}{2ik}\sum_{l=0}^{\infty}(2l + 1)\, P_l(\cos\theta)(S^N_l - 1)\exp(2i\sigma_l). \qquad (2.4)$$

Thus, when there is no nuclear interaction $S^N_l = 1$, and eq. (2.4) becomes eq. (2.1).

The elastic scattering of heavy-ions is broadly divided into two parts, this division is characterised by the Sommerfeld parameter η. When $\eta \gg 1$, (i.e. for heavier ions) the shape of the angular distribution is similar to the Fresnel-type diffraction structure, i.e. a small oscillatory structure at smaller angles ($\theta \leq 50^0$) and then a rapid fall of the cross section at larger angles. While, for $\eta < 1$ (i.e. for light heavy-ions) the cross section is similar to the Fraunhofer diffraction structure. In this case the scattering is mostly dependent on the nuclear potential since η is small. In fact, in simple qualitative calculations, the Coulomb force is usually neglected.

For these systems, the light heavy-ions, the sharp cut-off (SCO) model [Bla 54] gives a good description of the scattering process, because $|S_\ell|$ is one or zero for all but one partial waves involved in the scattering, at energies above the Coulomb barrier. For example, Gobbi et al [Gob 73] have shown that in the elastic scattering of $^{16}O + {}^{16}O$, there is only one even partial wave (even because of symmetrisation) that has a value of $|S_\ell|$ which is appreciably different from zero or unity. This leads to an effective ℓ-windowing of the S-matrix in the scattering. Rowley [Row 80] has shown that such an ℓ-windowing effect can be seen more explicitly by rewriting the scattering amplitude in terms of SCO Coulomb amplitudes. The SCO Coulomb amplitudes are defined as (for L>0)

$$\tilde{f}_L(\theta) = f_c(\theta) - \frac{1}{2ik}\sum_{\ell=0}^{L-1}(2\ell + 1)\, P_\ell(\cos\theta)\exp(2i\sigma_\ell) \qquad (2.5)$$

where $\tilde{f}_0(\theta) = f_c(\theta)$, as defined in eq. (2.1). The scattering amplitude in terms of the SCO amplitudes $f(\theta)$ becomes,

$$f(\theta) = \sum_{\ell=0}^{\infty} Z_\ell \tilde{f}_\ell(\theta) \qquad (2.6)$$

where $Z_\ell = S^N_\ell - S^N_{\ell-1}$ and $Z_0 = S^N_0$. This rearrangement of $f(\theta)$ allows us to sum over the region where S^N_ℓ is changing only i.e. $Z_\ell \neq 0$, thus effectively creating an ℓ-window on the scattering amplitude.

Frahn and Venter [Fra 63] defined the grazing angle θ_g as the position where the "quarter point recipe" holds, that is

$$\sigma(\theta_g) = \tfrac{1}{4}\sigma_R(\theta_g)$$

where σ_R is the Rutherford cross section. This angle is used to define the grazing partial wave as

$$\ell_g = \eta\cot(\tfrac{1}{2}\theta_g). \qquad (2.7)$$

This is the region in ℓ-space where $Z_\ell \neq 0$.

The angular distribution (eq. (2.2)) is proportional to the factor $(\sin\theta)^{-1}$, both classically and quantum mechanically. Classically, the Rutherford cross section is proportional to $(\mathrm{cosec}\frac{1}{2}\theta)^4$. While in the quantal expression of the scattering amplitude, replacing the Legendre polynomial by its asymptotic value, for $1/\ell \leq \theta \leq \pi - 1/\ell$, introduces a factor $(\sin\theta)^{-\frac{1}{2}}$ in the amplitude (see [Abr 65]). Therefore, for large angles, the cross section should strongly decrease with increasing scattering angle. This is the case for most ions, but for symmetric and nonsymmetric ions (that differ by few nucleons), large diffraction structures were observed in the cross section at large angles, suggesting that other physical process must be responsible for this.

2.1.1 IDENTICAL IONS.

For symmetric spin-zero bosons, like $^{12}C + {}^{12}C$, the elastic angular distribution is symmetric about $\theta = 90^0$. It is symmetric because after scattering, the system is indistinguishable. That is, we can not distinguish the two possible scattering processes that might have taken place. For example in $^{12}C + {}^{12}C$, the ^{12}C emerging at an angle θ could either be the projectile carbon or the target. If it is the projectile carbon, then we are observing a normal scattering process. However, if the emerging carbon at θ is the target carbon, then the projectile is observed at $\pi-\theta$, i.e. the backward angles. The two forms can not be distinguished from one another, as illustrated schematically in fig. 2.1. Therefore, the scattering amplitude is a coherent superposition of the two amplitudes at θ and $\pi-\theta$ (since the ions are spinless bosons), i.e.

$$f_s(\theta) = f(\theta) + f(\pi-\theta).$$

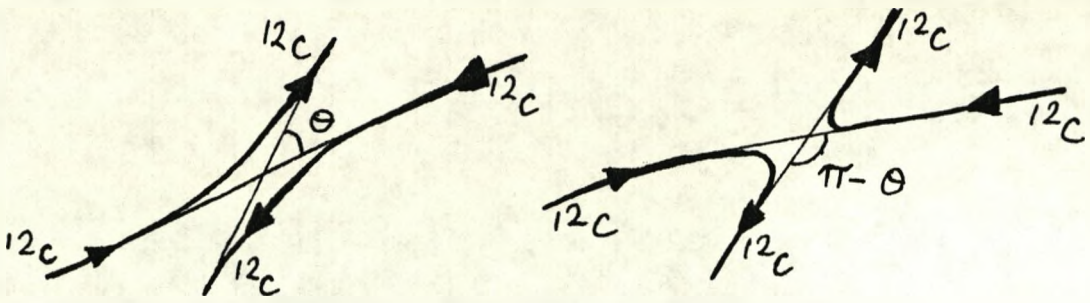

Fig. 2.1 A schematic representation of the two possible elastic scattering processes for symmetric ions.

Using the relation $P_\ell(\cos\pi-\theta) = (-1)^\ell P_\ell(\cos\theta)$ and eq. (2.4), but ignoring $f_c(\theta)$, the scattering amplitude becomes (note we have dropped the superscript N on S_ℓ for convenience),

$$f_s(\theta) = \frac{1}{ik}\sum_{\text{l even}}(2\ell + 1)\, P_\ell(\cos\theta)(S_\ell - 1)\exp(2i\sigma_\ell). \qquad (2.8)$$

Thus all the odd partial waves are removed.

2.1.2 NON-IDENTICAL IONS.

In some non-identical heavy-ions the angular distribution of the elastic scattering shows a large increase in the cross section with increasing scattering angles. In particular, these structures were observed in the elastic scattering of two nuclei A and B≡(A+b), where B differs from A by one or few nucleons (denoted by b). Von Oertzen [Von 73] explained that such structures can be accounted for by treating the scattering in the same way as the symmetric ions. That is the scattering amplitude is the sum of two different scattering amplitudes. One dominant at the forward angles $f(\theta)$ and the other at the backward angles $f(\pi-\theta)$. The forward angle scattering amplitude is the normal scattering process, i.e. A + B → A + B. While the backward scattering amplitude is a process in which there is an elastic transfer of the particle(s) b between the two cores, i.e.

$A_1 + B \equiv (A_2+b) \rightarrow (A_1+b) + A_2$ with $(A_1 \equiv A_2)$. This is indistinguishable from the forward angle scattering, since cores A_1 and A_2 are identical. For example, in the elastic scattering of $^{12}C + ^{16}O$, if a carbon nucleus emerging at an angle θ has picked up an α-particle, then we observe a carbon an angle $\pi-\theta$, as illustrated in fig. 2.2. Thus, the scattering amplitude for the nonsymmetric systems $f_u(\theta)$ is the sum of the two scattering amplitudes $f(\theta)$ and $f(\pi-\theta)$. Ignoring $f_c(\theta)$, the scattering amplitude in partial waves expansion becomes

$$f_u(\theta) = \frac{1}{2ik}\sum_{\ell=0}^{\infty}(2\ell + 1)\ [P_\ell(\cos\theta)S^D{}_\ell + P_\ell(\cos\pi-\theta)S^E{}_\ell]\ \exp(2i\sigma_\ell)$$

where S represent the nuclear scattering matrices in the direct (D) and exchange (E) processes. Using $P_\ell(\cos\pi-\theta) = (-1)^\ell P_\ell(\cos\theta)$ we obtain,

$$f_u(\theta) = \frac{1}{2ik}\sum_{\ell=0}^{\infty}(2\ell + 1)P_\ell(\cos\theta)\ [S^D{}_\ell + (-1)^\ell S^E{}_\ell]\ \exp(2i\sigma_\ell) \quad (2.9)$$

Thus, the effective nuclear scattering matrix for this reaction is $[S^D{}_\ell + (-1)^\ell S^E{}_\ell]$. In ℓ-space, an odd-even staggering of the effective scattering matrix will be seen. This procedure was shown, by Von Oertzen and many collaborators, to be successful in describing the scattering cross section of many nuclei, for example in $^{12}C + ^{11}B$ [Gut 73], $^{12}C + ^{13}C$ [Boh 71], $^{13}C + ^{14}N$ [Von 75], $^{12}C + ^{16}O$ [Gut 73], and many other combinations of ions.

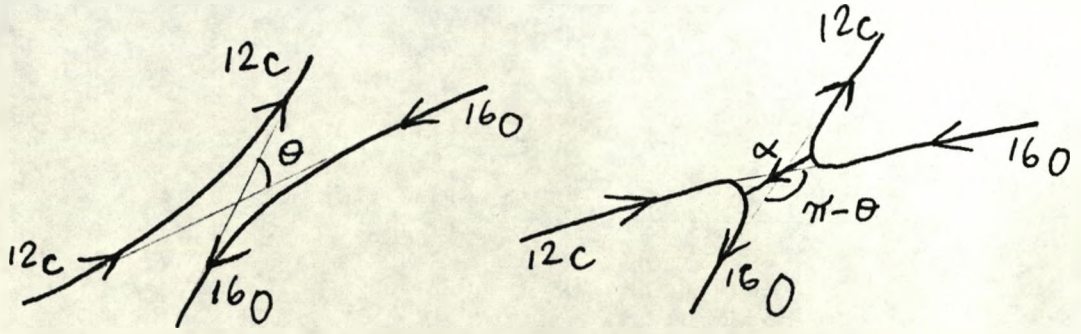

Fig. 2.2 A schematic representation of the two possible elastic scattering processes for nonsymmetric ions.

There are other procedures for reproducing this phenomena using optical model calculations. For example, Mailandt et al [Mai 73] have shown that with a weakly absorption imaginary potential, the sum of the forward and backward scattering amplitudes are reproduced by the interference between waves reflected at the angular momentum barrier and at the nuclear surface [Kue 69]. However, a weakly absorbing potential is not all that physical for a pair of heavy ions scattering. Another suggestion is that the odd-even staggering could be simulated by an ℓ-dependent imaginary potential, (Chatwin et al [Cha 70]). However, with this procedure, a parameter L_c (the cut-off partial wave) was introduced in the imaginary potential, which sometimes takes ambiguous values [Gut 73]. Furthermore, the physical reasons for an ℓ-dependent imaginary potential are still not very clear.

The exchange of particles between two cores was based on a procedure similar to the atom-ion exchange in atomic physics. Von Oertzen [Von 73] extended this method to nucleus-nucleus interactions by proposing a two-state molecular model with the molecular wave function constructed from linear combinations of nuclear orbitals (LCNO). One of the properties of the model is its ability to differentiate the exchange of particles and holes between the two cores. However, the model was based on the transfer of particles with $j \leq \frac{1}{2}$ and requires laborious calculations for $j > \frac{1}{2}$ [Von 73]. A DWBA calculation was suggested in this case.

The two-state molecular model assumes that we have two identical cores A_1 and A_2 (of the same masses M_A) and a valence particle b (assuming that $M_b << M_A$) sitting on top of one of the cores. It produces a Schrodinger equation containing a parity dependent potential. The parity dependent term in the potential accounts for core permutations and it vanishes at large separations between the cores. Von Oertzen

showed that the potential has a role similar to the Yukawa exchange potential in nuclear forces. Therefore, the form factor of this potential should be similar to the Yukawa potential. Also, it is related to the spectroscopic strength and thus the binding energy of the valence particle. Its sign and range has also been discussed by Baye [Bay 77 & 86].

2.1.3 THE TWO CHANNEL APPROACH

To derive the parity dependent potential in the Schrodinger equation without going through the details of the two-state molecular model, we consider a two coupled channels scattering problem. The first channel describes the direct reaction while the other channel accounts for the elastic transfer reaction. The Schrodinger equation becomes,

$$(K_\ell - V + E)\chi_d = V_e\chi_e$$
$$(K_\ell - V + E)\chi_e = V_e\chi_d \qquad (2.10)$$

where $K_\ell = \hbar^2/2\mu(d^2/dr^2 - \ell(\ell+1)/r^2)$, with V as the central potential and V_e the coupling potential. The direct elastic wave function is χ_d and χ_e is the transfer wave function. Writing in a compact form we have,

$$D\chi = V_{cc}\chi$$

where $D = \begin{pmatrix} K_\ell - V + E & 0 \\ 0 & K_\ell - V + E \end{pmatrix}$, $\chi = \begin{pmatrix} \chi_d \\ \chi_e \end{pmatrix}$ and $V_{cc} = \begin{pmatrix} Ve & 0 \\ 0 & V_e \end{pmatrix}$

We can follow the formulations similar to that of Lindsay and Rowley [Lin 84], by making a unitary transformation that would allow us to decoupled the Schrodinger equation. The coupling matrix V_{cc} is diagonalised by the unitary transformation:

$$\tilde{V}_{cc} = AV_{cc}A^+ = \begin{pmatrix} 1 & 0 \\ 0 & -1 \end{pmatrix}V_e$$

where $A = \sqrt{\frac{1}{2}}\begin{pmatrix} 1 & 1 \\ -1 & 1 \end{pmatrix}$. Since D is diagonal, then $ADA^+ = D$. Thus we can decouple the two equations into two independent 'elastic' equations. The wave function is now different, since

$$ADA^+ A\chi = AV_{cc} A^+ A\chi.$$

Letting $\phi = A\chi$, the two independent equations are

$$[K_\ell - V - V_e + E]\phi_1 = 0 \qquad (2.11a)$$

$$[K_\ell - V + V_e + E]\phi_2 = 0. \qquad (2.11b)$$

Boundary conditions are imposed on the wave functions ϕ, since it is only χ_d that has an incoming flux. This is realised by (see [Lin 84])

$$\chi = A^+ \Lambda \phi$$

where $\Lambda_{ij} = \delta_{ij} A_{i1}$ i.e. $\Lambda = \sqrt{\frac{1}{2}}\begin{pmatrix} 1 & 0 \\ 0 & -1 \end{pmatrix}$. The two 'elastic equations', when solved would give the scattering matrices $\tilde{S}_1$ and $\tilde{S}_2$. In terms of the uncoupled matrices of eq. (2.10) we have, $S = A^+ \Lambda \tilde{S}$ i.e.

$$S_d = \tfrac{1}{2}(\tilde{S}_1 + \tilde{S}_2)$$

$$S_e = \tfrac{1}{2}(\tilde{S}_1 - \tilde{S}_2)$$

However, we know from the scattering amplitude of eq. (2.9) that the scattering matrix is $S = S_d + (-1)^\ell S_e$, thus

$$S = S_d + S_e = \tilde{S}_1 \qquad \text{for even } \ell$$

$$S = S_d - S_e = \tilde{S}_2 \qquad \text{for odd } \ell.$$

On comparison with the way the two matrices $\tilde{S}$ are calculated, we see that for even ℓ we simply need to solve eq. (2.11a) while for odd ℓ it is eq. (2.11b) that is to be solved. Thus, we can simplify the problem by solving only one equation with a different potential for odd and even ℓ, as

$$[K_\ell - V - (-1)^\ell V_e + E]\phi = 0. \qquad (2.12)$$

This form with a $(-1)^\ell$ (parity) factor is similar to the final form of the Schrodinger equation obtained in the two-state molecular model.

2.2 FUSION REACTION OF HEAVY IONS.

When two heavy ions fuse a compound nucleus is formed which, in most cases, has a short life and is not in equilibrium with its internal degrees of freedom. Therefore, it may evaporate into residues that are "stable" by emitting particles which allow the experimentalist to measure the event. The sum of the cross sections of all the evaporation residues of the compound nuclei formed, of masses greater than the heaviest ion colliding, is called the cross section for complete fusion, which we call the fusion cross section for short. This sum is made over these masses so as to differentiate fusion from other forms of reactions.

The most commonly used model for describing the fusion cross section is the semi-classical barrier penetration model (BPM). The BPM assumes a one dimensional potential barrier, which is formed by the nuclear, Coulomb and centrifugal potentials. At any given energy the flux (partial wave) that fuse are those that penetrate the barrier and are those that we measure their cross sections. Therefore, at energy E, the fusion cross section is the sum of the transmission coefficients of each partial wave ℓ, i.e.

$$\sigma_f = (\pi/k^2)\sum_{\ell=0}^{\infty}(2\ell + 1)\, T_\ell(E), \tag{2.13}$$

where $T_\ell(E)$ is the transmission coefficient of a partial wave ℓ at the energy $E = \hbar^2k^2/2\mu$, μ being the reduced mass of the system. The task, in general, is simply to calculate the transmission coefficient for each ℓ. For a given barrier, as shown in fig. 2.3, we define the grazing partial wave ℓ_g as

$$\ell_g^{\,2} \simeq 2\mu R_B^{\,2}(E - V_B)/\hbar^2 \tag{2.14}$$

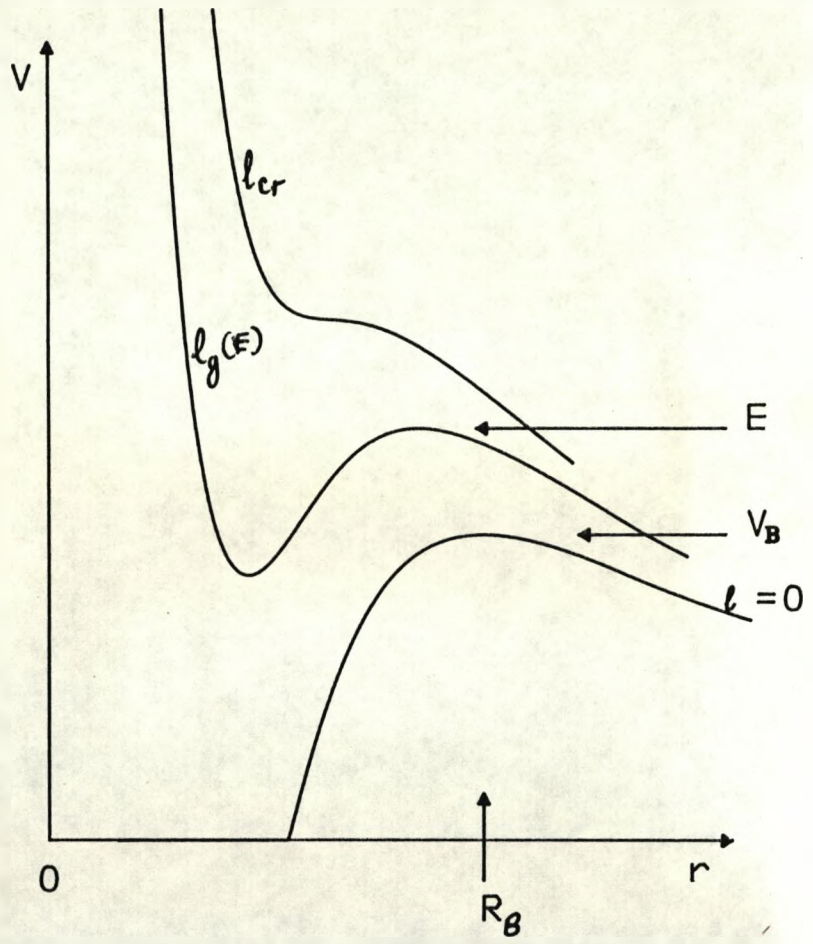

Fig. 2.3 A schematic representation of the nucleus-nucleus potential for various partial waves. The Coulomb barrier ($\ell = 0$) appears at the position R_B and height V_B. The grazing partial wave $\ell_g(E)$ for an incident energy E is the partial wave with a barrier height equal to E. The critical partial wave ℓ_{cr} is the partial wave with no barrier height.

where V_B is the barrier height formed by the nuclear and Coulomb potential at R_B. At energy E, the transmission coefficient for $\ell < \ell_g$ is simply one while for $\ell > \ell_g$ is zero. However, for $\ell \simeq \ell_g$ the transmission coefficient is model dependent and is the main contributing factor to the fusion cross section. For example, the sharp cut-off model (SCO) approximates the transmission coefficient as

$$T_\ell = 1 \quad \text{for } \ell \leq \ell_g$$
$$T_\ell = 0 \quad \text{for } \ell > \ell_g. \tag{2.15}$$

In the classical approximation, since the angular momentum is a continuous parameter, the fusion cross section becomes [Bas 77]

$$\sigma_f \simeq \pi R_B^2 (1 - V_B/E) \qquad E \geq V_B \tag{2.16}$$

and zero for $E < V_B$, using eqs. (2.13) and (2.14). Thus, classically, fusion can not take place at energies below the Coulomb barrier, and at higher energies σ_f saturates to πR^2_B. Bass [Bas 77], Glas and Mosel [Gla 76] and Kovar et al [Kov 79] (and many others) have made calculations for various systems using this model. In particular, Kovar et al have calculated the parameters V_B and R_B for a variety of light heavy ions.

However, when the quantum mechanical nature of ℓ is taken into account, at the energy E, where ℓ_g is grazing (see fig. 2.3), the fusion cross section becomes

$$\sigma_f = (\pi/k^2)(\ell_g + 1)^2. \tag{2.17}$$

To illustrate the shape of the fusion excitation function produced by the SCO model, we calculated the grazing partial wave ℓ_g using eq. (2.14) at various energies and the fusion cross section using eq. (2.17). The parameters we used in eq. (2.14) are the classical parameters of $^{12}C + ^{16}O$ system (obtained from Kovar et al [Kov 79]), i.e.

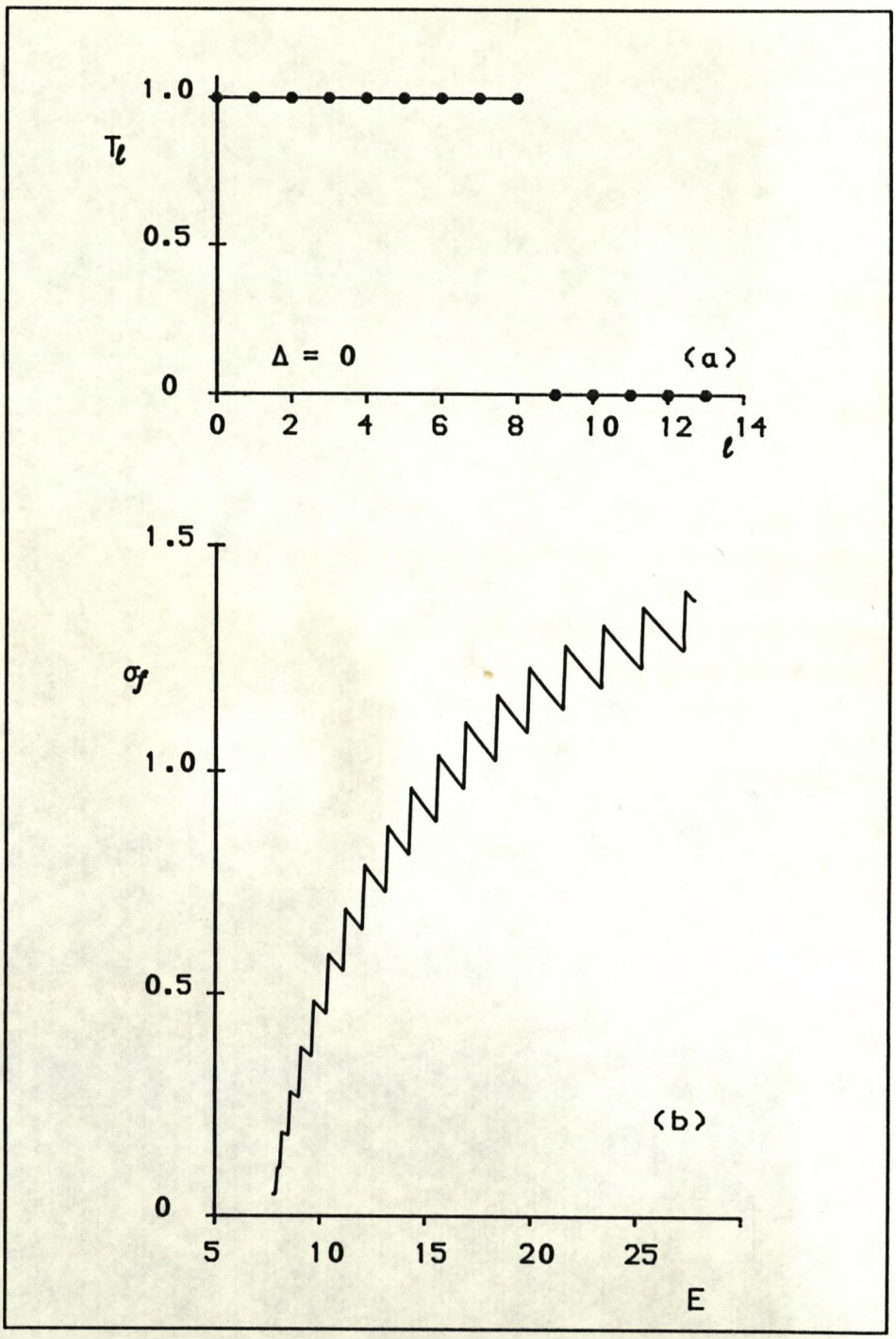

Fig. 2.4 The transmission coefficient at E= 11.6 MeV and the fusion excitation function for a SCO model.

R_B= 7.5 fm and V_B= 7.7 MeV. We choose $^{12}C + {}^{16}O$ as a typical example of a light heavy-ion system that possesses oscillatory structure in σ_f. In fig. 2.4a, we show the transmission coefficient produced by the SCO model at E= 11.6 MeV where ℓ_g= 8. The fusion excitation function produced by this model is shown in fig. 2.4b. The shape of σ_f we obtained, a "saw tooth", is clearly non-physical. Fusion cross sections are rather smooth functions of energies. Therefore, the SCO model is an extreme model. The fusion excitation function takes a "saw tooth" shape because the individual partial wave contribution to the summation in eq (2.13) is rather abrupt and T_ℓ is extremely sharp.

A realistic transmission coefficient should have a finite fall-off region in ℓ-space. For example, in the simplest approximation, the transmission coefficient could be

$$T_\ell = 1/\{1 + \exp[(\ell^2 - \ell_g{}^2)/\Delta]\}, \qquad (2.18)$$

at energy E where ℓ_g is grazing and Δ is assumed to be a constant that determines the rate of fall-off of T_ℓ in ℓ-space. For the extreme sharp cut-off model $\Delta = 0$, and the smaller Δ is the sharper T_ℓ would be. Using this approximation for the transmission coefficient, the fusion cross section would be smooth since individual partial waves are added to σ_f more gradually. Repeating the calculations as in fig. 2.4, we calculate T_ℓ at E = 11.64 MeV using eqs. (2.14) and (2.18) for two different values of Δ. These are shown in figs. 2.5 (a) and (c). The corresponding fusion excitation functions for the two values of Δ are shown in figs. 2.5 (b) and (d).

Since our aim is to produce oscillations in σ_f, the calculations of σ_f with $\Delta = 4$ show that one can easily achieve this using small values of Δ. For systems that do not possess oscillatory structure in σ_f, the present approximation is still valid if large values of Δ (say $\Delta \geq 8$)

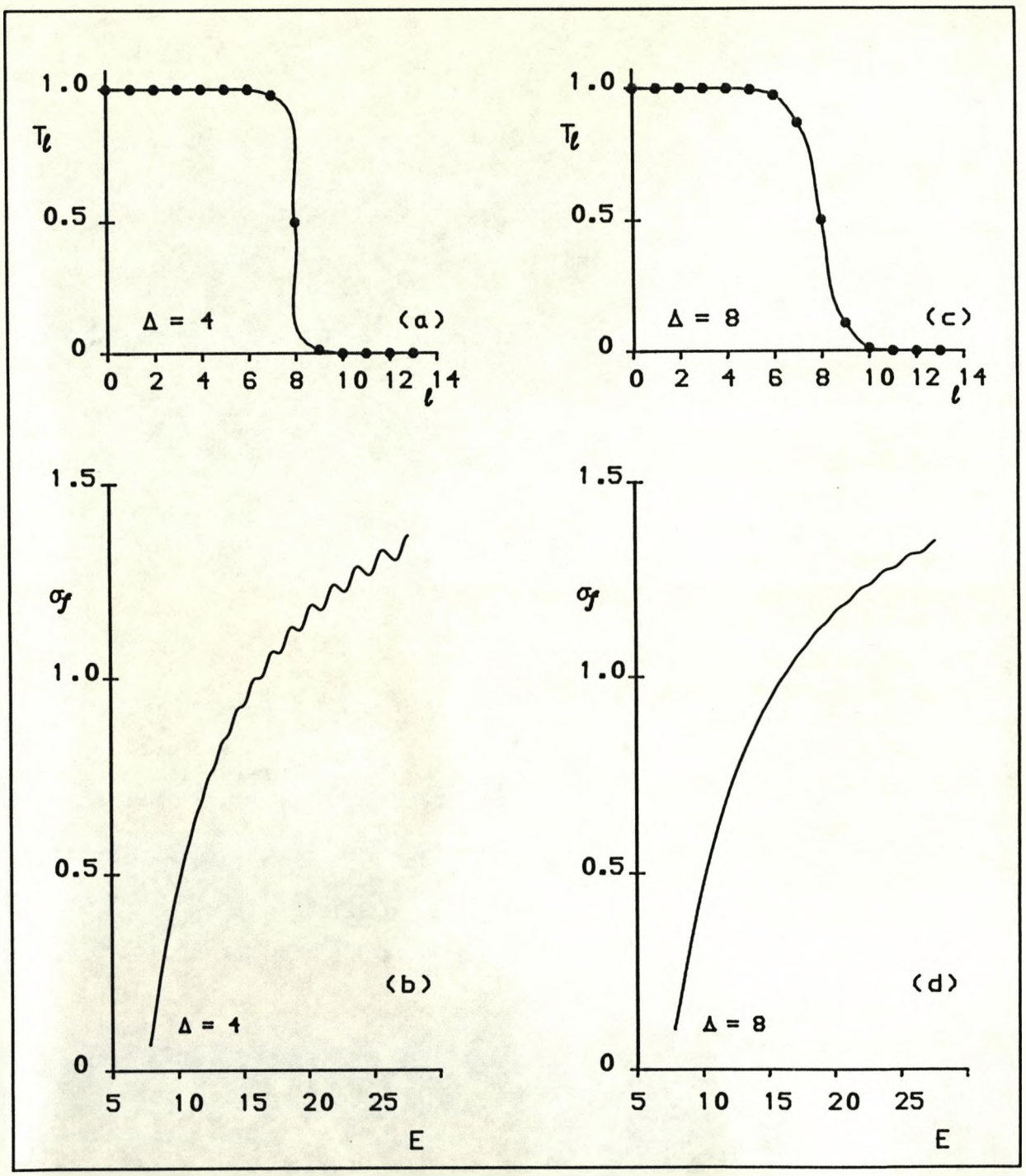

Fig. 2.5 The transmission coefficient at E= 11.6 MeV and the fusion excitation functions. (a) T_ℓ when $\ell_g = 8$ and $\Delta = 4$. (b) The corresponding fusion cross section for $\Delta = 4$. (c) T_ℓ when $\ell_g = 8$ and $\Delta = 8$. (d) The corresponding fusion cross section for $\Delta = 8$.

are used. Thus, for $^{12}C + ^{16}O$ system, $\Delta = 4$ should in principle reproduce the oscillations in σ_f.

A physical model that corroborates our approximation of T_ℓ above is a BPM which assumes a real potential with barriers formed from the sums of the nuclear, Coulomb and centrifugal potentials. For example, Cujec and Barnes [Cuj 76] approximated the top of the Coulomb barrier with an inverted parabola and used the Hill and Wheeler [Hil 53] expression for the transmission coefficient;

$$T_\ell = 1/\{1 + \exp[2\pi(V_{B\ell} - E)/\hbar\omega_\ell]\} \tag{2.19}$$

where $V_{B\ell}$ is the height of the interacting barrier for a given ℓ, defined as

$$V_{B\ell} = V(R_B) + \hbar^2\ell(\ell+1)/2\mu R_B^2 \tag{2.20}$$

and $\omega_\ell^2 = \frac{1}{\mu}\{\partial^2[V(r) + \ell(\ell+1)\hbar^2/2\mu r^2]/\partial r^2\}_{R_B}$.

Here $V(r)$ is the sum of the Coulomb and nuclear potentials. If $E \simeq V(R_B) + \hbar^2\ell_g(\ell_g+1)/2\mu R_B^2$, then T_ℓ in the above equation becomes approximately the same as eq. (2.18) with

$$\Delta \simeq \mu R_B^2\omega_\ell/\hbar\pi.$$

Thus, Δ should be energy dependent and related to the geometrical properties of the potential barrier.

Assuming that the tail of the real nuclear potential is roughly exponential with a surface diffuseness a_r, i.e.

$$V_N(r) = -V_o\exp(-r/a_r), \tag{2.21}$$

Poffe et al [Pof 83] derived a relationship between ω_ℓ and a_r from the above expressions. We can also use the relationship to express Δ in terms of the physical parameters of the system. We have

$$\Delta \simeq \frac{R_B^2}{\hbar\pi}\left[-\mu(V''_N + V''_C)\right]^{1/2}_{r=R_B} = \frac{eR_B}{\hbar\pi}\left[Z_1Z_2\mu\left(\frac{1}{a_r} - \frac{2}{R_B}\right)\right]^{1/2} \tag{2.22}$$

where V_C is the Coulomb potential and we have used the fact that at R_B, $V_N' = V_C' = Z_1 Z_2 e^2 / R_B^2$ for the s-wave. Thus, for light ions and a reasonably large surface diffuseness, Δ may be small.

To make a comparison of the possible values of a_r we would expect for given Δ, we calculate the surface diffuseness for two systems. A lighter system $^{12}C + ^{16}O$ and a slightly heavier system $^{16}O + ^{40}Ca$. Using eq. (2.22) with R_B = 7.5 fm for $^{12}C + ^{16}O$ and 9.0 fm for $^{16}O + ^{40}Ca$ (from [Kav 79]), we calculate a_r for the following Δ, as shown below.

	Surface diffuseness (fm)	
Δ	$^{12}C + ^{16}O$	$^{16}O + ^{40}Ca$
0	3.75	4.50
4	1.94	3.95
8	0.79	2.88
12	0.40	1.99
18	0.23	1.39
20	-	0.99

In the previous calculations of σ_f we made (fig. 2.5), it was shown that for $^{12}C + ^{16}O$, where experimentally σ_f possesses oscillatory structure, the oscillations can only be observed using smaller values of Δ. However, the above table shows that smaller values of Δ correspond to unrealistic a_r. This means that our present model can not produced the oscillatory structure in the excitation function even with a reasonably large a_r. For the heavier ions, clearly we do not expect any oscillations, since a reasonably large a_r corresponds to a large value of Δ. For these ions, the heavier ones, experimental results confirm our prediction, i.e., no oscillations were observed. However, for the lighter systems, we have to find another model that would explain the oscillations.

Another approach is to solve a standard optical model, with an imaginary potential included, so that all the flux that penetrates the barrier is absorbed. This approach is consistent with standard scattering calculations, since it takes into account that some of the flux that penetrates the barrier may not necessarily contribute to fusion but could go into other inelastic channels. The significance of the imaginary potential will be discuss in the latter part of this chapter. With the optical model approach, the transmission coefficient is calculated from the S-matrix as $T_\ell = (1 - |S_\ell|^2)$. However, this approach does not also reproduce the oscillatory structure in its present form (see attempts by [Fro 76]). Thus, for light heavy-ions, other physical properties of the system will have to be taken into account.

2.2 (A) SYMMETRIC IONS

For symmetric spin-zero bosons, it was shown in the previous section that, because of symmetrisation, the odd partial waves do not contribute to the elastic scattering amplitudes. Poffe et al [Pof 83] have shown that, because of the symmetrisation of the system the fusion cross section becomes

$$\sigma_f = (\pi/k^2)\sum_{\ell=0}^{\infty}(2\ell + 1)\, T_\ell[1 + (-1)^\ell]. \qquad (2.23)$$

These authors showed that because of the absence of the odd partial waves in the summation, oscillations are more likely to be seen in σ_f as a function of energy. To illustrate that the oscillations in σ_f can be obtained using the approximation of T_ℓ in eq. (2.18), we calculated σ_f using the same parameters as in fig. 2.5 (c) and (d) with $\Delta = 8$. Figure 2.6 shows that the oscillations in the cross section are clearly restored even though $\Delta = 8$. The transmission coefficient is shown in fig. 2.6a and it is the same as that in fig. 2.5c but it

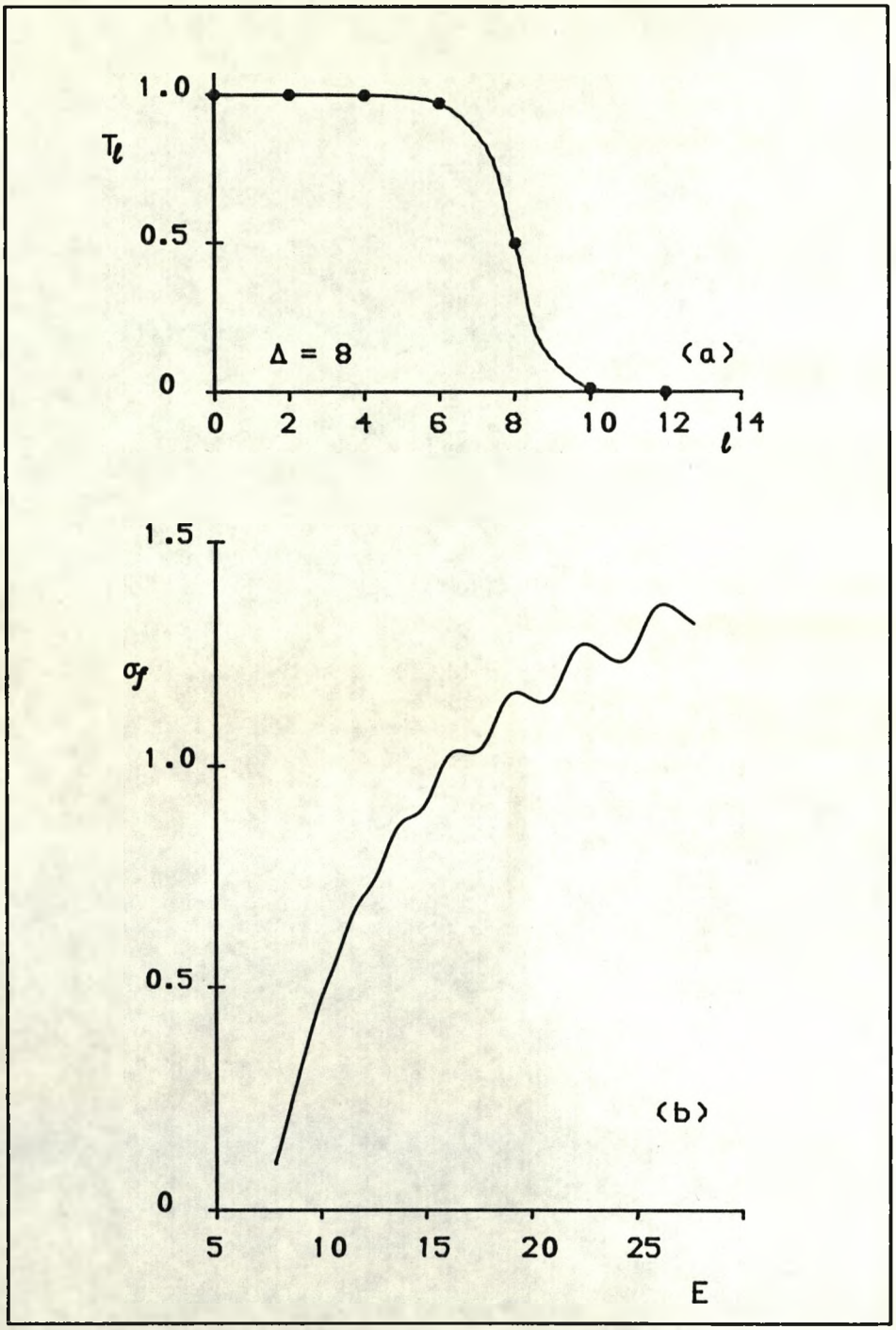

Fig. 2.6 The transmission coefficient at E= 11.6 MeV and the fusion excitation function for symmetric ions when $\Delta = 8$. (a) T_ℓ when $\ell_g = 8$. (b) The corresponding fusion excitation function.

now contains less partial waves in the transition region and is, therefore, effectively sharper. The reason for the restoration of the oscillations, in this case, can easily be seen if the effect of each barrier on the fusion cross section is considered.

Consider the difference between the barrier heights of three successive partial waves ℓ_1 (even), ℓ_1+1 and ℓ_1+2, as shown in fig. 2.7. Suppose that at energy E_{ℓ_1} the transmission coefficient for ℓ_1 is $\frac{1}{2}$, for partial waves $\ell<\ell_1$ we have $T_\ell = 1$ and $T_\ell = 0$ for $\ell>\ell_1$ (a "reasonable" sharp cut-off in T_ℓ as in fig. 2.5c). The cross section is then the sum up to ℓ_1. As the energy is increases, since ΔE_{ℓ_1} is small for light ions (~1 MeV), the next term in σ_f is easily reached. However, in symmetric ions the odd partial waves are removed. Therefore, before the summation in σ_f is increased by the term with ℓ_1+2, the energy has to increase by a value of ΔE_{ℓ_1+2}, but since $\sigma_f \propto 1/k^2$ (i.e., 1/E) then as the energy increases, σ_f decreases. Once the energy reaches E_{ℓ_1+2}, the summation will abruptly increase, and this results to a net increase in σ_f. As the energy increases again the summation remains constant but σ_f would start falling again, until another partial wave. This phenomena brings the oscillations. It should be noted that this can only occur when T_ℓ is reasonably sharp (i.e. with a thick barrier) and is true of all symmetric systems. However, oscillations are not likely in the heavier symmetric ions because ΔE_{ℓ_1+2} is small.

2.2 (B) NONSYMMETRIC IONS.

For the nonsymmetric system, oscillatory structure in the fusion cross section of many ions have also been observed, for example in $^{12}C + ^{16}O$, $^{12}C + ^{11}B$, $^{12}C + ^{24}Mg$ and many other combinations. The model we have presented so far does not explain any of these oscillations, since larger values of Δ are required. For the symmetric system it

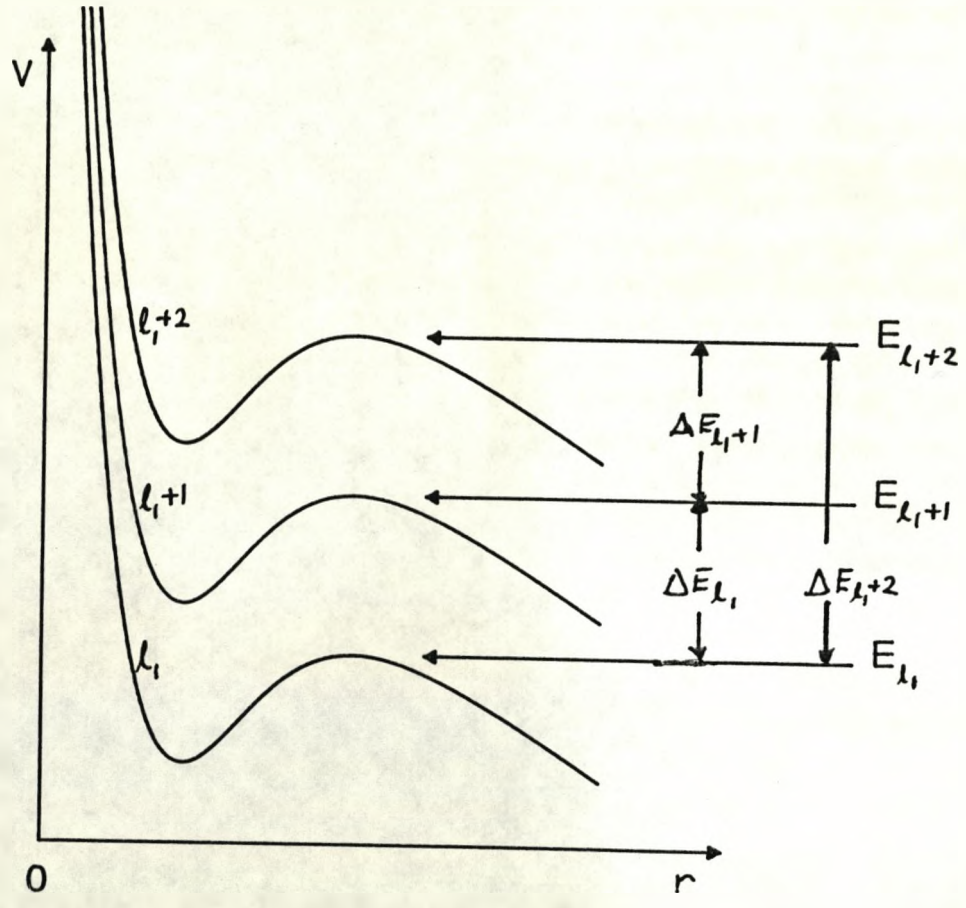

Fig. 2.7 A schematic representation of the barrier heights of three consecutive partial waves.

was shown that taking account of the elastic scattering process, the oscillatory structure in σ_f can easily be reproduced. We can extend the same argument here to the nonsymmetric systems. That is, since in the elastic scattering of two nonsymmetric ions (that differ by few nucleons) a parity dependent potential was used, then the same potential can be used in calculating the fusion cross section. This potential would effectively shift the barrier heights of different partial waves, as such it lowers or raises the grazing energy of a partial wave ℓ. This leads to a situation where the barrier heights of some odd partial waves is the same as the neighbouring even ones. Thus the system would look like the symmetric ones, and oscillations may reappear in the fusion excitation function.

If $(-1)^{\ell}\Delta V$ is the contribution of the parity dependent potential to the barrier height and is added such that the barriers for the odd partial waves are depressed and those for the even partial waves are raised by about half the original separation of the original barriers, then the barrier height of the two new barriers will be similar, and $T_\ell \simeq T_{\ell+1}$. This is shown schematically in fig. 2.8. If ΔV is constant and $T_\ell \simeq T_{\ell+1}$, then the adjacent pairs of odd-even partial waves would also have approximately the same transmission coefficient and at energies in the region of these barriers we have

$$\sigma_f = (\pi/k^2)\sum_{\ell=0}^{\infty}(2\ell + 1)T_\ell \simeq (\pi/k^2)\sum_{\ell=0}^{\infty}(2\ell + 1)(T_\ell + T_{\ell+1})$$

$$\simeq (2\pi/k^2)\sum_{\ell\ \text{even}}(2\ell + 1)T_\ell. \qquad (2.24)$$

This expression is the same as eq. (2.23) for the symmetric system. Therefore, we expect the oscillatory structure to be restored in the energy region where the eq. (2.24) is valid.

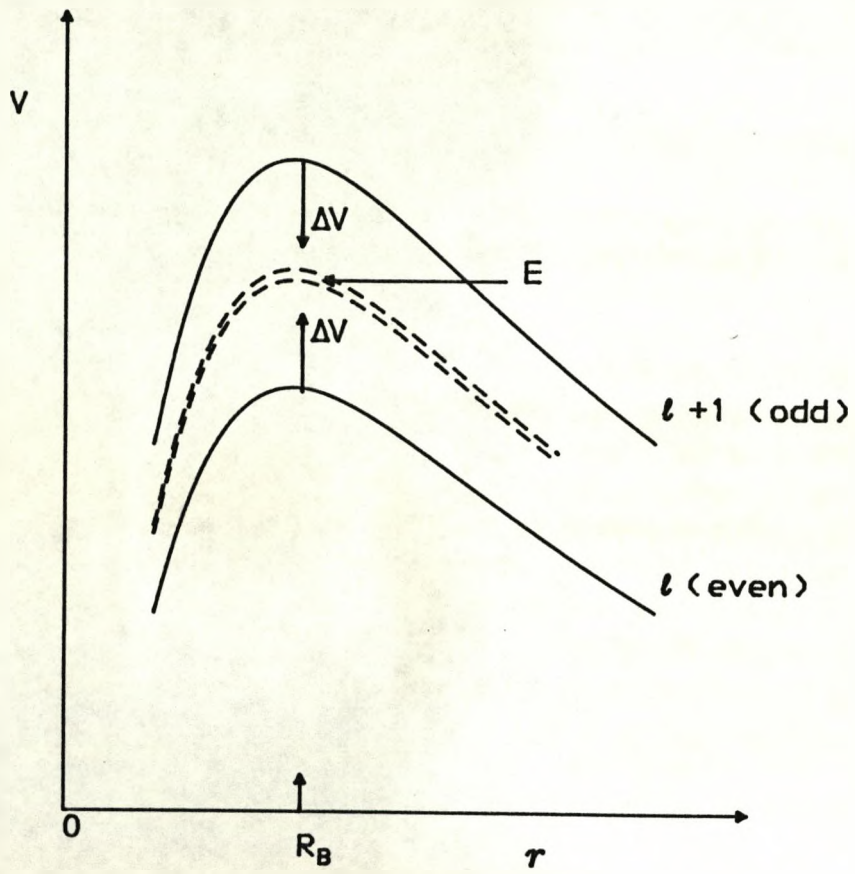

Fig. 2.8 A schematic representation of the effect of a parity dependent potential on two barrier heights; ℓ and ℓ + 1. The full curves represent the barriers when no parity dependent potential was added. The two dashed curves represent the barrier after a parity dependent potential was added.

The expression for the grazing partial waves at energy E is now different for the odd and even ℓ,

$$\ell_e^2 = 2\mu R_B^2(E - V_B + \Delta V)/\hbar^2$$
$$\ell_o^2 = 2\mu R_B^2(E - V_B - \Delta V)/\hbar^2 \qquad (2.25)$$

for the even (e) and odd (o) partial waves. Similarly, the transmission coefficient in our approximation is now different for both the even and odd partial waves, i.e.

$$T_{even} = 1/\{1 + \exp[(\ell^2 - \ell_e^2)/\Delta_e]\}$$
$$T_{odd} = 1/\{1 + \exp[(\ell^2 - \ell_o^2)/\Delta_o]\} \qquad (2.26)$$

The width Δ for the odd and even partial waves should be similar if the two barrier heights do not differ too much so we can take $\Delta_e = \Delta_o = \Delta$. The value ΔV at R_B can easily be calculated from the change in two successive ℓ. Using eq. (2.25) we obtained

$$\Delta\ell_g = |\ell_e - \ell_o| \simeq \frac{R_B \Delta V}{\hbar}\sqrt{\frac{2\mu}{E - V_B}} \qquad (2.27)$$

If $\Delta\ell_g = 1$, then the expression for σ_f (eq. (2.24)) is valid at energies where $T_\ell \simeq T_{\ell+1}$ and we expect the oscillations in σ_f to be restored. However, if $\Delta\ell_g = 2$ or even, then in the region where the barrier heights are the same $T_\ell \simeq T_{\ell+2}$ and $T_{\ell+1} \simeq T_{\ell+3}$. The expression for σ_f in this case is not all that different from the expression when $\Delta V = 0$, and thus the oscillations in σ_f will not appear.

To illustrate that our model restores the oscillatory structure in σ_f, we repeated the calculations we made in figs. 2.5 and 2.6. Using the same parameters as those in the figures but with $\Delta V = 0.4$ MeV, we calculated T_ℓ using eqs. (2.25) and (2.26). The value of ΔV was chosen so that $\Delta\ell_g = 1$ and $T_7 \simeq T_8$ at 11.6 MeV. The transmission coefficient for the odd and even partial waves is shown in fig. 2.9a. Using eq.

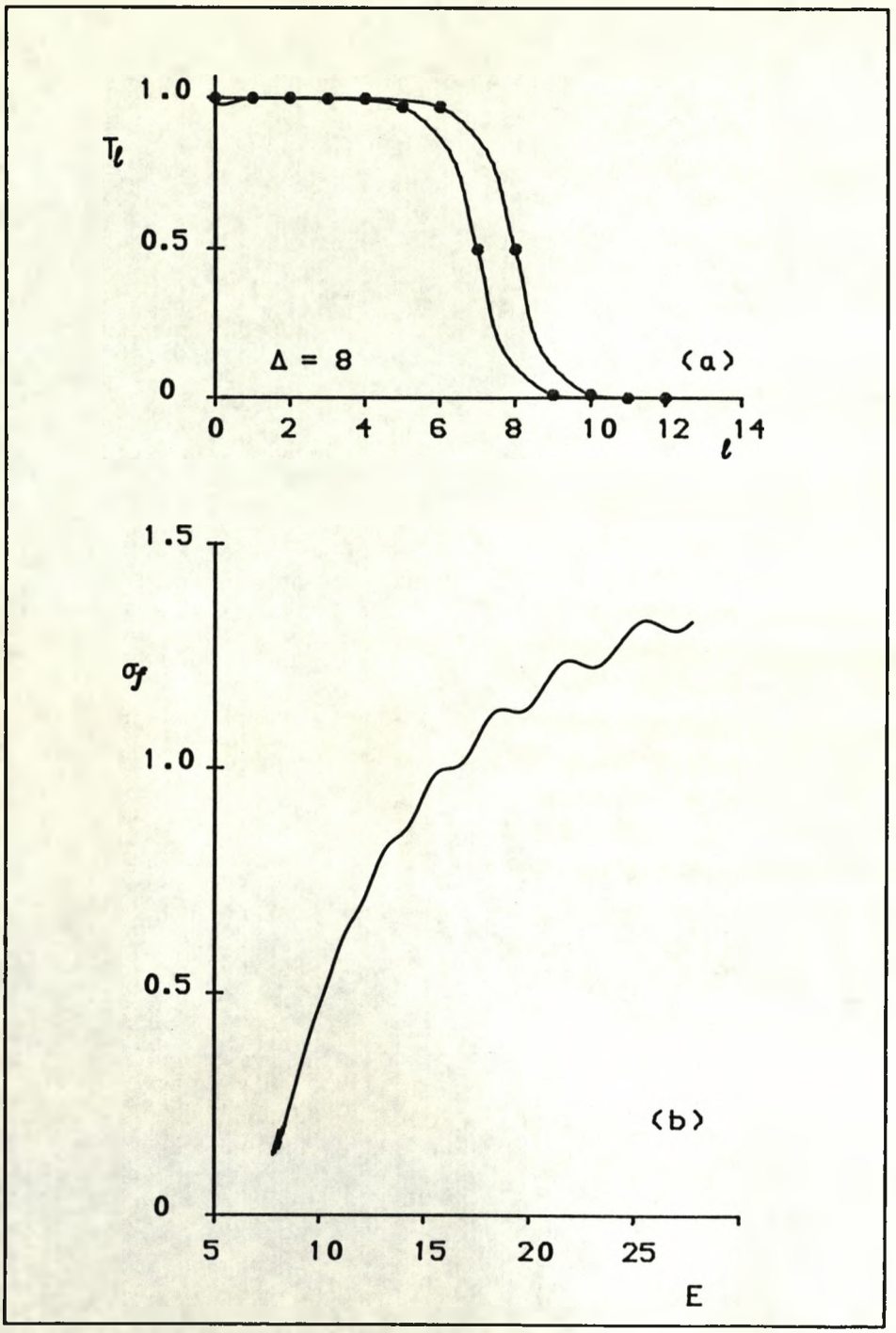

Fig. 2.9 (a) The transmission coefficients at E= 11.6 MeV for even and odd partial waves. The grazing energies are ℓ_g = 7 and 8, because of the parity dependent potential. (b) The corresponding fusion excitation function.

(2.13), we calculated the fusion cross section at various energies. This is shown in fig. 2.9b. The oscillatory structure is clearly restored at the energies where changes in barrier heights are significant.

It is important to note that, to restore these oscillations in physical systems the difference in the barrier height of two successive partial waves has to be significantly large. That is, even if the barrier heights are shifted but the difference between the shifted barriers (ℓ and $\ell+2$ if $\Delta\ell_g=1$) is small, no oscillations will be seen. The importance of the difference in the barrier heights was explained by Poffe et al [Pof 83]. They showed that, σ_f in eq. (2.13) can be decomposed into two parts, a gross cross section term σ_w which possesses no oscillation and an oscillatory term σ_{osc}, i.e. $\sigma_f = \sigma_w + \sigma_{osc}$, with

$$\sigma_{osc} \simeq \frac{4\pi\mu R_B \hbar\omega}{k^2} \exp\left(\frac{-\pi\mu R_B \omega}{\ell_g+\frac{1}{2}}\right) \sin(2\pi\ell_g). \tag{2.28}$$

For the symmetric systems, the oscillatory term becomes

$$\sigma_{osc} \simeq \frac{4\pi\mu R_B \hbar\omega}{k^2} \exp\left(\frac{-\pi\mu R_B \omega}{2\ell_g+1}\right) \sin(\pi\ell_g). \tag{2.29}$$

Therefore, the magnitude of oscillations in the nonsymmetric and symmetric systems is mainly determined by the exponents in the above equations. For the nonsymmetric system, we have

$$\frac{\pi\mu R_B \hbar\omega}{\ell+\frac{1}{2}} = \frac{\pi\hbar\omega}{\partial V_B(\ell)/\partial\ell} \simeq \frac{\pi\hbar\omega}{V_B(\ell+1) - V_B(\ell)} \tag{2.30}$$

and for the symmetric systems, we have

$$\frac{\pi\mu R_B \hbar\omega}{2\ell+1} = \frac{\pi\hbar\omega}{2\partial V_B(\ell)/\partial\ell} \simeq \frac{\pi\hbar\omega}{V_B(\ell+2) - V_B(\ell)} \tag{2.31}$$

These expressions show the importance of the difference in the barrier heights, and thus the reduced mass of the system.

For the nonsymmetric case, in the energy region where the barrier heights are the same and $\Delta\ell_g = 1$, the expression in eq. (2.31) applies and in the other regions where the barrier heights are shifted but not equal eq. (2.30) is applicable. Therefore, for lighter systems with small values of μ, oscillations are likely to appear. However, for the heavier systems, i.e. large μ, oscillations are likely to appear at higher energies where ℓ is large, but not at the lower energies.

2.3 CONNEXION BETWEEN THE ELASTIC AND FUSION CROSS SECTIONS IN OPTICAL MODEL

In the proceeding section, we used the properties of the elastic scattering of symmetric and nonsymmetric systems to explain the fusion reactions and we showed that these properties are important in restoring the oscillatory nature of σ_f. Though the model was not applied to a specific system of light heavy-ions, we argued that the model applies to all nonsymmetric systems. In chapter 3 the model is applied to physical system of light heavy-ions using an optical model potential and the elastic scattering properties of the system.

Through an optical model, Udagawa et al [Uda 85] and later Satchler et al [Sat 87] proposed that the two processes can be treated simultaneously. The aim of this section is to briefly present the proposal of Udagawa et al, so that we can discuss the significance of the imaginary potential in future calculations we shall make.

Essentially, Udagawa et al showed that given a Schrodinger equation for elastic scattering in an optical model, as

$$(K_a + U_a)\chi_a = E_a\chi_a \qquad (2.32)$$

where $U_a = -V_a - iW_a$ the optical model potential, the reaction cross section is

$$\sigma_R = (2/\hbar v_a) \ \langle \chi_a \ | W_a | \chi_a \rangle \qquad (2.33)$$

$$= (2\pi/k_a^2) \sum_{\ell=0}^{\infty} (2\ell + 1) \ T_\ell$$

with

$$T_\ell = (4/\hbar v_a) \int_0^R |\chi_\ell|^2 \ W_a(r) \ dr.$$

Here χ_a is the elastic scattering wave function, which in partial wave expansion has χ_ℓ partial waves. The reaction cross section is then the sum of all the non-elastic cross sections, which can be decomposed into two parts: the fusion cross section σ_f and other direct scattering processes cross section σ_d, i.e. $\sigma_R = \sigma_f + \sigma_d$. We can write the fusion cross section in the same way as in eq. (2.33), i.e.

$$\sigma_f = (2/\hbar v_a) \ \langle \chi_a \ | W_f | \chi_a \rangle,$$

where W_f is the imaginary potential that allows the absorption of the flux that fused only. Similarly, for the direct reaction we have

$$\sigma_d = (2/\hbar v_a) \ \langle \chi_a \ | W_d | \chi_a \rangle,$$

here W_d is the imaginary potential for the direct processes. Thus,

$$\sigma_R = (2/\hbar v_a) \ \langle \chi_a \ | W_f + W_d | \chi_a \rangle.$$

Therefore, we may write

$$W_a = W_f + W_d.$$

That is, the imaginary potential used in the elastic scattering is the sum of two potentials, namely: the fusion and the direct imaginary potentials. Thus, once the correct choice of U_a is made in calculating the elastic scattering (i.e. χ_a), the same real potential can be used to calculate σ_f, but with an imaginary potential that is smaller than W_a. This deduction is important because we have shown that the real potential in the elastic scattering of nonsymmetric systems contains a $(-1)^\ell$ factor (this is also true for the symmetric ions but the

factor is now $[1+(-1)^{\ell}]$), and we used this fact to restore the oscillatory nature of σ_f. Thus, the model we have presented for the nonsymmetric systems is consistent with the Udagawa et al [Uda 83] proposal and therefore a valid one. Therefore, the fusion imaginary potential in BPM should be short ranged and confined inside the barrier, since the flux that fuses is that which penetrates the barrier.

Another important thing we can deduce from this is that, if we solve the Schrodinger equation with the aim of fitting σ_f, then we may still be able to reproduce the elastic scattering data with a larger imaginary potential. However, it should not be surprising if in some cases the elastic scattering data is not reproduced, since χ_a is not used and U_a in eq. (2.32) may be non-local. It was in fact suggested [Nag 86a] that to be able to fit both σ_f and the elastic scattering cross sections, the "ideal" thing to do is to fit the elastic scattering cross sections at various energies and use these potentials to calculate σ_f at the appropriate energies. This procedure should reproduce the fusion cross sections at energies both below and above the Coulomb barrier. Our main concern in this thesis is the fusion reaction, therefore we shall not adapt the "ideal" procedure. Though we shall attempt to fit both σ_f and the elastic scattering cross section in the following chapter.

CHAPTER 3

FUSION OF SPINLESS NUCLEI (APPLICATION)

In the previous chapter the theory behind the oscillatory structure in σ_f was presented and a simple model was used to illustrate the shape of σ_f for symmetric and nonsymmetric systems. In this chapter, we shall apply the theory to symmetric and nonsymmetric ions using an optical model potential. For the symmetric ions like the $^{12}C + ^{12}C$ system, previous calculations that reproduced the oscillations used an inverted parabola as the approximate shape of the Coulomb barrier [Pof 83]. We shall replace the inverted parabola barrier with a barrier formed by an optical potential and repeat the calculations for $^{12}C + ^{12}C$ system. For $^{16}O + ^{16}O$ system, Tanimura [Tan 80] used an optical model to calculate the elastic and fusion excitation functions, but included the 3^- inelastic state of ^{16}O in the calculations. Similarly, Kondo et al [Kon 80] explained the oscillations in terms of the band-crossing model and obtained a fit similar to that of Tanimura.

For the nonsymmetric ions, we shall take account of the properties of the system discussed in the previous chapter to fit the fusion excitation functions of $^{12}C + ^{16}O$ [Kab 88], $^{12}C + ^{24}Mg$ and $\alpha + ^{40}Ca$ systems. For the $^{12}C + ^{16}O$ system, the elastic scattering cross sections will also be calculated at various energies and we shall compare the result with the experimental data available at those energies. In general, this calculation can be applied to other systems that exhibit the "anomalous large angle scattering cross section" (ALAS) in the elastic angular distribution and oscillatory structure in the fusion excitation function. We shall discuss this generalisation, to other systems, in the last section of this chapter.

The effective interaction potential, we shall be using, is the sum of a complex nuclear potential $V_N(r)$, a Coulomb potential $V_C(r)$ and a centrifugal potential. For nonsymmetric systems where there is exchange of particles, a parity dependent potential $V_\pi(r)$ is included. That is

$$U(r) = V_N + V_C + \ell(\ell + 1)\hbar^2/2\mu r^2 \quad + (-1)^\ell V_\pi, \tag{3.1}$$

where the Coulomb potential defined as

$$V_C(r) = \begin{cases} Z_1 Z_2 e^2/r & r > R_c \\ Z_1 Z_2 e^2[3-(r/R_c)^2]/2R_c. & r \leq R_c \end{cases} \tag{3.2}$$

The real nuclear potential is described by a Woods-Saxon form factor, though later we shall see some variations for different systems when the normal Woods-Saxon form factor does not describe the nuclear potential satisfactorily. The imaginary part of the potential is also parameterised by a Woods-Saxon form factor. That is

$$V_N(r) = -V_0 f(r,R_r,a_r) \quad - iW_0 f(r,R_i,a_i) \tag{3.3}$$

$$\text{where} \quad f(r,R_0,a_0) \quad = [1 + \exp((r-R_0)/a_0)]^{-1}, \tag{3.4}$$

$R_0 = r_0(A_1^{1/3} + A_2^{1/3})$ and A_1, A_2 are the mass number of the target and the projectile. The same form is used for the Coulomb radius R_c, with r_c usually fixed for a given system (between 1.2 and 1.5 fm).

The form factor of the exchange potential according to the two-state molecular model should be a Yukawa form factor, though Baye [Bay 86] used an exponential form factor in his calculations. For convenience, we assume that the form factor of $V_\pi(r)$ is the form factor of real part of the nuclear potential multiplied by a dimensionless parameter α. That is

$$V_\pi(r) = -\alpha V_0 f(r,R_r,a_r). \tag{3.5}$$

As was shown in fig. 2.8, the parity dependent potential is added to the interaction potential so that it shifts the exact barrier heights to get the appropriate changes in the heights. Therefore, the precise shape of $V_{\pi}(r)$, in the interior of the real potential, is not important. Since the barriers occur around the tail of the nuclear potential.

In fitting the fusion cross sections, we shall adapt the following procedure:-

1. The imaginary potential is confined to the interior of the interacting barrier. This is to ensure that only the flux that penetrates the barrier are absorbed. Thus the range of the imaginary potential should be less than the range of the real potential and the depth should be large enough to allow complete absorption of all the flux that penetrate.
2. A large value of a_r will always be used (about 0.95 fm). This is to ensure that a reasonably sharp T_ℓ is obtained.
3. When these conditions are satisfied, a χ^2 (chi squared) fit is made to the experimental data by varying all the potential parameters.

We shall now present the details of our calculations for each system in the following sections. The computer code we used to calculate the fusion excitation function and the elastic cross sections is a modified version of the code HI-OPTIM-85 [Cla 85]. We modified the code so that it takes account of the elastic exchange process and symmetrisation in the symmetric systems.

3.1 THE $^{12}C + ^{12}C$ SYSTEM.

These are symmetric spin-zero bosons, so the odd partial waves are not present in either the elastic or the fusion cross section calculations (see eqs. (2.8) and (2.23)). As mentioned in the introduction to this chapter, calculations for the fusion excitation function of this system were made by Poffe et al [Pof 83] using an inverted parabola barrier approximation. The model reproduced the oscillatory structure in σ_f satisfactorily up to 25 MeV. Above this energy the fit was over estimating the data. More recently, Ohkubo and Brink [Ohk 87a] used an optical model potential to calculate σ_f. However, their fit was not satisfactory because they used a shallow real potential with a small surface diffuseness a_r. They argued that the origin of the oscillations in σ_f is due to the interference of the "internal" and "barrier" waves, which are produced at the two turning points of the interacting potential. That is, the barrier wave is the reflected wave at the angular momentum barrier and the reflected wave at the nuclear surface is the internal wave. Internal and barrier waves have been used previously to explain some of the features of the elastic scattering of $^{12}C + ^{12}C$ system (see [Row 77]).

We repeated the calculations of σ_f for this system using an optical model potential with large a_r, so that the effect of individual ℓ contribution to the cross section can be seen. Figure 3.1 shows the results of our calculations. The values of the potential parameters we used are given in table 3.1. The fit was made using a deep real potential with a strongly absorbing imaginary potential. From the figure, we note that there is a good agreement between the calculated σ_f and the experimental values up to 25 MeV. Above 25 MeV our fit is not in phase with the data. However, the general trend seems to be in close agreement, i.e. decreasing. At those energies, i.e. above

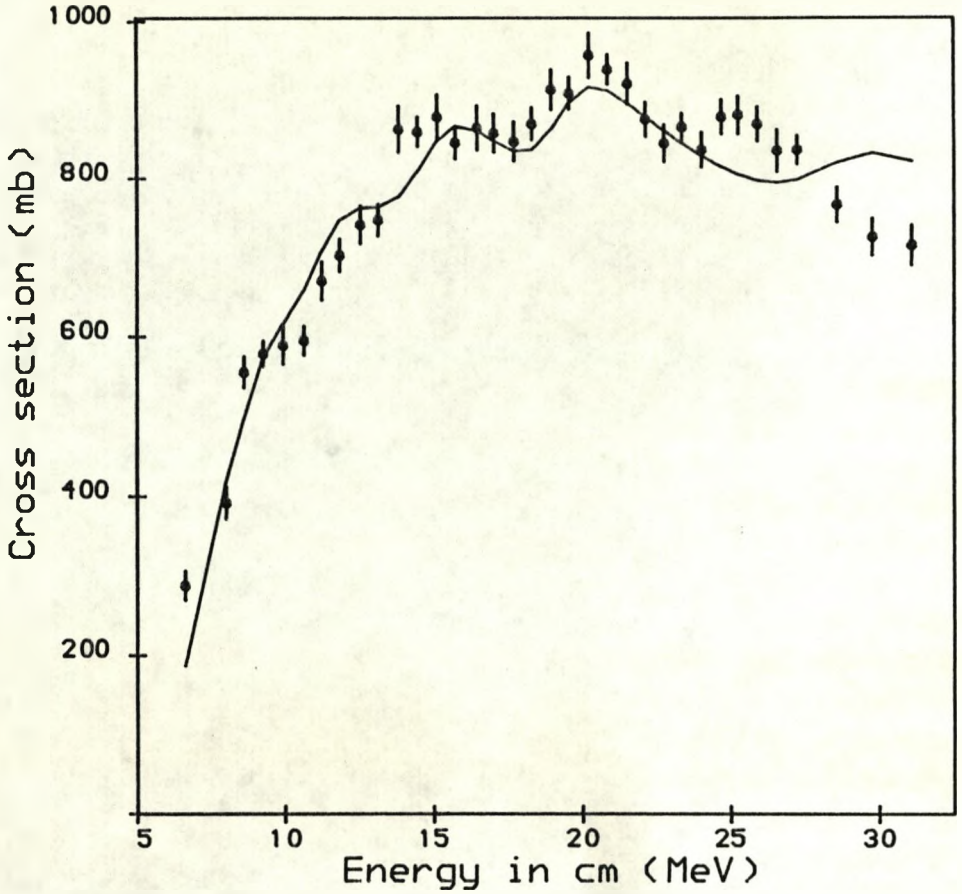

Fig. 3.1 The fit to the fusion cross section of $^{12}C + ^{12}C$ system. The values of the potential parameters given in table below. Experimental data points were obtained from [Kav 79].

TABLE 3.1

	V (MeV)	r (fm)	a(fm)
Real	102.77	0.67	0.94
Imaginary	82.32	0.40	0.53
Coulomb	-	1.40	-

25 MeV, our potential does not yield the correct barrier heights, but the correct critical angular momentum was obtained, that is why σ_f is decreasing. A similar problem was encountered by Poffe et al. Therefore, it is likely that at those energies conventional form factors do not adequately describe the nuclear potential or there are other direct processes taking place.

The most important conclusion of these calculations is that a qualitatively good fit to the fusion cross section was obtained when the symmetrisation of the system was taken into account and a reasonably thick barrier (i.e. small Δ) was used.

3.2 THE $^{12}C + ^{16}O$ SYSTEM.

Until recently [Kab 88], all attempts to explain the mechanism responsible for the oscillatory structure in σ_f for this system have not been successful, largely because the exchange process of the system has not been taken into consideration. Optical model calculations by Frohlich et al [For 76], the inverted parabola approximation by Glas and Mosel [Gla 74] and many other models have reproduced the average fusion cross section but not the oscillations.

In the previous chapter, it was shown that a parity dependent potential is required for this system, since the elastic angular distribution possesses the "anomalous large angle scattering cross sections" (ALAS). The parity dependent potential is to make the barrier heights of two successive ℓ the same, as was shown in fig 2.8. The choice of which barriers should be depressed and which are to be raised can be deduced from the experimental spin assignment of the system.

Experimental spin assignment of the system for elastic scattering was made by Charles et al [Cha 76] and Malmin et al [Mal 72] and for

the fusion reaction by Frohlich et al [Fro 78]. In these assignments, the positions of $J^{\pi} = 7^{-}$, 9^{-}, 11^{-} and 13^{-} were shown to correspond to the positions where peaks of the fusion oscillations occur. The intermediate even J^{π} states are absent except for the 14^{+} state which was observed at ≃2 MeV from the position of the 13^{-} state. The even states of J^{π} were missing because they occur approximately at the same energies as the odd states of J^{π}. On the other hand, the 14^{+} state was observed separately because the parity dependence is small compared with the difference of the barrier heights for successive large values of ℓ. This suggests that the parity dependent potential should be constant or should not vary significantly from one set of partial waves to another. The presence of the 14^{+} state near the 13^{-} state signifies that the parity dependent potential has raised the barrier height of $\ell = 13$ and has depressed that of $\ell = 14$. Thus α in eq. (3.5) is a positive quantity, so the odd partial waves are raised and the even ones are depressed. The sign of α from this deduction is consistent with the work of Baye [Bay 86]. A negative α will produce oscillations, but out of phase with the experimental data. This will be shown in the subsequent figures.

The exact magnitude of α can be deduced either from a minimisation of χ^2 or by comparing the average σ_f (where there is no oscillation, i.e. α=0) with the experimental data. The comparison should reveal roughly the position where the difference between the average σ_f and the data is maximum. This point corresponds to approximately the position where two partial waves have exactly the same barrier heights, thus we can deduce the value of ΔV (in fig 2.8) and the magnitude of α. On comparison, we observed that the difference in the two cross sections is maximum at the position where $J^{\pi} = 7^{-}$ state occurs. Therefore, the initial value of α was chosen so that the barrier

heights of $\ell = 7$ and $\ell = 8$ are approximately the same, i.e. $T_7 \simeq T_8$. When we adopted the second option, i.e. minimising χ^2 with respect to α, we observed that whenever $\Delta\ell_g$ is odd oscillations are always obtained, but no oscillation when $\Delta\ell_g$ is even. In fact, we obtain a good fit to σ_f at higher energies with $\Delta\ell_g = 3$ [Kab 87d] (note that the sign of α is positive not as was quoted in the reference). This confirms that the shift in the barrier heights of the even and odd partial waves is important in restoring the oscillatory nature of σ_f.

Following these procedures, we obtained a good fit to σ_f for energies greater that 12 MeV but the lower-energy fusion cross sections were over estimated. By reducing the range r_r of the real potential, we reproduced the low energy σ_f. However, the higher energy σ_f were then greatly under estimated. We observed that the difference between the two radii required to fit σ_f in the higher and lower energy ranges decreases with decreasing values of a_r, but then of course the oscillatory structure is damped down because of large Δ. In fig. 3.2 we show the fits to σ_f for two different potentials, so as to illustrate these effects. The potential parameters we used are given in table 3.2. The first potential we used to calculate σ_f (fig. 3.2a) has a large a_r, and the second (fig. 3.2b) has a smaller a_r. The figure shows that the oscillatory structures in σ_f are reproduced satisfactorily at higher energies using the first potential (i.e. the solid curve in fig. 3.2a). However, the difference between the higher and the lower energy σ_f fits (the solid and dashed curves in fig. 3.2a) is large compared to the fits in fig. 3.2b. Thus, we can effectively make the two curves the same by decreasing a_r (as in fig. 3.2b), but as a_r decreases the fit to the higher energy data deteriorates.

The potential that fits the low energy cross sections underestimates σ_f at the higher energies because the grazing angular momentum

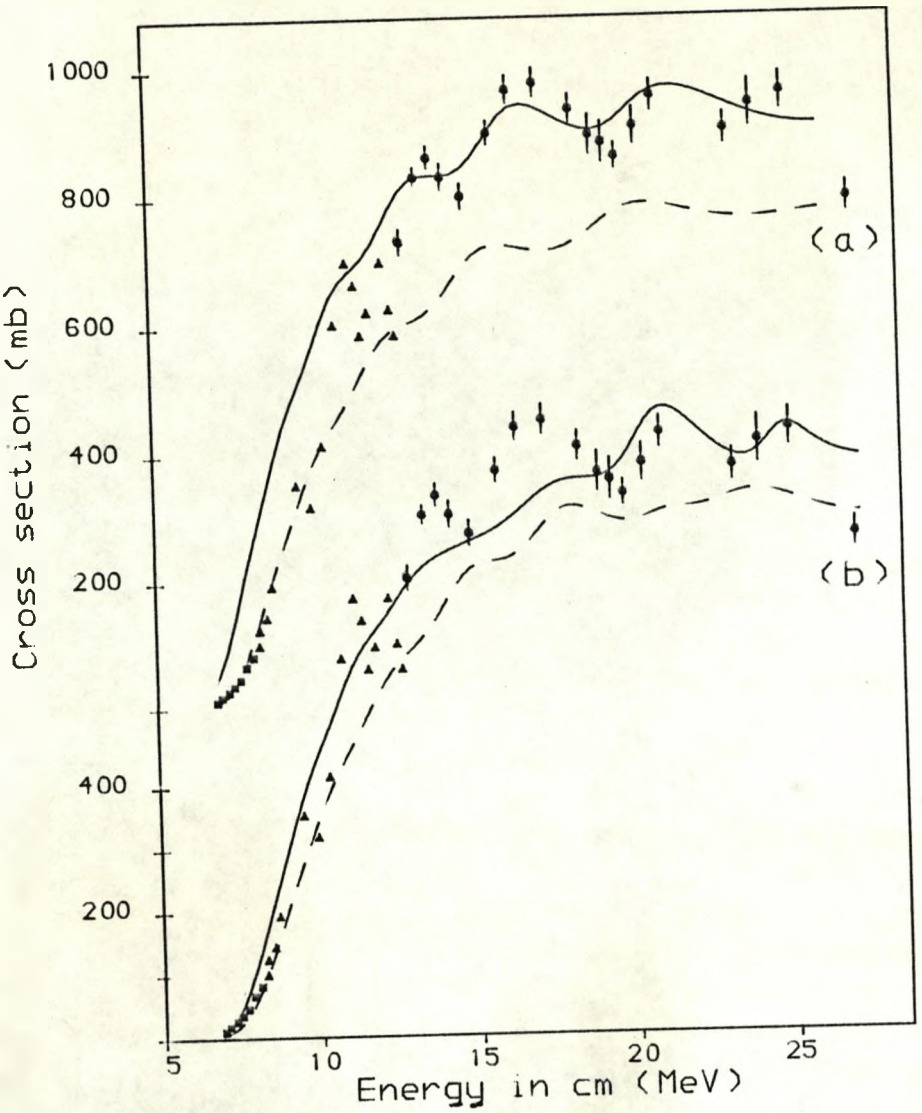

Fig. 3.2 Fusion cross section for $^{12}C + ^{16}O$ system. (a) Full curve represent the fit using potential I and the broken curve using potential II. (b) Same as (a) but using potentials III and IV respectively. The potential parameters are given in table 3.2. Experimental data were obtained from: ● (dot) [Spe 76], ▲ (solid triangle) [Fro 76] and ■ (solid square) [Pat 71].

TABLE 3.2

The potential parameters used in figure above. The Coulomb radius is $r_c = 1.4$ fm.

Potential	V_0 (MeV)	r_r (fm)	a_r (fm)	W_0 (MeV)	r_i (fm)	a_i (fm)	α
I	81.84	0.69	1.20	54.27	0.46	0.66	0.16
II	81.84	0.57	1.20	54.27	0.46	0.66	0.16
III	64.80	0.87	0.96	26.60	0.40	0.78	0.18
IV	64.80	0.81	0.96	26.60	0.40	0.78	0.18

it yields is too small for higher incident energy, i.e. the barrier heights for the higher ℓ were not correctly obtained. The "high energy" potential overestimates the low energy cross sections because it adds more than the required number of partial waves. That is, the barrier heights obtained with this potential for $\ell \leq 6$, should be higher. For the other partial waves i.e. $\ell > 6$ the correct heights of the barriers, and thus the correct fusion cross sections were obtained.

The difference in the radii suggests that either the fusion cross section may be affected by coupling to channels other than the elastic transfer channel or that there are details of the shape of the nuclear potential that are not adequately described by a Woods-Saxon form factor when large values of a_r are used. In the next section we shall investigate the effect of coupling to an additional channel.

3.2.1 COUPLING TO AN INELASTIC CHANNEL

To see the effect of another channel in the calculations of σ_f, we couple the reaction to a fictitious 0^+ inelastic channel and solve the problem by using the "adiabatic" approximation of Nagarajan et al [Nag 86]. Where the excitation energy of the inelastic channel is assumed to be approximately equal to zero. We assume that the coupling potential between the elastic and the transfer channel is V_{12} and the coupling potential between the elastic and the inelastic channel is the same as the coupling potential between the transfer and the inelastic channels, represented by V_{23}. The Schrodinger equation for this process at energy E becomes

$$\begin{pmatrix} K_\ell & 0 & 0 \\ 0 & K_\ell & 0 \\ 0 & 0 & K_\ell \end{pmatrix} \begin{pmatrix} \chi_1 \\ \chi_2 \\ \chi_3 \end{pmatrix} = \begin{pmatrix} 0 & V_{12} & V_{23} \\ V_{12} & 0 & V_{23} \\ V_{23} & V_{23} & 0 \end{pmatrix} \begin{pmatrix} \chi_1 \\ \chi_2 \\ \chi_3 \end{pmatrix}$$

where $K_\ell = \hbar^2/2\mu[d^2/dr^2 - \ell(\ell+1)/r^2] - V + E$, and V is the central potential. The direct elastic wave function is χ_1, the transfer wave function is χ_2 and χ_3 is the inelastic wave function. Writing in a compact form we have,

$$D\chi = V_{cc}\chi$$

where D is the diagonal 3x3 matrix containing K_ℓ and V_{cc} is the 3x3 matrix containing the coupling potentials. We can follow the formulation similar to that of Lindsay and Rowley [Lin 84] (and also sect. 2.1.3), by making a unitary transformation that decouples the three equations into "elastic" form, i.e.

$$ADA^+ A\chi = AV_{cc} A^+ A\chi.$$

where A is a unitary matrix. Defining the coupling matrix as

$$\tilde{V}_{cc} = AV_{cc} A^+$$

where $\tilde{V}_{cc}$ is diagonal with λ_i as the elements. We obtain

$$\lambda_1 = -V_{12} \qquad \lambda_2, \lambda_3 = \tfrac{1}{2}[1 \pm (1 + 8\beta^2)^{\frac{1}{2}}]V_{12}$$

where $\beta = V_{23}/V_{12}$. These are clearly independent of the sign of β, changes in the sign of β will only affect the wave functions. The decoupled "elastic" equations become

$$[K_\ell - \lambda_i(r)]\phi_i = 0, \qquad i=1,2,3$$

where ϕ is the decoupled wave function obtained from $\chi = A^+\Lambda\phi$ with $\Lambda_{ij} = \delta_{ij} A_{il}$. When the above equation is solved, three S-matrices $\tilde{S}_i$ are obtained, which form a vector $\tilde{S}$. The coupled vector S (matrix) is obtained from

$$S = A^+\Lambda \tilde{S}.$$

The elastic and inelastic scattering matrices are $S_{el} = S_1 + (-1)^\ell S_2$ and $S_{inel} = S_3$ respectively. The fusion cross section is the difference between the reaction and inelastic cross sections,

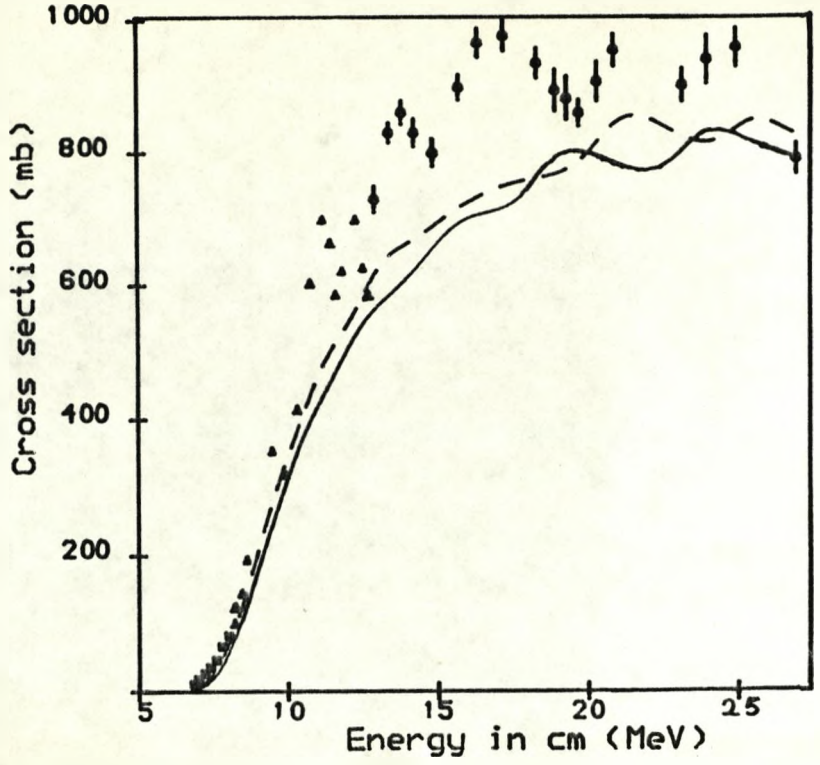

Fig. 3.3 Fusion cross section for $^{12}C + ^{16}O$ system. Full curve represents the fusion cross section when the reaction is coupled to an inelastic channel (see text). Broken curve represents the fit without the coupling. The potential parameters are given in the table below. Experimental data points are the same as those in fig. 3.2.

TABLE 3.3

Potential parameters used in the figure above. Here $\beta^{-1} = V_{12}/V_{23}$, assuming V_{23} has the same form factor as V_{12}. Where V_{12} the exchange potential (= $V_{\pi}(r)$).

	V (MeV)	r (fm)	a(fm)
Real	61.80	0.81	0.92
Imaginary	26.60	0.40	0.78
r_c = 1.4 fm	α = 0.183		β = 0.4

$$\sigma_f = \sigma_{rxn} - \sigma_{inel}$$

$$= (\pi/k^2)\sum_{\ell=0}^{\infty}(2\ell + 1)[1 - |S_{el}|^2 - |S_{inel}|^2].$$

When we modified the program to take these formulations into account, we observed that for whatever values of β we take the fusion cross section is not enhanced at higher energies. Rather, the oscillations are simply shifted. However, the reaction cross section was enhanced. In fig. 3.3 we show the results of our calculations. The potential parameters are given in table 3.3. We assumed that V_{23} has the same form factor as V_{12}.

Therefore, we conclude that the coupling to an inelastic channel is not capable of solving the problem of two potentials fitting two segments of the fusion cross section data. We can now look at the other possibility, i.e. the Woods-Saxon form factor does not adequately describe the nuclear potential.

3.2.2 THE WOODS-SAXON FORM FACTOR.

To obtain a good description of the real nuclear potential, we can either modify the Woods-Saxon potential or choose entirely a new form factor. When we modified the Woods-Saxon potential in such a way that it reproduced the correct values of the two previous potentials in the appropriate regions, we obtained a good fit to both the low and high energy fusion cross sections. The potential was chosen by using the sum of two Woods-Saxon terms such that the first term is similar to the "lower energy" potential. The other term, a relatively weak one, was chosen such that it is non-zero in the region where the "higher energy" potential barrier occurs for $\ell>6$ but is negligible at large values of r. This term was added to the "lower energy" potential so that the barrier heights produced by the sum of the two Woods-Saxon

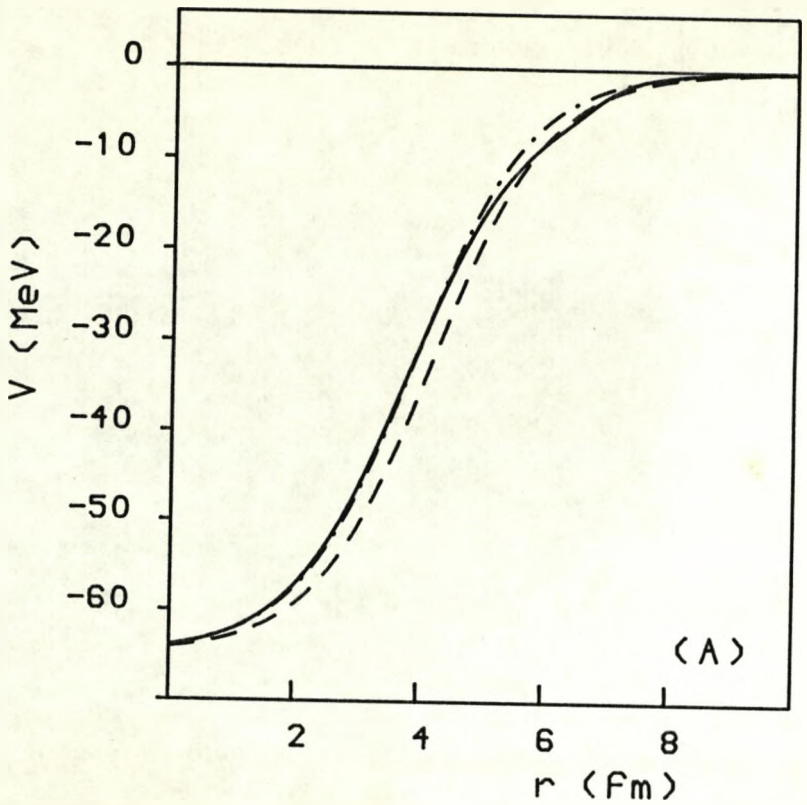

Fig. 3.4 The radial dependence of the real nuclear potentials that fit: (i) the lower energy region of the fusion cross section (←•— • —•→), potential I. (ii) the higher energy region of the fusion cross section (← — — — →), potential II. (iii) the average σ_f over the whole range of energies we considered, potential III (————). Potential III is the sum of III (a) and (b). See table 3.4 for the parameter values.

TABLE 3.4

The potential parameters used in figs. 3.4, 3.5 and 3.6. The Coulomb radius is r_c = 1.4 fm.

Potential	V_0 (MeV)	r_r (fm)	a_r (fm)	W_0 (MeV)	r_i (fm)	a_i (fm)	α
I	64.80	0.81	0.96	26.60	0.40	0.78	0.18
II	64.80	0.87	0.96	26.60	0.40	0.78	0.18
III (a)	61.80	0.79	0.92	26.60	0.40	0.78	0.18
(b)	3.15	1.41	0.28				
IV (a)	61.80	0.79	0.92	66.60	0.80	0.88	0.18
(b)	3.15	1.41	0.92				

terms for $\ell>6$ are approximately the heights produced by the "higher energy" potential, but the barrier heights for $\ell\leq 6$ are the same as those produced by the "lower energy" potential. In fig. 3.4, we show the radial dependence of the form factors and also the new "interpolated" form factor. A slight modification to the "lower energy" potential was made so that it does not become deeper in the interior when the shallow Woods-Saxon term is added. In table 3.4 the values of the parameters for the form factors used are given.

Using the new potential we calculated the fusion cross section at all energies. Fig 3.5a shows the results of our calculations. Clearly the fusion excitation function is well reproduced at all energies, thus the mechanisms we have discussed are capable of producing the gross structure in qualitative agreement with the magnitude and phase of the experimental oscillations. In fig 3.5b shows a comparison of the cross sections using the correct sign of α (positive) and the wrong sign of α (negative). The fit with a negative α, is clearly out of phase with the experimental data and the calculated σ_f.

Note that we have used the same imaginary potential W(r) in each of the fits (see table 3.4). As suggested earlier, W(r) is not sensitive to the fit provided it is confined to the interior of the real potential. Though we noticed that at higher energies (>25 MeV) σ_f is sensitive to W(r). This is because at those energies the barrier heights of the grazing partial waves occur in the region where the imaginary potential is significantly large. Hence, some flux may be absorbed even before the barrier is encountered.

To conclude this section, we have shown that the oscillatory structure in σ_f are qualitatively reproduced using an optical model potential that also accounts for elastic α-particle transfer between the two carbon cores. Without taking account of the transfer process, the

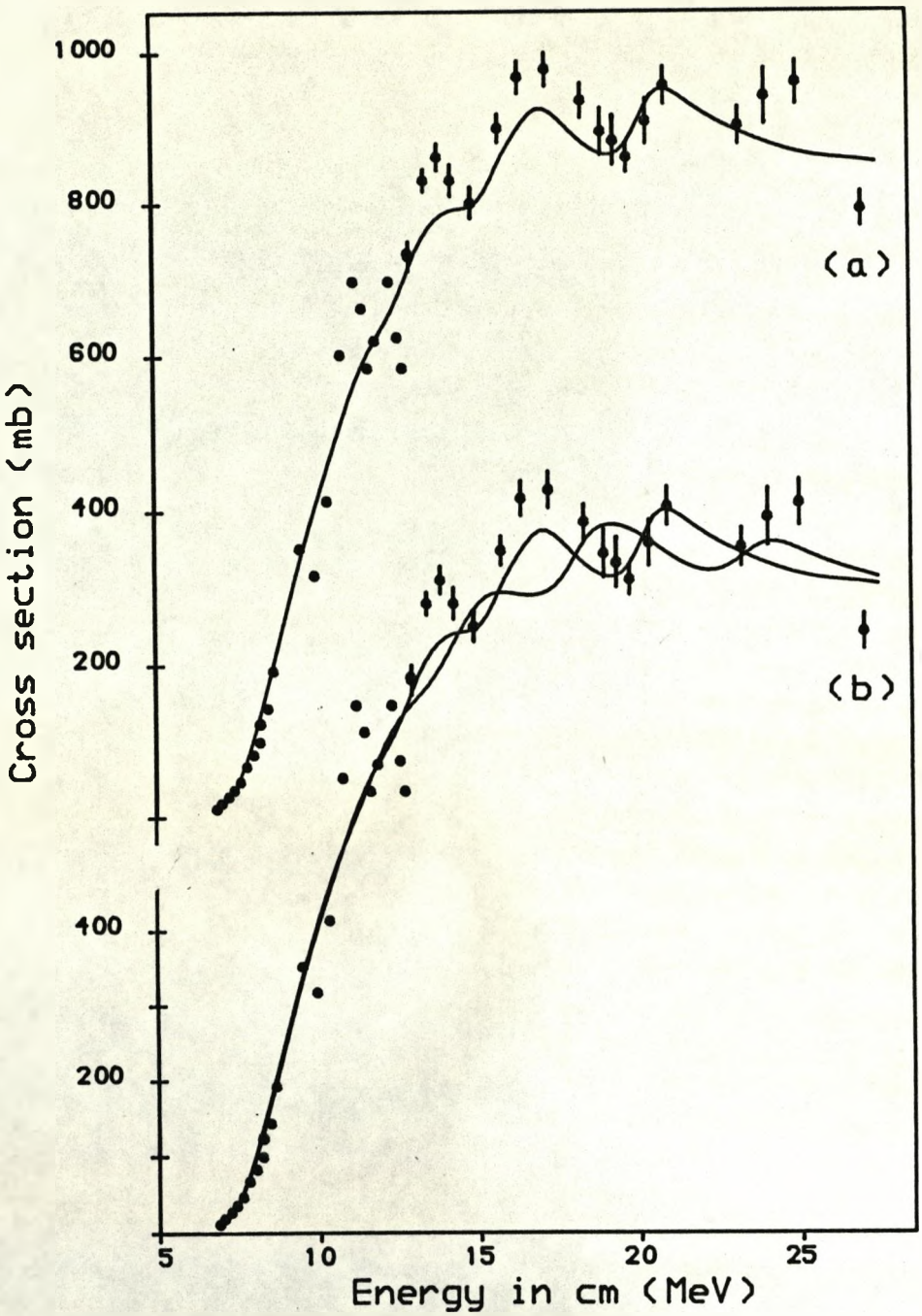

Fig. 3.5. The fit to the fusion cross section of ^{12}C on ^{16}O. (a) Using the modified Wood Saxon potential (potential III of table 3.4). (b) A comparison with the fit when α has the opposite sign. Experimental data are the same as those in fig 3.2.

oscillatory structure in the cross section can not be obtained. A modified Woods-Saxon potential was used and a good fit to the whole energy range was obtained, as shown in fig 3.5a. Even though the peak at E > 25 MeV was not reproduced, we have reproduced all the peaks at E < 25 MeV and also the correct values of σ_f near the Coulomb barrier were obtained. At E > 25 MeV, the general trend of σ_f is in agreement with the experimental data, i.e. decreasing. Like in the $^{12}C + ^{12}C$ system, the potential we used here does not yield the correct barrier heights at those energies, but the correct ℓ_{cr} was obtained. At those energies, either the potential does not give a satisfactory description of the nuclear potential or there are other direct processes taking place.

3.2.3 THE ELASTIC SCATTERING

In the previous section, the fusion cross section was reproduced using a parity dependent potential which is similar to the one used in calculating the elastic scattering cross sections of the system [Gut 73]. Udagawa et al [Uda 85] suggested that the elastic and the fusion cross section can be reproduced using the same real potential but with a different W(r). In this section we shall calculate the elastic scattering cross sections for $^{12}C + ^{16}O$ system using the same real potential that reproduced σ_f.

Using the parameters of potential III in table 3.4, we calculated the angular distribution of the system at three energies: 10.29 MeV, 17.28 MeV and 18.0 MeV. The fits to the angular distributions are shown in fig. 3.6. From the figure, it is noticeable that at 10.29 MeV the angular distribution is well reproduced at the forward angle cross sections, while at 17.28 MeV and 18.0 MeV the large angle cross sections are in good agreement with the data. However, the fit to the

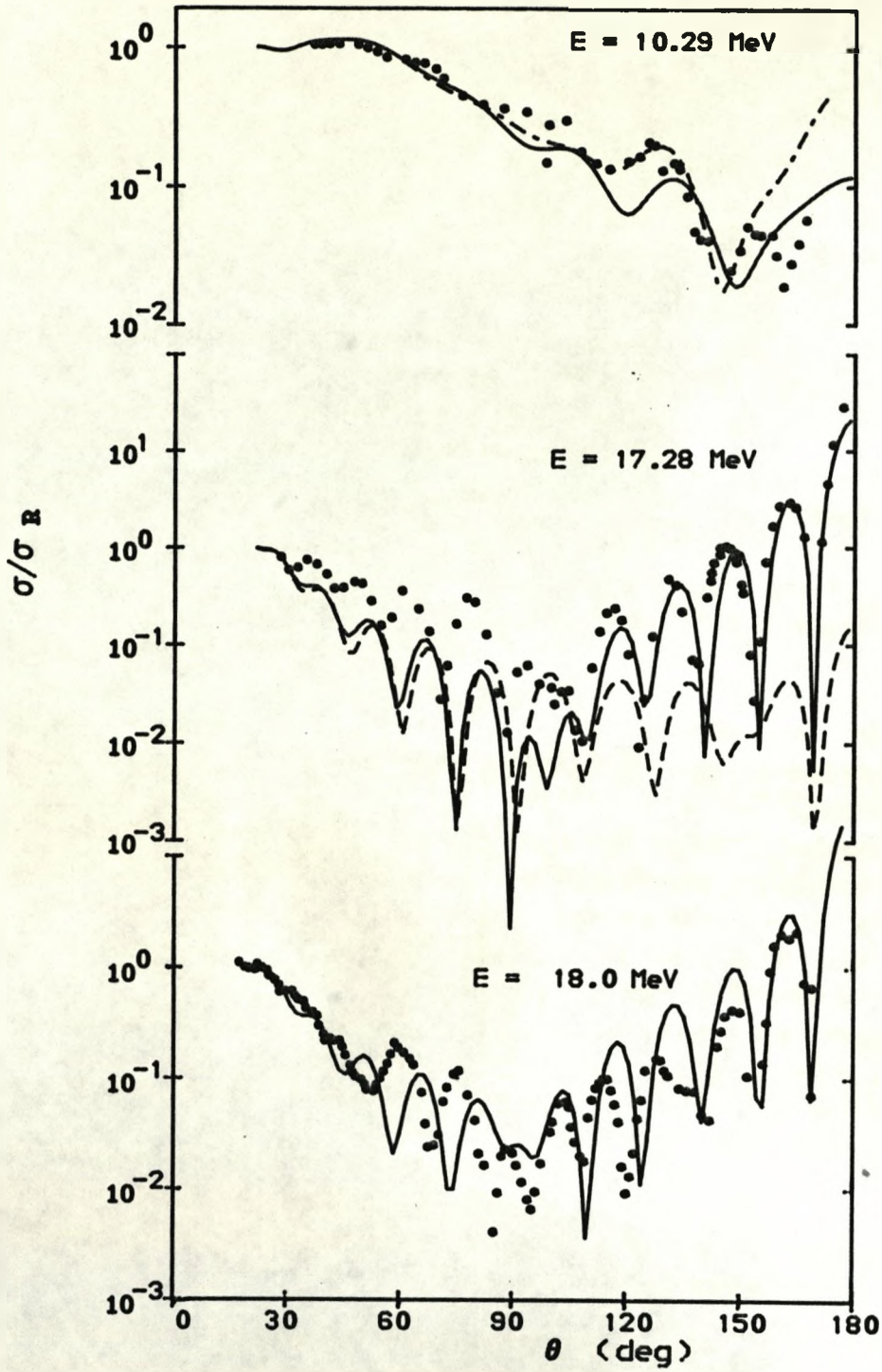

Fig. 3.6. Fits to the elastic scattering cross sections of ^{16}O on ^{12}C at different centre of mass energies, using potential III of table 3.4. The solid curve represents the fit when the parity dependent potential is included. The broken curve at 10.29 MeV shows the fit using a different imaginary potential; potential IV of table 3.4. The broken curve at 17.28 MeV shows the fit without the parity dependent potential. Data were obtained from: Gutbrod et al [Gut 73] for E = 10.29 MeV and E = 18.0 MeV, Charles et al [Cha 76] for E = 17.28 MeV.

forward angle cross sections at 17.28 MeV and 18.0 MeV are not in close agreement with the data. Since the imaginary potential required for the elastic scattering is usually larger than that needed for the fusion, then we may improve the fit by increasing W(r). When we increased W(r), we obtained a good fit at the large angles for 10.29 MeV data. The dashed curve at 10.29 MeV fit in fig 3.6 represents the improved fit and the values of the potential parameters are given in table 3.4 (potential IV). However, the forward angle cross sections at the other two energies were not significantly improved.

To understand the physical phenomena taking place in the angular distribution, in general for systems like $^{12}C + {}^{16}O$, we can divide the elastic scattering cross section roughly into three angular regions: 0° to 60°, 60° to 120° and 120° to 180° with each region exhibiting a different physical process.

In the first region, the dominant structure is the direct elastic scattering, and the cross section is approximately proportional to $s(\ell_g) = |\sum_{\ell=0}^{\ell_g}(2\ell + 1)P_\ell(\cos\theta)|^2$ for a sharp cut-off in S_ℓ. At a particular energy, $s(\ell_g)$ is usually not in phase with $s(\ell_g \pm 1)$ for $0 \geq\theta \geq 60^\circ$. Thus whenever the experimental ℓ_g (determined from the "quarter point recipe") is different from the theoretical grazing ℓ, then the two cross sections will not be phase. For example, at 17.28 MeV, $\ell_g = 11$ experimentally [Cha 76] but theoretically $\ell = 11$ grazes at 15.63 MeV and $\ell = 12$ at 16.46 MeV (see table 3.5), that is why the experimental data is not in phase with our calculations. However, at E = 18.00 MeV, the two cross sections are reasonably in phase with each other, in this region, because from theory $\ell = 12$ is still grazing and experimentally $\ell = 12$ is the most likely partial wave that would graze. Therefore, if the two cross sections are not in

phase, the only parameters that would bring them in phase are those that change the barrier heights.

Table 3.5 Grazing energies obtained from experiment and theory (using potential III in table 3.4).

Partial wave (J^{π})	Grazing energy (MeV)	
	Theory	Experiment
9	13.12	13.75 [Mal 72]
10	13.76	
11	15.63	17.29 [Cha 76]
12	16.46	
13	22.06	20.79 [Cha 76]

For $120^0 \leq \theta \leq 180^0$, the scattering is because of the elastic exchange and the parameters responsible for this are essentially those in $V_{\pi}(r)$. If the parity dependent potential is switched off (i.e. $\alpha = 0$), then the experimental cross sections are not reproduced (see the dashed line at E = 17.28 MeV in fig. 3.6). At low energies, for example at 10.28 MeV, the scattering cross section is over estimated because $V_{\pi}(r)$ is energy independent and it was determined at higher energies. However, at higher energies, with the right choice of $V_{\pi}(r)$, the "anomalous larger angle scattering cross section" (ALAS) can easily be reproduced. The W(r) in this region is important because it can easily suppress the physical significance of $V_{\pi}(r)$.

The region $60^0 \leq \theta \leq 120^0$ is where the two decomposed amplitudes $f(\theta)$ and $f(\pi-\theta)$ interfere strongly. The magnitude of the cross section is dependent on the way the amplitudes interfere. For example at $\theta=90^0$ it was observed that there is always a maximum in the cross section whenever a particle is exchanged, but a minimum is obtained whenever a hole is been exchanged. Therefore, the fit to the cross sections in this region depends on how the fits in the two other re-

gions are reproduced. For example at 17.28 MeV and 18.00 MeV, since the large angle cross sections are reproduced, the cross sections for $90^0 \leq \theta \leq 120^0$ are reasonably good. But for $60^0 \leq \theta \leq 90^0$, this is not so because the forward angle cross sections were not well reproduced.

To sum up, the fits at these energies clearly illustrate some important features of the elastic scattering process. However, the most important thing in this fit, is that the correct magnitude of the large-angle scattering cross section was obtained using the same potential that reproduced the oscillatory structures in σ_f.

3.2.4 SCATTERING AT LARGE ANGLES

In the previous section we have shown that the ALAS was qualitatively reproduced at energies above the Coulomb barrier even though at some energies the fit to the forward angle cross sections were not in close agreement with the data. As was pointed out, the potential we used is energy independent containing $V_\pi(r)$, and the transfer process was reproduced because of this potential. This seems to suggest that transfer is more or less energy independent. In particular, we observe that at angles near π the cross section is constant over a wide range of energies.

In this section we want to make an analytical proof of these deductions. We shall do this by expanding the amplitude in terms of the SCO Coulomb amplitudes (this was introduced in the previous chapter) and investigate the energy dependence of the amplitude. A detailed discussion of the scattering amplitude in terms of the SCO Coulomb amplitudes is given in the paper [Row 80], we shall use the results of this reference to derive our observations.

The scattering amplitude in terms of the SCO Coulomb amplitudes $\tilde{f}_\ell(\theta)$ is (see chap. 2)

$$f(\theta) = \sum_{\ell=0}^{\infty} (S_\ell - S_{\ell-1}) \tilde{f}_\ell(\theta). \tag{3.6}$$

For a sharp cut-off in the nuclear scattering matrix S_ℓ, the above expression allows the effective ℓ-window created to be seen. Therefore, the summation above is made over the region where $\ell \simeq \ell_g$. Decomposing the scattering matrix into the direct (D) and exchange (E) matrices as

$$S_\ell = S^D{}_\ell + (-1)^\ell S^E{}_\ell,$$

the scattering amplitude becomes,

$$f(\theta) = \sum_{\ell=0}^{\infty} [(S^D{}_\ell - S^D{}_{\ell-1}) + (-1)^\ell (S^E{}_\ell + S^E{}_{\ell-1})] \tilde{f}_\ell(\theta). \tag{3.7}$$

For angles near π, a good approximation to $\tilde{f}_\ell(\theta)$ was given by Frahn and Venter [Fra 63] as

$$\tilde{f}_\ell(\theta) \simeq \frac{(-1)^\ell \ell}{2ik\cos\frac{1}{2}\Theta(\ell)} \left(\frac{\pi-\theta}{\sin(\pi-\theta)}\right)^{1/2} \exp(2i\sigma_\ell)\, J_o[\ell(\pi-\theta)] \tag{3.8}$$

where $\Theta(\ell) = 2\tan^{-1}(\eta/\ell)$ is the classical Coulomb deflection function. For energies sufficiently high above the barrier, the cut-off in S_ℓ is quite sharp and only a few ℓ-values around the grazing partial wave ℓ_g contribute to the summation in eq. (3.7). In this region $\Theta(\ell)$ is quite small and $\sigma_\ell \simeq \sigma_{\ell_g}$. Therefore, we can approximate $\tilde{f}_\ell(\theta)$ as

$$\tilde{f}_\ell(\theta) \simeq (-1)^{\ell-\ell_g} \left[\frac{(-1)^{\ell_g} \ell_g}{2ik} \left(\frac{\pi-\theta}{\sin(\pi-\theta)}\right)^{1/2} \exp(2i\sigma_{\ell_g})\, J_o[\ell_g(\pi-\theta)]\right]$$

$$\simeq (-1)^{\ell-\ell_g} \tilde{f}_{\ell_g}(\theta). \tag{3.9}$$

Substituting the above expression into eq. (3.7) we obtain

$$f(\theta) \simeq \tilde{f}_{\ell_g}(\theta) \sum_{\ell=0}^{\infty} (-1)^{\ell-\ell_g} [(S^D{}_\ell - S^D{}_{\ell-1}) + (-1)^\ell (S^E{}_\ell + S^E{}_{\ell-1})]. \tag{3.10}$$

Note that we have factored $\tilde{f}^{g}_{\ell}(\theta)$ out of the summation since it is now constant. The phase $(-1)^{\ell}$ in the above expression causes the direct contribution $(S^{D}_{\ell} - S^{D}_{\ell-1})$ to the sum to be small and the scattering amplitude becomes

$$f_{\ell}(\theta) \simeq (-1)^{\ell} \tilde{f}^{g}_{\ell}(\theta) \sum_{\ell=0}^{\infty} (S^{E}_{\ell} + S^{E}_{\ell-1}) \qquad (3.11)$$

That is, the exchange contribution is dominant at large angles. Since S^{E}_{ℓ} is constant for a sharp cut off in S_{ℓ}, the summation is independent of energy. The energy dependence in the above expression is in $\tilde{f}^{g}_{\ell}(\theta)$ only. Thus we do not expect any strong energy dependence of the scattering amplitude at large angles. This result is in full agreement with the results of our calculations in the previous sections.

3.3 THE $^{12}C + ^{24}Mg$ SYSTEM.

In this system, both the "anomalous large angle scattering cross section" in the elastic angular distribution and oscillatory structure in the fusion cross section have been observed [Dan 82]. However, the oscillations appeared only at E > 20MeV and they are not as pronounced as those in lighter system, like the $^{12}C + ^{16}O$ system.

We can use our model to explain the oscillations and also why they appear only at higher energies. As was discussed, to reproduce ALAS, we require a $(-1)^{\ell}$ factor in both the scattering amplitude and the effective interacting potential. This factor, in the interacting potential, causes a shift in the barrier heights of the odd-even partial waves, but the oscillations in the fusion excitation function will only appear if the difference in the shifted barrier heights is large enough (see eqs. (2.30) and (2.31)). For lower ℓ, the difference in the barrier heights is small, so the effect of shifting the barriers is not noticeable. Thus we do not expect any oscillations at lower energies.

However, at higher energies the difference between the barrier height of the grazing partial wave and the neighbouring ℓ is large enough for the oscillations to appear. That is why the oscillations were observed at higher energies.

To reproduce the oscillations for this system, the procedure used in the previous section can be applied here. Using an optical model potential containing a $V_{\pi}(r)$, we calculated the fusion excitation function. As expected, oscillations were obtained at higher energies. However, the calculated excitation function was not in agreement with the experimental data when an ordinary Woods-Saxon potential was used. Using a "Woods-Saxon squared" for both the real and imaginary potentials, a satisfactory fit to the data was obtained. The correct magnitude of the experimental cross section was obtained at all energies. This is shown in fig. 3.7. The values of the potential parameters used are given in table 3.6. In principle, the same potential can be used to reproduce the elastic scattering cross sections for this system. However, the experimental data available at the backward angles is not complete, therefore no fit to the elastic scattering data was made.

From the above analysis, we conclude that the mechanism responsible for the fusion oscillations in the $^{12}C + ^{16}O$ system is the same as that in $^{12}C + ^{24}Mg$ system, which is a slightly heavier system. The exchange particle (cluster) in this case is a ^{12}C nucleus. Therefore, in general, we can reproduce the oscillations in the fusion excitation function of any system that possesses ALAS in the elastic angular distribution. For example in $\alpha + ^{40}Ca$ system, discussed in the following section.

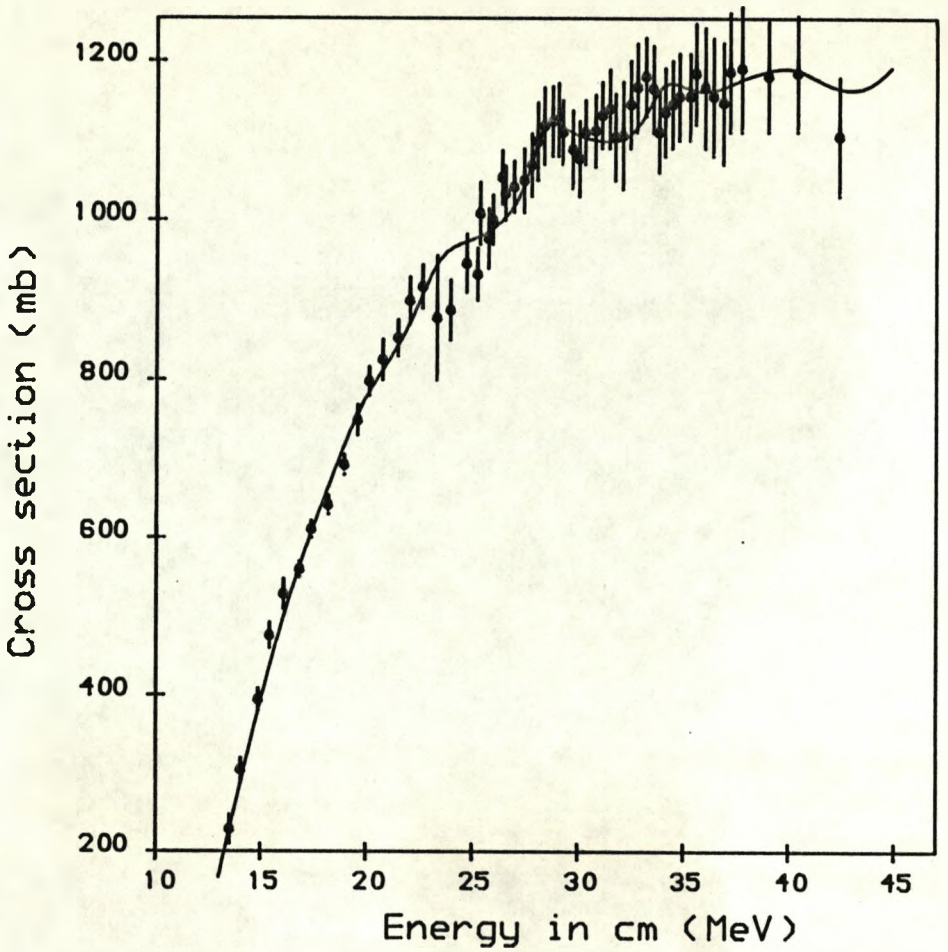

Fig. 3.7 The fit to the fusion cross section of $^{12}C + ^{26}Mg$ system. The potential parameters are given in the table below. Experimental data points are from [Dan 82].

TABLE 3.6

Optical model potential parameters used in figure above. The real and the imaginary form factors used to fit the data are not those in eq. (3.4) but

$$f(r,R_0,a_0) = [1 + \exp[(r-R_0)/2a_0]]^{-2}$$

	V (MeV)	r (fm)	a(fm)
Real	100.30	1.300	0.343
Imaginary	89.00	0.490	0.400
r_c =1.40 fm		α = 0.309	

3.4 THE $\alpha + {}^{40}Ca$ SYSTEM.

For the $\alpha + {}^{40}Ca$ system, the elastic angular distribution possesses the "anomalous large angle scattering cross sections" (ALAS) at energies above the Coulomb barrier [Eck 75]. The theoretical explanation to the ALAS was not in terms of the elastic exchange model, since the particle to be exchanged is heavier than the core, i.e. a ^{36}Ar between two α-cores. Rather, the process was explained in terms of the internal and barrier waves. In this scattering process, where it was shown that the α-particle has a small probability of penetrating the nuclear interior and leave out again in the elastic channel, the internal waves are important. It was further shown that, the internal waves are significant only with certain potentials, such as a weakly absorbing imaginary potential and a deep real potential (see Rowley et al [Row 80a] and the references therein). In this case, the internal waves could then be deflected at backward angles which explains the ALAS [Bri 77].

Experimental measurements of the fusion excitation function for this system also reveal oscillations in σ_f [Ebe 79]. Ohkubo and Brink [Ohk 87] have shown that the origin of these oscillations is due to the interference of the internal and barrier waves. They used a deep real potential to reproduce the oscillations in σ_f.

The mechanism responsible for the fusion oscillations in nonsymmetric system, like $^{12}C + {}^{16}O$ and $^{12}C + {}^{24}Mg$ systems, can not be the same mechanism responsible for the oscillations in this system. However, the same procedure, that was used in the two systems, can be applied to this system. That is, since the scattering matrix in this system exhibits the odd-even staggering effect in ℓ-space (see [Sat 83]), similar to that produced in the two systems above, the scattering matrix can be represented by a pseudo-sum of direct and exchange matri-

ces, which contains a $(-1)^{\ell}$ factor (the actual scattering matrix is the sum of the scattering matrices produced by the internal and barrier waves). Thus the potential will also be parity dependent. This potential would then shift the barrier heights of the odd-even partial waves and consequently produce oscillations in the fusion excitation function.

Using this procedure we calculated the fusion cross sections for the system. Fig. 3.8 shows the results of our calculations, using an optical model potential containing $V_{\pi}(r)$. The potential we used is a relatively weak one compared to the one required for the internal and barrier wave model. Initially, when fitting the data we experienced a problem similar to that encountered when fitting the fusion cross section of $^{12}C + ^{16}O$ system, where two potentials (that differ by the radii) fitting two different regions of the data. We solved this problem using a modified Woods-Saxon potential i.e., the sum of two Woods-Saxon terms (similar to the one used in $^{12}C + ^{16}O$). This potential gives a good fit to the data. The potential parameters are given in table 3.7.

To conclude this section, the $\alpha + ^{40}Ca$ system shows that the model on elastic exchange of particles can not be applied to every system that possesses ALAS. However, we can still use the same procedure to reproduce the fusion oscillations of systems that possess ALAS in the angular distribution. For this particular system, we can deduce that, in terms of the cross section they yield, the potential that allows the effect of the internal waves to be seen is analogous to a parity dependent potential.

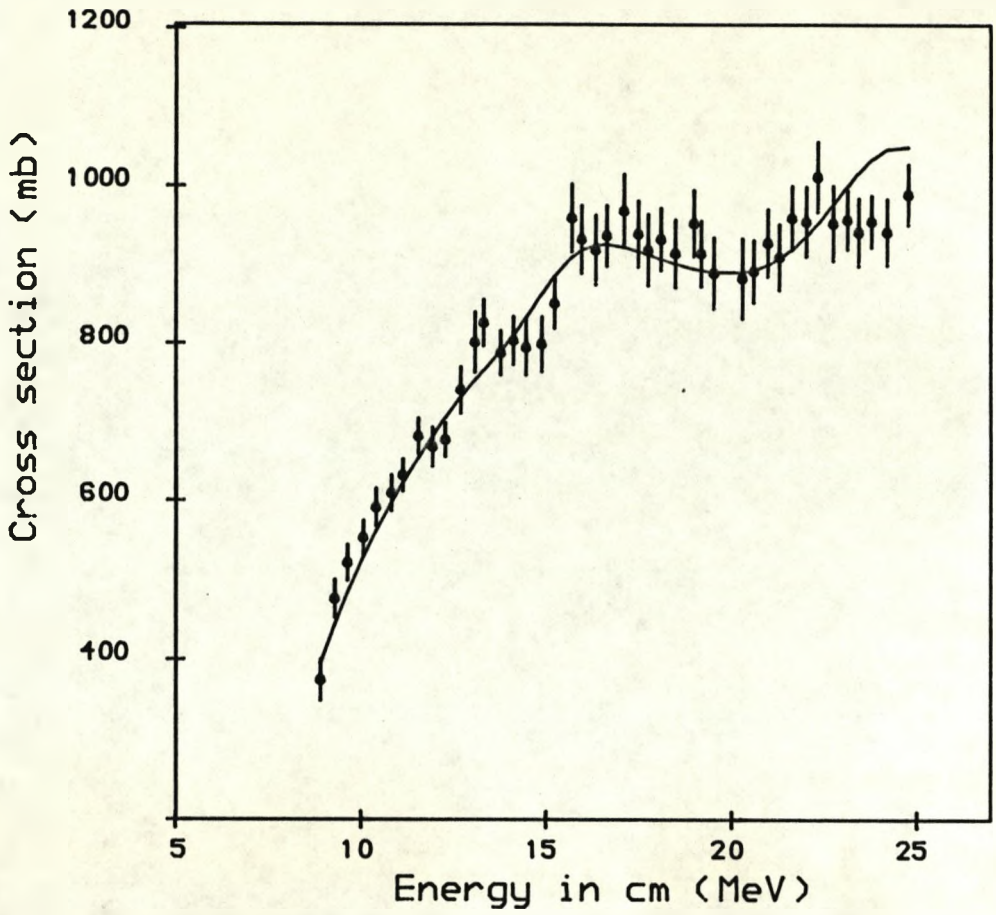

Fig. 3.8 The fit to the fusion cross section of $\alpha + {}^{40}Ca$ system. The potential parameters are given in the table below. Experimental data points are from [Ebe 79].

TABLE 3.7

Optical model potential parameters for the $\alpha + {}^{40}Ca$ system. The form factor used is the sum of two Woods-Saxon terms (similar to that used in the ${}^{12}C + {}^{16}O$ system).

	V (MeV)	r (fm)	a(fm)
Real I	39.51	0.855	0.860
Real II (added)	6.28	1.140	0.200
Imaginary	33.97	0.580	0.647
r_c =1.30 fm		α = -0.189	

3.5 CONCLUSION

We conclude this chapter with a discussion on the fusion cross section of other spinless systems. For the symmetric spin-zero bosons, experimental measurements have been made on almost all the light ions. Oscillations were observed in the lighter ions from $^{12}C + ^{12}C$ to $^{20}Ne + ^{20}Ne$ [Pof 83]. Systems with reduced mass greater than that of ^{20}Ne system possess no oscillations, for example in $^{24}Mg + ^{24}Mg$ [Jac 81] and $^{28}Si + ^{28}Si$ [Cen 81]. The explanation given by Poffe et al for the symmetric systems seems conclusive, except for cases where other direct processes are important. For example in $^{16}O + ^{16}O$, it was shown [Tan 80] that the 3^- inelastic state of ^{16}O is strongly coupled to the fusion reaction channel.

For the nonsymmetric spin-zero systems, apart from the effect of the reduced mass of the system, large angle scattering in the elastic channel is the other most important factor that determines the oscillations. That is, to reproduce the oscillations, we need to shift the barrier heights of the system so that at certain energies the system would look like the symmetric ones. This is achieved by adding a parity dependent potential that reproduces ALAS in the elastic scattering. Therefore, all the systems that possess oscillations in the fusion excitation function should also possess ALAS. However, some systems may possess ALAS but with no oscillations in σ_f. This is possible when either $\Delta\ell_g$ is even or the reduced mass of the system is large.

The reduced mass, on the other hand, is important because it determines where the oscillations should appear. For example, in systems with large μ, oscillations only may appear at higher energies and in most cases closely spaced. To illustrate the importance of the reduced mass, consider the fusion reaction of the ^{12}C on ^{24}Mg and ^{26}Mg systems [Dan 82] and also the reaction of the α on ^{40}Ca and ^{44}Ca systems

[Ebe 79]. In these examples, going from the lighter targets to the heavier ones results in a significant reduction in the number of peaks of the oscillations and the spacing between the peaks. The values of μ could also explain why there is no evidence of any oscillation in $^{16}O + ^{20}Ne$ and $^{16}O + ^{24}Mg$ systems [Tab 78], while oscillations appeared when the projectile is a ^{12}C (not ^{16}O) nuclei.

Therefore, we can generalise on which nonsymmetric system should possess oscillatory structure in the fusion excitation function. There are essentially two factors, namely: the ALAS in the angular distribution and a small reduced mass. Whenever these are satisfied, oscillations in σ_f are likely to appear.

CHAPTER 4

FUSION OF NUCLEI THAT POSSESS SPIN.

In this chapter, we explain the mechanism responsible for the oscillatory structure in the fusion excitation function of symmetric and nonsymmetric ions that possess spin. In some of these ions significant changes in the structure of the fusion cross section was observed for systems differing by one or two nucleons. For example, pronounced oscillatory structure was observed in the $^{12}C + ^{16}O$ system but the oscillations were absent in the $^{12}C + ^{17}O$ and $^{12}C + ^{15}N$ systems [Kov 79]. In some other systems, like the $^{12}C + ^{12}C$ and $^{12}C + ^{11}B$ systems pronounced oscillations were observed, but the magnitude of the oscillations was significantly different. However, the $^{12}C + ^{13}C$ system, which differs by one and two nucleons, very small structure (which could even be regarded as statistical) was observed.

For the symmetric ions, similar changes in the oscillatory structure can be seen. For example in the previous chapters, it was shown that for symmetric ions apart from the symmetrisation of the system the other most important factor that determines the oscillatory structure is the reduced mass of the system. Therefore, since pronounced oscillatory structure was observed in the $^{16}O + ^{16}O$ system, then one would expect oscillations in the $^{14}N + ^{14}N$ system. However, experimental measurements by DeYoung et al [DeY 82] reveal that there are no oscillations in the fusion excitation function of this system.

One of the differences of these systems is the spin they possess. Therefore, the model we presented in the two previous chapters can be used to explain the mechanism responsible for the oscillatory structure in the fusion excitation function of these systems, if the spin dependent forces are considered. We shall consider these forces for

three systems: the $^{14}N + {}^{14}N$, $^{11}B + {}^{12}C$ and $^{12}C + {}^{13}C$ systems, in this chapter.

4.1 SYMMETRIC SYSTEMS

The elastic scattering amplitude of two identical ions, that possess spin, is similar to that given in eq. (2.4) for spinless particles. However, we must take account of the projections of the spins when writing the scattering amplitudes. Consider the elastic scattering of two identical ions that possess spin I. Let the projectile spin projection before and after scattering be M_1 and M_1' respectively. Suppose the target spin projection is M_2 before scattering and M_2' after scattering. Then the scattering amplitude can be written as [Sat 83]

$$f_{M_1M_2\to M_1'M_2'}(\theta,\phi) = \frac{1}{2ik}\sum \langle I\ I\ M_1\ M_2|S\ M\rangle\langle L\ S\ 0\ M|J\ M\rangle$$
$$\langle I\ I\ M_1'\ M_2'|S'\ M'\rangle\langle L'\ S'\ M-M'\ M'|J\ M\rangle\ (2L+1)^{\frac{1}{2}}$$
$$\exp[i(\sigma_L+\sigma_{L'})]\ (S^J_{LSL'S'} - \delta_{LL'}\delta_{SS'})\ Y^{M-M'}_{L'}(\theta,\phi) \quad (4.1)$$

where the summation is over L, L', S, S' and J. Here it is assumed that the incident beam direction is along the z-axis and M, M' are the z-projection of S and S'. The couplings

$$\underline{S} = \underline{I} + \underline{I} \quad \text{and} \quad \underline{J} = \underline{L} + \underline{S}. \quad (4.2)$$

were used. The primes on S, L and M indicate the corresponding quantum numbers after scattering. Note that J has no prime because it is conserved.

For symmetric ions, the scattering amplitude is the sum of amplitudes (see fig. 2.1), one dominant at the forward angles and the other important at the backward angles. The forward angle scattering amplitude is the same as the above expression. The other component of the scattering amplitude, i.e. at backward angles $(\pi-\theta,\phi+\pi)$, is similar to the forward angle scattering amplitude but now the projectile and

the target spin projections after scattering are M_2' and M_1' respectively. The scattering amplitude is the same as eq. (4.1) but with M_1' and M_2' interchanged. Therefore, the symmetric scattering amplitude is

$$f^{sym}_{M_1M_2\ M_1'M_2'}(\theta,\phi) = f_{M_1M_2\to M_1'M_2'}(\theta,\phi) + (-1)^{2I} f_{M_1M_2\to M_2'M_1'}(\pi-\theta,\phi+\pi)$$

where the phase $(-1)^{2I}$ differentiates between bosons and fermions. The symmetric relations of the Clebsch-Gordan coefficients give,

$$\langle I\ I\ M_2'\ M_1' | S'M' \rangle = (-1)^{2I+S'} \langle I\ I\ M_1'\ M_2' | S'M' \rangle, \tag{4.3}$$

and $Y^M_{L'}(\pi-\theta,\phi+\pi) = (-1)^{L'} Y^M_{L'}(\theta,\phi)$. Thus the scattering amplitude becomes

$$f^{sym}_{M_1M_2\ M_1'M_2'}(\theta,\phi) = \frac{1}{2ik} \sum [1 + (-1)^{L'+S'}]\ A^J_{LSL'\ S'}\ Y^{M-M'}_{L'}(\theta,\phi) \tag{4.4}$$

where $A^J_{LSL'\ S'}$ are the Clebsch-Gordan coefficients and the constants in eq. (4.1). The effective scattering matrix is

$$S = [1 + (-1)^{L'+S'}]\ S^J_{LSL'\ S'}. \tag{4.5}$$

Thus only the even $(L' + S')$ in the outgoing channel can contribute to the scattering amplitude. Since J and the parity $(-1)^{L'}$ are conserved, $(L + S)$ in the entrance channel will also be even. Therefore, $(L' + L)$ and $(S' + S)$ are even.

If the imaginary potential is confined inside the potential barrier, so that it allows the absorption of the fused flux only, then the fusion cross section is the reaction cross section. Thus the fusion cross section is

$$\sigma_f = \frac{\pi}{k^2} \frac{1}{(2I+1)^2} \sum_{JLS} (2J+1)\ [1 + (-1)^{L+S}]\ T^J_{LS}, \tag{4.6}$$

where $T^J_{LS} = 1 - \sum_{L'S'} |S^J_{LSL'\ S'}|^2$ is the transmission coefficient of the flux in the state (LSJ). If the transmission coefficient is independent of J and S (i.e. $T^J_{LS} \equiv T_L$), then we can factor T_L out of the

summations over S and J in the above equation. The summation of (2J + 1) over J is (2L + 1)(2S + 1), since $|L-S| \leq J \leq L+S$. Eq. (4.6) becomes

$$\sigma_f = \frac{\pi}{k^2} \frac{1}{(2I+1)^2} \sum_{LS} [1 + (-1)^{L+S}] (2L+1)(2S+1) T_L.$$

The summation over S can now be made with S =0,1,2,....,2I, we have

$$\sigma_f = \frac{\pi}{k^2} \sum_{L} \left[1 + \frac{(-1)^{2I+L}}{(2I+1)}\right](2L+1) T_L. \qquad (4.7)$$

The above expression means that the odd and even L are not added equally for I ≠0. For example when I=½ (eg $^{13}C + ^{13}C$) the ratio is 1 to 3, i.e.

$$\sigma_f = (\pi/k^2)[\ \tfrac{1}{2} \sum_{L\,even} (2L+1)T_L + \tfrac{3}{2} \sum_{L\,odd} (2L+1)T_L], \qquad (4.8)$$

while for systems with I=1 (like $^{14}N + ^{14}N$ system) the ratio is 2:1, i.e.

$$\sigma_f = (\pi/k^2)[\ \tfrac{4}{3} \sum_{L\,even} (2L+1)T_L + \tfrac{2}{3} \sum_{L\,odd} (2L+1)T_L]. \qquad (4.9)$$

Therefore, the oscillatory structure in σ_f now depends on the way the odd-even partial waves are added. Of course, the oscillations also depend on the physical properties of the system such as the reduced mass.

For lighter systems with I=½ and a small reduced mass, oscillatory structure in σ_f is likely to appear because the ratio is large, for example in $^{13}C + ^{13}C$ system. To illustrate the shape of the excitation function of systems with I=½, we calculated the transmission coefficient at various energies using the approximation of T_L in eq. (2.18). The fusion cross section was calculated using eq. (4.8). Its energy dependence is shown in fig. 4.1a. Similar calculations were made for systems with I=1 (eg $^{14}N + ^{14}N$) and I=3/2 (eg $^{11}B + ^{11}B$). The excitation functions are shown in fig 4.1 (b) and (c) respectively.

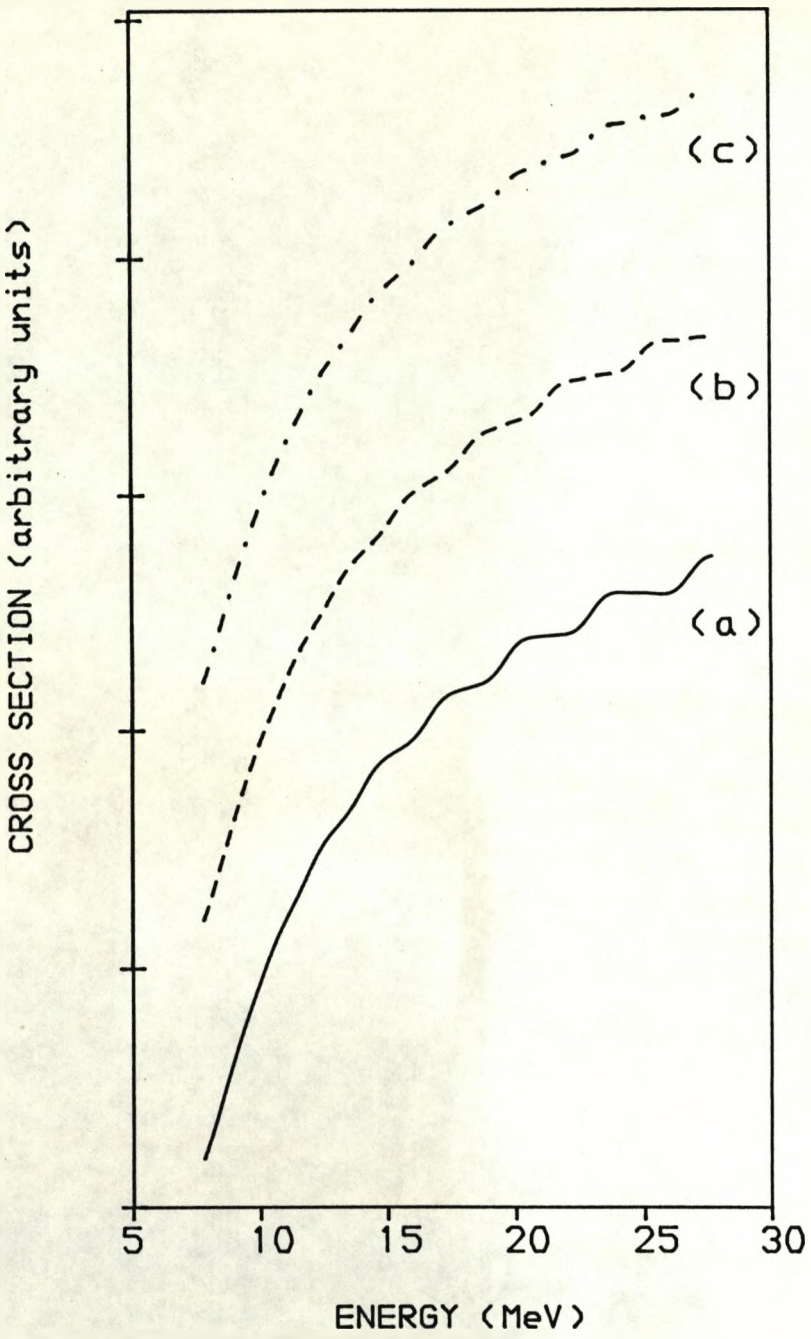

Fig. 4.1 The fusion excitation function of symmetric ions with: (a) I = 1/2. (b) I = 1. (c) I = 3/2. The fusion cross section was calculated using eq. (4.8). The parameters used in calculating the transmission coefficients are $\Delta = 8$, $R_B = 7.5$ fm and $V_B = 7.7$ MeV.

chapter. The fusion cross section was calculated using eq. (4.9). The fit to the experimental data is shown in fig. 4.2. In this fit, even though there are no oscillations in the fusion cross section, a reasonably large surface diffuseness a_r was used; smaller values of a_r do not yield the correct magnitude of the fusion cross sections at all energies. The form factor for the real potential used in fitting the data is a "Woods-Saxon squared". The convention Woods-Saxon form factor does not give a satisfactory fit the data. We note that, the fit gives a close agreement with the data at the lower energies. At higher energies there are some discrepancies with the data, which could be due to higher order interactions (like quadrupole). However, our ability to fit the lower energies suggests that these secondary interactions are negligible. Moreover, at higher energies other direct process channels will be open.

One thing of interest we note with this system is that the maximum fusion cross section is much smaller than that of the $^{12}C + ^{16}O$ system even though the two systems form the same ^{28}Si compound nucleus. Our model can not be used to explain this. However, it is likely that this has to do with the nuclear structure of the nuclei involved. For example, the $^{14}N + ^{14}N$ system has four unpaired nucleons which could "fly off" before fusion, while for the $^{12}C + ^{16}O$ system all the nucleons are part of a complete shell. DeYoung et al [DeY 82] have made an interesting comparison of the two systems in terms of the critical angular momentum trajectory.

4.2 NONSYMMETRIC SYSTEMS.

To investigate the fusion reaction of two nonsymmetric ions, the elastic scattering process of the system will have to be examined. Suppose the projectile possesses spin I and the target is spinless

(for targets with spin, the same could apply if the coupling between the target spin and I is negligible). If the z-projection of I before scattering is M_1 and after scattering it changes to M_2, then the scattering amplitude can be written as [Sat 83]

$$f_{M_1M_2}(\theta,\phi) = \frac{1}{2ik}\sum_{LL'J} \langle L\ I\ 0\ M_1 | J\ M_1\rangle \langle L'\ I\ M_1-M_2\ M_2 | J\ M_1\rangle\ (2L+1)^{\frac{1}{2}}$$
$$\exp[i(\sigma_L+\sigma_{L'})]\ (S^J_{LL'} - \delta_{LL'})\ Y^{M_1-M_2}_{L'}(\theta,\phi) \qquad (4.10)$$

assuming that the incident beam direction is along the z-axis. Here we used the coupling $\underline{J} = \underline{L} + \underline{I} = \underline{L'} + \underline{I}$ where L' is the angular momentum in the exit channel.

A detailed analysis of the scattering amplitude for systems that differ by a few nucleons and for which an elastic transfer process is possible has been given by Von Oertzen and Norenberg [Von 72]. They showed that if the cores (in the two-state molecular model) are spinless, then the scattering amplitude is the sum of two amplitudes, one which dominates at the forward angles $f^D(\theta,\phi)$, and the other important at backward angles $f^E(\pi-\theta,\phi+\pi)$, as discussed in chapter 2. The amplitude $f^D(\theta,\phi)$ is the same as the expression in eq. (4.10) with $S^{JD}_{LL'}$ in place of $S^J_{LL'}$. The amplitude $f^E(\pi-\theta,\phi+\pi)$ is similar to eq. (4.10) but with a different scattering matrix ($S^{JE}_{LL'}$) and the angles changed to $(\pi-\theta,\phi+\pi)$. Using the relation $Y^M_{L'}(\pi-\theta,\phi+\pi) = (-1)^{L'} Y^M_{L'}(\theta,\phi)$, the scattering amplitude for the nonsymmetric system is similar to eq. (4.10) but with an effective scattering matrix as

$$S^J_{LL'} = [S^{JD}_{LL'} + (-1)^L S^{JE}_{LL'}]. \qquad (4.11)$$

If the cores are not spinless eg in $^{13}C + {}^{14}C$, then the coupling of the core spins to the valence particle spin would have to be considered and the scattering amplitude is different from eq. (4.10). Also, the interference of the two components of the scattering amplitudes in-

troduces an extra phase $(-1)^{2S_c}$ in the scattering matrix (eq. (4.11)), where that S_c is the spin of the core. A detailed description of the scattering amplitude for this case is given in [Von 73]. In this chapter we shall discuss systems with spinless cores only.

The fusion cross section becomes

$$\sigma_f = (\pi/k^2) \frac{1}{(2I+1)} \sum_{JL} (2J+1)\ T_{JL} \qquad (4.12)$$

where the transmission coefficient is $T_{JL} = 1 - \sum_{L'} |S^J_{LL'}|^2$, and the scattering matrix is defined by eq. (4.11). When $I > 1/2$, L' can be different from L, but J and the parity have to be conserved throughout. That is $(L' + L)$ should always be even. For cases where $L' \neq L$ is possible, the Schrodinger equation contains coupling terms that allow multipole interactions. These will be discussed in detail for $I = 3/2$ in sect. 4.2.2.

A generalisation of the form of σ_f can not be made, since individual systems would have different physical properties. Therefore, we shall discuss individual systems separately in the following sections.

4.2.1 THE $^{12}C + ^{13}C$ SYSTEM.

Studies on the elastic scattering of $^{12}C + ^{13}C$ system have shown that the angular distribution possesses the anomalous large angle scattering cross section for various energies. Optical model fits to the elastic and inelastic angular distributions have been made by Von Oertzen and many collaborators [Von 73]. Recently Voit et al [Voi 88] have investigated molecular effects in the elastic and inelastic scattering of this system. Most of the calculations for the elastic scattering use the elastic transfer model and reproduce the angular distribution satisfactorily. It was argued [Voi 88] that the model is particularly suited for this system because the ^{13}C nuclei exhibit

single-particle states with a small binding energy (4.9 MeV) of the valence neutron. However, measurements of the fusion cross section do not reveal any strong oscillatory structure in the excitation function for energies above the Coulomb barrier.

The formulations we presented above apply to this system since the valence neutron has spin $\frac{1}{2}$. Using these formulations we made an optical model fit to the fusion cross section data. We assumed that $T_{JL} \equiv T_L$ and the barriers are degenerate for a given L. Figure 4.3 shows the results of our calculations. Since σ_f is more or less structureless, we obtain a reasonable fit to the data for different values of the potential parameters and α. However, the correct value and sign of α was not determined because both the positive and negative values of α give a good χ^2 fit to the fusion cross section data. On the other hand, the elastic scattering cross sections have definite oscillations at large angles which can be used to determine the correct value of α. Thus, the correct sign and value of α was determined from an optical model fit to the elastic scattering data. The results of the calculations are shown in fig. 4.4. The sign of the value of α we obtained from these fits is consistent with sign used by Von Oertzen [Von 75] (i.e. negative). The opposite sign of α produces the backward angle cross section but 90^0 out phase with the experimental data.

One of the reasons why there are no oscillations in σ_f is that the value of α, determined from elastic scattering, gives $\Delta L_g \simeq 2$ (see eq. (2.27)). Since, we argued in chapter 2 that whenever ΔL_g is even, oscillations will not appear. Then, we do not expect any oscillations in the $^{12}C + ^{13}C$ system.

Through the elastic exchange model (transfer model) we can also explain the reasons why there is no oscillatory structure in σ_f. Since the ^{13}C nucleus exhibits pure single-particle states and with a small

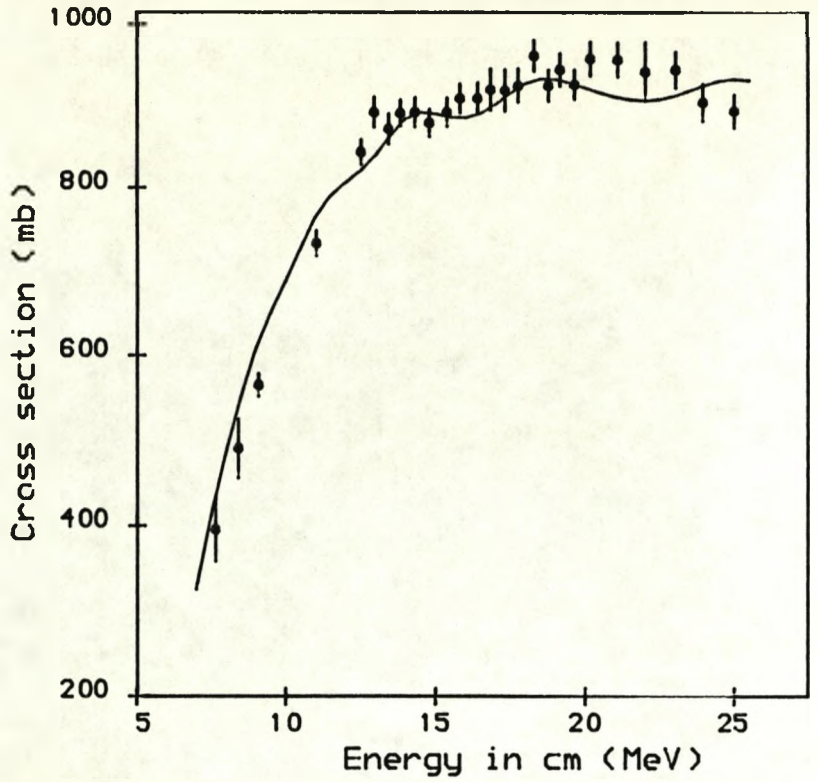

Fig. 4.3 The optical model fit to the fusion cross section of $^{12}C + ^{13}C$ system. The potential parameters used are given table 4.1. The experimental data points were obtained from [Kov 79].

TABLE 4.1

The potential parameters used in figs. 4.3 and 4.4. The Coulomb radius is $r_c = 1.4$ fm.

	V_0 (MeV)	r_r (fm)	a_r (fm)	W_0 (MeV)	r_i (fm)	a_i (fm)	α
Fusion	50.0	0.85	0.99	6.14	1.0	0.42	-0.41
Elastic scattering							
E=7.8 MeV	50.0	0.85	0.99	45.00	1.30	0.40	-0.41
E=9.9 MeV	50.0	0.85	0.99	45.00	1.23	0.38	-0.41

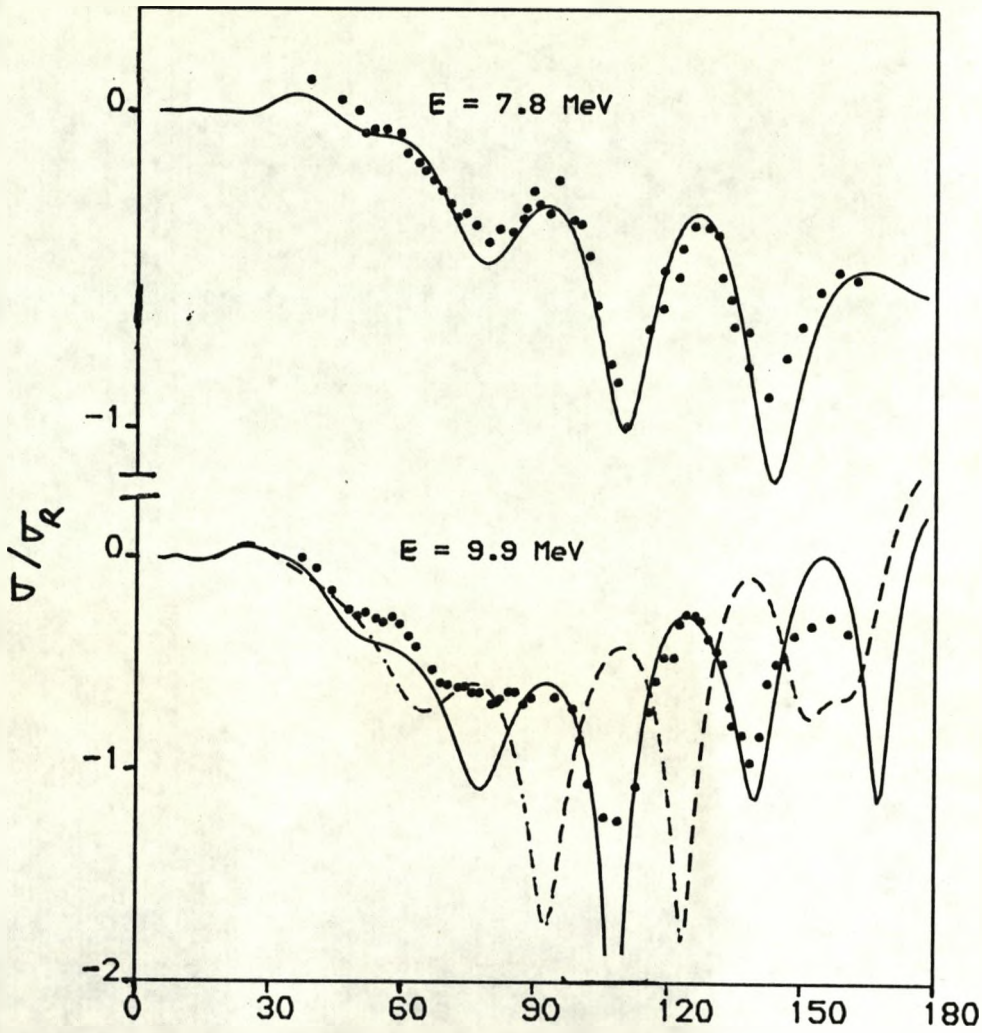

Fig. 4.4 The optical model fit to the elastic scattering cross section of $^{12}C + ^{13}C$ system. The solid curve represents the fit with $\alpha \neq 0$. The dashed curve represents the fit with α positive (the wrong sign). The potential parameters used are given table 4.1. The experimental data points were obtained from [Von 79].

binding energy for the valence neutron, then during the scattering process the neutron can be exchanged at long distances because the wave function of the neutron is long-ranged. This enhances the exchange process and thus the large angle cross section. However, the fusion cross section is not enhanced, because the exchange process could take place at large separation of the cores. Therefore, the exchange contribution to the fusion is very small, i.e. during the exchange process the probability of the ions coming close enough to overlap and fuse is small. Hence the fusion cross is not significantly different from the average fusion cross section (i.e. $\alpha=0$), for which there are no oscillations.

4.2.2 THE $^{11}B + ^{12}C$ SYSTEM

The elastic scattering of this system exhibits ALAS at energies above the Coulomb barrier. A two-state molecular model [Von 69] and DWBA calculations [Boh 74] have been used to reproduce the elastic angular distribution. It was shown that the particle transferred between the two carbon cores is a hole, in the $1p_{3/2}$ state. That is why the angular distribution possesses a minimum at $\theta = 90^0$ [Boh 74].

Experimental measurements [Mat 82] of the fusion cross section of this system reveal that the fusion excitation function possesses oscillatory structure at energies above the Coulomb barrier. Like other nonsymmetric systems, a satisfactory explanation for the reasons why the oscillations appear in fusion cross sections has not been given. To explain the oscillations, the model we have presented can be applied to this system. That is, since ALAS exists in the angular distribution, the exchange of the $1p_{3/2}$ hole should introduce a parity dependent potential that shifts the barrier heights of various partial waves, and thus cause oscillations in σ_f.

The formalism we have presented in this chapter applies to this system, since the cores are spinless. If the barriers are independent of J, i.e. $T_{JL} \equiv T_L$, then the fusion cross section can easily be calculated using eq. (4.12). When we assume that $T_{JL} \equiv T_L$ and calculated the fusion cross section, we observed that the correct magnitude and phase of the oscillations were not reproduced, for all values of the potential parameters we used. However, the average cross section was reproduced (i.e. with no oscillations). The imaginary potential required to fit the average fusion cross section was long ranged, extending beyond the interior of the barrier. Thus, the imaginary potential allows the absorption of flux that does not even penetrate the barrier. Therefore, the transmission coefficient is not sharp and the transition region (where T_ℓ is different from 1 or 0) contains more than one partial wave.

Our inability to reproduce the correct magnitude and phase of the oscillations suggests that either our assumption $T_{JL} \equiv T_L$ is wrong or there are other coupled channels involved in the scattering process. If the latter is the case, then some of the flux may go into these channels and the imaginary potential required to allow the absorption of the remaining flux would then be smaller, and thus confined inside the barrier. Therefore, the transmission coefficient will be sharper as few partial waves are involved in the transition region, and thus the oscillations may reappear. For this system, since the total angular momentum of the hole is 3/2, the scattering involves two coupled channels, one with an orbital angular momentum L and the other channel with either L-2 or L+2. In this case, if the J-dependence of the system is considered, the imaginary potential may be confined to the interior of the barrier and this may lead to a sharper transmission coefficient.

To investigate the J-dependence of the fusion cross section, we calculated the σ_f using a parity dependent optical model potential and a spin-orbit $\underline{L}\cdot\underline{S}$ (Thomas type) potential. The reason for adding a spin-orbit potential is simply to introduce a J-dependence in the transmission coefficient, since the barrier heights for each J state are now different. Using these potentials, we obtained a remarkably good fit to the fusion cross section [Kab 88b]. The fit shows that indeed the transmission coefficient is J-dependent. However, the imaginary potential required to reproduce the cross section is shallow; W_0= 2.5MeV. The strength of the spin-orbit potential is quite large compared to a normal nucleus-nucleus spin-orbit potential used in polarisation calculations. The values of the spin-orbit potential parameters we obtained are: V_{so}= 4.0MeV, r_{so}= 0.5fm and a_{so}= 0.4fm. At higher energies, because W(r) is shallow, the lower partial waves are not completely absorbed, which is uncharacteristic of nucleus-nucleus scattering. Therefore, the fit we obtained is unlikely to be a physically acceptable fit. Nonetheless, the fit shows that the reaction and thus the transmission coefficients are J-dependent.

To solve the problem properly, all possible elastic interactions taking place have to be considered. These interactions would then be included when calculating the fusion cross section. The possible interactions for a given state defined by the quantum numbers I,L,J and π, where the π represent a process with or without elastic transfer of a particle between the cores, are:-

a) The direct elastic scattering process where the entrance channel is the same as the exit channel, i.e. $|I\ L\ \pi\ J\rangle \rightarrow |I\ L\ \pi\ J\rangle$ ("L → L direct" for short).

b) The elastic transfer process of the valence particle from one core to the other, without a change in the orbital angular momentum of the system, i.e. $|I\ L\ \pi\ J\rangle \rightarrow |I\ L\ \pi' J\rangle$ ("L → L with a transfer" for short).

c) The direct elastic scattering process without a transfer, but the orbital total angular momentum has changed in the exit channel, i.e. $|I\ L\ \pi\ J\rangle \rightarrow |I\ L'\pi\ J\rangle$ ("L → L′ direct" for short). Note that J and the parity $(-1)^L$ have to be conserved.

d) The elastic transfer of the valence particle from one core to the other and with a change in the orbital angular momentum of the system in the exit channel, i.e. $|I\ L\ \pi\ J\rangle \rightarrow |I\ L'\pi'\ J\rangle$ ("L → L′ with a transfer" for short). Again, parity and J have to be conserved.

The Schrodinger equation for these processes is

$$(K_{L'} - V(R) + E)U^{J}_{L'\pi}(R) = \sum_{L''\pi'' \neq L'\pi} V^{J}_{L'\pi:L''\pi''}(R)\ U^{J}_{L''\pi''}(R), \qquad (4.13)$$

for $L' = L$ and $L\pm2$ (note that $L' = L-2$ or $L+2$ but not both) since $I=3/2$ and $\pi = \pi_1, \pi_2$, where π_1 represents the direct process and π_2 represents the transfer process. Here the couplings $\underline{J} = \underline{I} + \underline{L'}$ in the entrance channel and $\underline{J} = \underline{I} + \underline{L''}$ in the exit channel were used. The radial wave function for the state $(IL'J\pi)$ is $U^{J}_{L'\pi}(R)$. The kinetic energy operator for the angular momentum L′ is $K_{L'}$ and V(R) is the sum of the monopole nucleus-nucleus potential and the Coulomb potential. Other multipole interactions between the state $|I\ L'\pi\ J\rangle$ and $|I\ L''\pi' J\rangle$, are the potentials on the right hand side (RHS) of the above equation, defined as

$$V^{J}_{L'\pi:L''\pi'}(R) = \langle I\ L'\pi\ J\ |V(\underline{R},\xi)|\ I\ L''\pi' J\rangle \qquad (4.14)$$

where ξ are the internal coordinates of the system. Normally $V(R,\xi)$ is expressed in terms of spherical tensors, i.e. an expansion in higher order multipole interactions. Thus (see [Sat 83])

$$V(\underline{R},\xi) = \sum_{KQ} V^{\pi}_{KQ}(\underline{R},\xi)[i^K Y^Q_K(\hat{R})]^* \qquad (4.15)$$

where V^{π}_{KQ} are the components of the tensors of rank K. The components allow the transfer of the angular momentum K between the internal nuclear states and the nuclear states of the relative motion of the system. The z-projection of K is Q. Using the Wigner-Eckart theorem (see Brink and Satchler [Bri 62]) the coupling potential $V_{L\pi:L''\pi'}(R)$ becomes

$$V^{J}_{L'\pi:L''\pi'}(R) = \sum_{K} i^{L''-L'-K}\,(-1)^{J-I}\,\hat{L}'\,\hat{L}''\,\hat{I}\,\langle L'\,L''\,0\;0|K\;0\rangle \\ W(L'\,L''\,I\;I;\;K\;J)\,\langle I\|V^{\pi'}_{K}(R,\xi)\|I\rangle \qquad (4.16)$$

where W is a Racah coefficient and $\hat{a} = (2a+1)^{\frac{1}{2}}$. The reduced matrix element $\langle I\|V^{\pi'}_{K}(R,\xi)\|I\rangle$ is now a function of R only. The potential V(R) in eq. (4.13) contains the "L → L direct" (monopole interaction). Suppose we represent the other forms of interaction as:-

L → L with transfer	as $\alpha(R)$ i.e.	$V^{J}_{L\pi_1:L\pi_2}(R)$
L → L±2 direct	as $\beta(R)$ i.e.	$V^{J}_{L\pi_1:L\pm2\ \pi_1}(R)$
L → L±2 with transfer	as $\gamma(R)$ i.e.	$V^{J}_{L\pi_1:L\pm2\ \pi_2}(R)$

assuming that α, β, and γ are all dependent on I, L′ and J as in the expression above (eq. (4.16)). Then, the coupling matrix on the RHS of eq. (4.13) becomes

$$\mathbf{V} = \begin{pmatrix} 0 & \alpha & \beta & \gamma \\ \alpha & 0 & \gamma & \beta \\ \beta & \gamma & 0 & \alpha \\ \gamma & \beta & \alpha & 0 \end{pmatrix}$$

Equation (4.13) becomes, in matrix form,

$$\mathbf{D}\cdot\mathbf{U}^J = \mathbf{V}\cdot\mathbf{U}^J \qquad (4.17)$$

where $\mathbf{D}$ is a 4x4 diagonal matrix with $D_{11} = D_{22} = K_L - V(R) + E$ and $D_{33} = D_{44} = K_{L\pm2} - V(R) + E$. The elements of the column matrix $\mathbf{U}^J$ are the wave functions $U^J_{L\pi_1}$, $U^J_{L\pi_2}$, $U^J_{L\pm2;\pi_1}$, and $U^J_{L\pm2;\pi_2}$. To calculate the fusion cross section, the above coupled differential equations would have to be solved, and this requires a lengthy computation. However, the four coupled equations can be simplified by decoupling them into four "elastic" equations using the adiabatic approximation of Nagarajan et al [Nag 86]. Here the "orbital sudden approximation" is used (see [Lin 83]), where the Coriolis potential is "frozen" for L and L±2, i.e. it is approximated by $\ell(\ell+1)\hbar^2/2\mu r^2$ where $\ell = (L\pm1)$ is the average of L and L±2. Thus, $\mathbf{D}$ is the unit matrix multiplied by K_ℓ and eq. (4.17) can be written as

$$\mathbf{A}^+\mathbf{D}\cdot\mathbf{A}\cdot\mathbf{A}^+\mathbf{U}^J = \mathbf{A}^+\mathbf{V}\cdot\mathbf{A}\cdot\mathbf{A}^+\mathbf{U}^J$$

where $\mathbf{A}$ is a unitary matrix. The coupling matrix can be diagonalised from the above equation. If we define $\phi = \mathbf{A}^+\mathbf{U}^J$ and $\mathbf{A}^+\mathbf{V}\,\mathbf{A} = \underline{\lambda}$, then we may write

$$(\mathbf{D} - \underline{\lambda})\phi = 0 \qquad (4.18)$$

where $\underline{\lambda}$ is now a diagonal matrix;

$$\underline{\lambda} = \begin{pmatrix} \alpha+\beta+\gamma & 0 & 0 & 0 \\ 0 & -\alpha+\beta-\gamma & 0 & 0 \\ 0 & 0 & \alpha-\beta-\gamma & 0 \\ 0 & 0 & 0 & -\alpha-\beta+\gamma \end{pmatrix}$$

and

$$\mathbf{A} = \tfrac{1}{2}\begin{pmatrix} +1 & +1 & -1 & +1 \\ +1 & -1 & -1 & -1 \\ +1 & +1 & +1 & -1 \\ +1 & -1 & +1 & +1 \end{pmatrix} \qquad \mathbf{A}^{-1} = \mathbf{A}^+ = \tfrac{1}{2}\begin{pmatrix} +1 & +1 & +1 & +1 \\ +1 & -1 & +1 & -1 \\ -1 & -1 & +1 & +1 \\ +1 & -1 & -1 & +1 \end{pmatrix}$$

Note that the elements of $\underline{\lambda}$ are unique for a given $\mathbf{V}$ but the order in which they are written is not unique and this, of course, affects $\mathbf{A}$, but not the final results. For example interchanging λ_2 with λ_3

gives a symmetric A which is equal to its inverse. However, this is not the most convenient way of writing $\underline{\lambda}$. We choose $\underline{\lambda}$ to have the above form so that it is consistent with the two coupled channel model we presented in section 2.1.3, when $\beta = \gamma = 0$. With this choice, the first decoupled "elastic" equation with λ_1 represents the "elastic" $L \to L$ direct, the second decoupled equation with λ_2 represents the "elastic" $L \to L$ with transfer channel, the third equation is the "elastic" $L \to L\pm2$ direct and the fourth equation is the "elastic" $L \to L\pm2$ with transfer.

Particular boundary conditions have to be imposed on the decoupled wave functions, as the incident flux is from one channel only [Nag 86]. This is realised by writing $U^J = A\Lambda\phi$ where $\Lambda_{ij} = \delta_{ij}\ A^+_{i1}$. The coupled scattering matrix S can be obtained from the decoupled matrix $\tilde{S}$ as

$$S = A\,\Lambda\,\tilde{S}$$

that is

$$\begin{pmatrix} S^{J\pi_1}_{L:L} \\ S^{J\pi_2}_{L:L} \\ S^{J\pi_1}_{L:L\pm2} \\ S^{J\pi_2}_{L:L\pm2} \end{pmatrix} = \frac{1}{4}\begin{pmatrix} \tilde{S}_1 + \tilde{S}_2 + \tilde{S}_3 + \tilde{S}_4 \\ \tilde{S}_1 - \tilde{S}_2 + \tilde{S}_3 - \tilde{S}_4 \\ \tilde{S}_1 + \tilde{S}_2 - \tilde{S}_3 - \tilde{S}_4 \\ \tilde{S}_1 - \tilde{S}_2 - \tilde{S}_3 + \tilde{S}_4 \end{pmatrix}$$

From these scattering matrices, we can now calculate the fusion cross section using eq. (4.12). As we have shown previously, the effective scattering matrix is

$$S^J_{LL'} = S^{J\pi_1}_{LL'} + (-1)^L\, S^{J\pi_2}_{LL'}$$

where π_1 is the direct contribution, and π_2 is the exchange contribution. Thus,

$$T_{JL} = 1 - |S^{J\pi_1}_{LL} + (-1)^L\, S^{J\pi_2}_{LL}|^2 - |S^{J\pi_1}_{L:L\pm2} + (-1)^L\, S^{J\pi_2}_{L:L\pm2}|^2.$$

In terms of the decoupled scattering matrices the transmission coefficient becomes

$$T_{JL} = 1 - \tfrac{1}{2}|\widetilde{S}_1|^2 - \tfrac{1}{2}|\widetilde{S}_3|^2 \qquad \text{for even L}$$

$$T_{JL} = 1 - \tfrac{1}{2}|\widetilde{S}_2|^2 - \tfrac{1}{2}|\widetilde{S}_4|^2 \qquad \text{for odd L.} \qquad (4.19)$$

From eq (4.18), we observe that the decoupled scattering matrix $\widetilde{S}_i$ is obtained when the Schrodinger equation containing the off-diagonal potential λ_i is solved. Thus $\widetilde{S}_1$ is associated with $\lambda_1 = \alpha + \beta + \gamma$, $\widetilde{S}_2$ with $\lambda_2 = -\alpha + \beta - \gamma$, $\widetilde{S}_3$ with $\lambda_3 = \alpha - \beta - \gamma$ and $\widetilde{S}_4$ with $\lambda_4 = -\alpha - \beta + \gamma$. Similarly, for the transmission coefficients from eq. (4.19), the even partial waves contribute to the matrices $\widetilde{S}_1$ and $\widetilde{S}_3$ only, while the odd partial waves contribute to the matrices $\widetilde{S}_2$ and $\widetilde{S}_4$ only. Thus a short form of writing the off-diagonal potentials is

$$(-1)^L\alpha + m[\beta + (-1)^L\gamma] \qquad (4.20)$$

where $m = +1$ for $L' = L$ and $m = -1$ for $L' \neq L$. Since $J>L$ when $L' = L$ and $J<L$ when $L' = L\pm2$, then an easier way of defining m is $m=+1$ if $J>L$ and $m=-1$ if $J<L$. In other words, the above expression shows that, the effect of a transfer monopole interaction is $(-1)^L\alpha(r)$, similar to the form we used in the previous calculations. The quadrupole interaction is $m\beta(R)$, but the transfer interaction introduces the phase $(-1)^L$ (from $(-)^L m\gamma(R)$) into the potential, similar to the phase introduced by the monopole transfer interaction.

If the Coulomb barrier height occurs at R_B (from the monopole interaction potential V(R) in eq. (4.13)), then the barrier height of the state (ILJ) would now be

$$V_L(R_B) = \text{Max}[V(R) + \ell(\ell+1)/2\mu R^2 + (-1)^L\alpha + m(\beta + (-1)^L\gamma)], \qquad (4.21)$$

where m is defined above. The barrier heights produced by these potentials are represented schematically in fig. 4.5. In this figure,

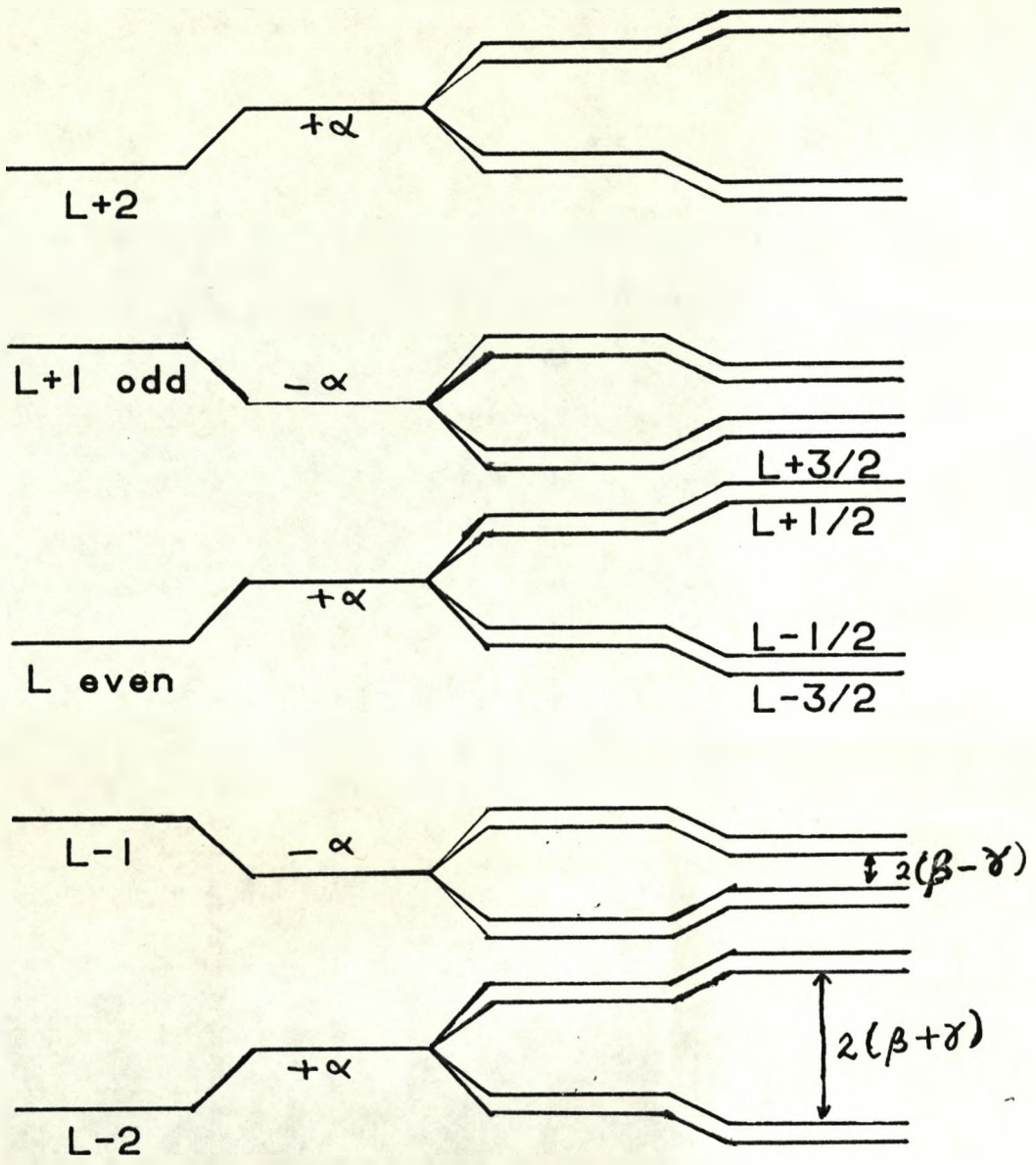

Fig. 4.5 A schematic representation of the effects of adding a monopole transfer term $(-1)^{L}\alpha$ and quadrupole terms $[\beta + (-1)^{L}\gamma]m$ to the barrier heights (represented by levels) of five successive partial waves (where L > 2). For the full meaning of α, γ, β and m see the text.

we initially assumed that for a given L the barriers are degenerate. Thus if the monopole transfer term is independent of J, then $(-)^L\alpha(R)$ would simply shift the barriers up or down as shown in the figure. Note that the barrier heights are represented by a straight line ("levels"). The quadrupole terms are J dependent. Therefore, the term without a transfer removes the degeneracy of the barrier heights, and the barriers are shifted by $m\beta(R_B)$. Similarly the other quadrupole term with a transfer would further shift the barriers by $(-1)^L m\gamma(R_B)$.

From this analysis, we can understand why the initial fit we made using a spin-orbit potential ($\underline{L}\cdot\underline{S}$) gives a good description to the data. This is because the $\underline{L}\cdot\underline{S}$ splitting of the barriers for a given L correspond to approximately the same splitting caused by the monopole and quadrupole interactions.

We shall now investigate the J-dependence of these interactions by expanding eq. (4.16).

4.2.2 (A) MONOPOLE INTERACTION WITH A TRANSFER $\alpha(R)$

Here $L' = L$, $\pi = \pi_2$, so there is no angular momentum transferred i.e. K = 0. Therefore, from eq. (4.16) we have

$$\alpha(R) = V_{L\pi_1 : L\pi_2}(R) = \hat{L}^2 \hat{I} \langle L\ L\ 0\ 0 | 0\ 0\rangle\ W(L\ L\ I\ I;\ 0\ J)\ \langle I \| V_0^{\pi_2}(R,\xi) \| I\rangle .$$

Expanding and substituting the values of the Racah and Clebsch-Gordan coefficients we obtain

$$\alpha(R) = \langle I \| V_0^{\pi_2}(R,\xi) \| I\rangle . \qquad (4.22)$$

Thus it is independent of L and J, as expected. The reduced matrix is simply a function of R. This is consistent with the assumption we made in the fig. 4.5 and in the previous calculations. Thus we can still approximate the form factor of this potential as

$$\alpha(R) = V_{\pi}(R) = \alpha V_N(R),$$

where α (the one without the brackets) is a dimensionless parameter and $V_N(R)$ is the monopole direct interaction, the "L → L direct" potential (see eq. (3.5)). It should be noted that $V_N(R)$ is the same expression as eq. (4.22) except that π_2 is now π_1

4.2.2 (B) QUADRUPOLE INTERACTION

Here $L' = L\pm2$, π is π_1 for $\beta(R)$ and π_2 for $\gamma(R)$. Therefore, the angular momentum transferred is 2, so K=0,1,2. The expression of β is the same as for γ except that the reduced matrix $\langle I\|V_K^{\pi}(R,\xi)\|I\rangle$ is different. The expression for β is

$$\beta(R) = \sum_{K=0}^{2} i^{L'-L-K} (-1)^{J-I} \hat{L}\hat{L}'\hat{I} \langle L\ L'\ 0\ 0|K\ 0\rangle$$
$$W(L\ L'\ I\ I;\ K\ J)\ \langle I\|V_K^{\pi_1}(R,\xi)\|I\rangle.$$

For $L' = L\pm2$, the above expression is zero for K=0,1. This is because $\langle L\ L'0\ 0|K\ 0\rangle = 0$ if $L+L'+K$ is odd or if K is zero (see [Bri 62]). Thus we obtain,

$$\beta(R) = (-1)^{J-I} \hat{L}\ (\hat{L\pm2})\ \hat{I}\ \langle L\ L\pm2\ 0\ 0|2\ 0\rangle$$
$$W(L\ L\pm2\ I\ I;\ 2\ J)\ \langle I\|V_2^{\pi_1}(R,\xi)\|I\rangle,$$

and

$$\gamma(R) = (-1)^{J-I} \hat{L}\ (\hat{L\pm2})\ \hat{I}\ \langle L\ L\pm2\ 0\ 0|2\ 0\rangle$$
$$W(L\ L\pm2\ I\ I;\ 2\ J)\ \langle I\|V_2^{\pi_2}(R,\xi)\|I\rangle.$$

The values of the Racah and Clebsch-Gordan coefficients can be obtained for different J from standard tables (see [Bri 62]) or computer subroutines. These values contain phase factors that make the above expression an absolute positive quantity except for the sign of the reduced matrix. The expressions of $\beta(R)$ and $\gamma(R)$ contain the same J-dependent factors. Therefore, we can assume that they are related to one another in a form similar to the relation between the two

monopole interactions. That is, if $\beta(R)$ is $F^{J}_{IL}(R)$, then the $\gamma(R)$ is expressed as $\gamma F^{J}_{IL}(R)$, where γ is now the scaling parameter.

We can also assume that $\beta(R)$ is a "surface" interaction, since quadrupole interaction is predominantly a surface interaction and it involves changes in the projection of the orbital angular momentum of the system which is normally at the nuclear surface. Therefore, we may write the radial part of $F^{J}_{IL}(R)$ as a derivative of the nuclear potential, similar to the Thomas type interaction in the L•S coupling. If the nuclear potential is parametrised by a Woods-Saxon form factor, then F(R) is

$$F(R) = -(V_q/R)[\partial(WS)/\partial R] \qquad (4.23)$$

where WS is Woods-Saxon form factor and V_q is the strength of the potential. The values of the parameters of this potential could either be the same as those in the nuclear potential or chosen independently.

4.2.2 (C) OPTICAL MODEL FIT.

When these formulations are taken into account, we now have an effective real potential as

$$V(R) = V_C(R) + [1+ (-1)^{L}\alpha]V_N(R) + \ell(\ell+1)\hbar^2/2\mu R^2 + [1 + (-1)^{L}\gamma]mF^{J}_{IL}(R) \qquad (4.24)$$

where m=+1 for J>L and m=-1 for J<L. The monopole interaction in eq. (4.13) is the sum of V_C and V_N. To calculate the fusion cross section, we need to solve only one Schrodinger equation (for each J and L) containing the above expression as the real part of the optical model potential. The transmission coefficient is then calculated using eq. (4.19).

When we made an optical model fit to the fusion cross section data for the $^{11}B + ^{12}C$ system, we observe the following:-

1. The fits with and without a J-dependence in $F^{J}_{IL}(R)$ are more or less the same. The χ^2 obtained in both cases are almost the same. When we calculated the I,L,J dependent factor of $\beta(R)$ and $\gamma(R)$ for different values of J, we observed that these values do not differ significantly from one another. They vary within the range 0.7 - 1.0, with the asymptotic value 0.9 easily reached. That is why we did not notice any significant difference in χ^2 for the two fits.

2. A significant difference in the χ^2 was obtained when the values of the parameters in F(R) are either the same as those in $V_N(R)$ or when they are different. The latter case yields the better χ^2 fit, but containing more independent parameters.

3. We observed that values of α and γ are almost the same, for most of the fits we made. When we made a χ^2 fit to the data with respect to α and γ, we obtain a minimum χ^2 when α is approximately equal γ. This is not completely unexpected, since the transfer interaction involves the same particle. Therefore, the transfer strength or probability should always be the same in either the quadrupole or monopole interaction.

In fig. 4.6, we show the optical model fit to the data with a J-independent F(R) and with the values of the parameters in F(R) varying independently of the nuclear potential parameters. The values of the potential parameters are given in table 4.2. The other fits, as described in the above cases, are more or less the same as the fit we present in fig. 4.6 expect that the χ^2 is different by about 1 to 10%.

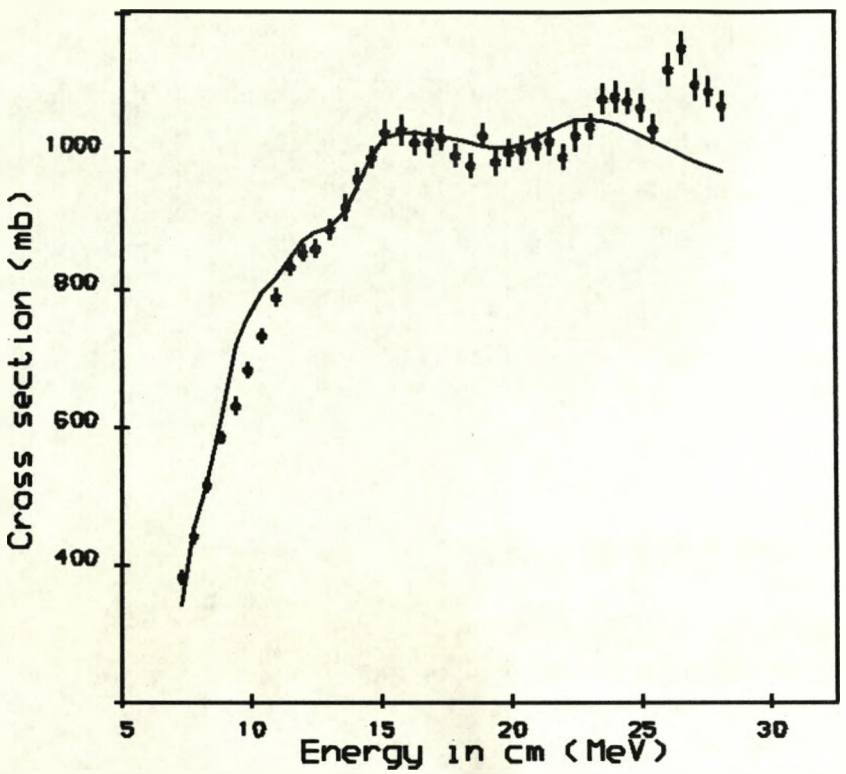

Fig. 4.6 The optical model fit to the fusion cross section of $^{11}B + ^{12}C$ system. The potential used is given in eq. (4.20). The potential parameters used are given in table 4.2.

TABLE 4.2

Potential parameters used in the figure above. Here F(R) is described in eq. (4.23)

	V (MeV)	r (fm)	a(fm)
Real	41.11	0.66	0.88
Imaginary	5.25	0.49	0.71
F(R)	30.00	0.53	0.39
r_c = 1.3 fm	α = 0.370		γ = 0.32

Notes added in proof: The fit to the data in fig. 4.6 is a satisfactory description of the fusion cross section. The imaginary potential used is, however, shallow and we observed that σ_f is sensitive to this potential even at lower energies (E > 11 MeV). There is, therefore, a partial absorption of the partial waves $L < L_g$ at all energies, thus suggesting a possible significance of internal waves. However, it is not obvious *a posteriori* that the internal waves should be significant in this system and also σ_f sensitive to W(R). To investigate these observations, we made another fit to the data. The fit is shown below. We observed that one can easily obtain a satisfactorily good fit to the data with a large imaginary potential, thus effectively removing any surface transparency effect that the previous potential seems to suggest. The fit was made using the sum of two Woods-Saxon terms to describe the nuclear potential and F(R) in eq. (4.24) is defined as: $F(R) = \beta \frac{1}{R} \frac{d}{dR}(V_N(R))$. Other potential parameters are:

	V	r	a
Real I	70.3	0.58	0.85
II	11.2	1.26	0.43
Imaginary	43.5	0.61	0.66
r_c=1.3	$\alpha = \gamma$ = 0.15		β = 0.5

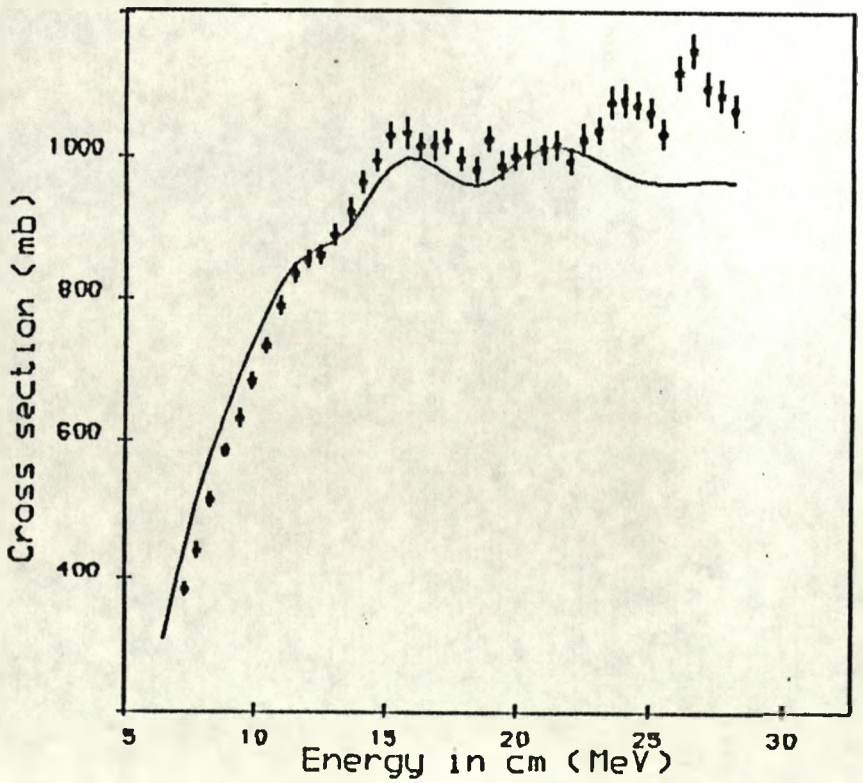

In the final analysis, the $^{11}B + ^{12}C$ system reveals some interesting features of the effect of the spin of the particle transferred. We have shown that the fusion cross section can only be reproduced if the spin-dependent forces are taken into account. This is similar to the observations by Bohne et al [Boh 74] when fitting the elastic scattering cross section for this system, i.e. without the spin-dependent forces the elastic scattering cross sections were not well reproduced.

4.3 CONCLUSION

Given the above analysis, we conclude this chapter with a comparison of the fusion reaction of $^{11}B + ^{12}C$ and $^{12}C + ^{13}C$ systems and the other three systems we introduced in the beginning of this chapter.

The two systems, $^{11}B + ^{12}C$ and $^{12}C + ^{13}C$, are similar because the cores in the two state molecular model are the same. In the $^{11}B + ^{12}C$ system a $1p_{3/2}$ hole is being exchanged between the two carbon cores, while in the $^{12}C + ^{13}C$ system the exchanged particle is a $1p_{1/2}$ neutron. Both systems possess ALAS at energies above the Coulomb barrier. However, their angular distributions are out of phase, when they are superimposed on one another at a particular energy. In particular, at $\theta=90^{0}$, $^{11}B + ^{12}C$ system has a minimum while $^{12}C + ^{13}C$ system has a maximum for all cases considered.

It was shown in fig. 4.4 that if α (the scaling parameter in the monopole interaction potential) has the wrong sign, then the oscillations in both the elastic and fusion cross sections are always out phase with the cross sections produced using the correct sign of α. This explains why the oscillations in the two systems are out of phase with each other and the values of α we obtained have opposite signs. This is also consistent with the two-state molecular model derivations [Von 73].

Another interesting phenomena taking place in the two systems is that, at all energies, the fusion cross section of the $^{11}B + ^{12}C$ system is greater than that for the $^{12}C + ^{13}C$ system. We argued that in the $^{12}C + ^{13}C$ system there are no oscillations in the cross section because the valence neutron is loosely bound (E_B = 4.95MeV). Therefore, the contribution of the exchange process to the fusion reaction is almost negligible, because the neutron can be exchanged at large separation between the two carbon cores. Comparing these properties with those in the $^{11}B + ^{12}C$ system, we see that the $1p_{3/2}$ hole is strongly bound, (E_B= 18.72MeV). As such the wave function of the hole is short-ranged. Thus, the exchange process can only take place at short separation of the two cores. Therefore, during the exchange process, the exchange force could be strong enough to bring the two cores close enough to overcome the Coulomb barrier, thus having a higher probability of fusing. As a result of this, σ_f has this interesting distinct structure and is much larger than that for the $^{12}C + ^{12}C$ and $^{12}C + ^{13}C$ systems. Also, because of the extra contribution from the quadrupole interaction, more absorption takes place. The barrier heights for each J will thus be lower than the heights of the barriers in the other two systems, so more terms are included in eq. (4.12). For this system ($^{11}B + ^{12}C$), because of the splitting of the barriers, it is unlikely to see a dominant signature of one state (J^{π}) at a particular energy.

A similar argument applies to the $^{12}C + ^{16}O$, $^{12}C + ^{15}N$ and $^{12}C + ^{17}O$ systems. In these cases, oscillations appear in the $^{12}C + ^{16}O$ system because of the exchange contribution to the fusion process. However, in the other two systems we do not have any oscillations because there is no elastic exchange process. Also, the average fusion cross section in the three systems is consistent with the classical prediction. That is, $^{12}C + ^{15}N$ has the smallest average σ_f

because it has the smallest R_B. Also, the average fusion cross section is the smallest because I=1/2 and there are no extra absorptive channels (unlike for example, the $^{11}B + ^{12}C$ system).

In conclusion, the above discussion has illustrated some of the important aspects of the fusion reaction that take place. Our model can be used to predict or explain other systems that possess an oscillatory structure in the fusion cross section.

CHAPTER 5

THE S MATRIX FOR COUPLED CHANNEL SCATTERING

5.1 INTRODUCTION

The S matrix can be defined as the operator that transforms an initial wave function $|\chi_{in}>$ of a nucleon (or particle), which is well defined before scattering at $t \to -\infty$, into a scattered wave function $|\chi_{out}>$ that is also well defined after the scattering at $t \to \infty$, i.e.

$$|\chi_{out}> = S|\chi_{in}>.$$

Flux conservation requires S to be unitary i.e. $SS^{+} = 1$. The matrix contains information on the scattering process, and thus is dependent on the Hamiltonian H of the system. If H is time reversal invariant, then S is symmetric.

For two spinless particles scattering in the presence of a central potential, the S matrix is a diagonal matrix. That is $S = \exp(2i\underline{\delta})$, where $\underline{\delta}$ is a diagonal matrix with real elements δ_{ℓ} (the phase shifts) for the angular momentum states $\ell = 0,1,2,3,.....$ Thus the particular S matrix associated with an angular momentum ℓ is simply $S_{\ell} = \exp(2i\delta_{\ell})$. When the scattering is inelastic, δ_{ℓ} is complex, with the imaginary part taking account for the loss of flux from the incident channel.

In the presence of a non-central potential some angular momentum states may be coupled. An example is the scattering of neutrons on protons in the presence of a tensor potential, where the states with $\ell = 0$ ($^3S_1$) and $\ell = 2$ ($^3D_1$) are coupled. The corresponding channel S matrix is a 2x2 symmetric and unitary submatrix of the main S matrix. For simplicity we refer to this submatrix as the S matrix.

The 2x2 S matrix requires three independent real parameters to fully describe the scattering process. The first two parameters may be thought as describing the direct scattering of each state while the other accounts for the coupling (mixing) of the two states. However, since the elements of S are complex, there are six real quantities in the matrix. Hence three parameters are redundant and can be expressed in terms of the other three. Alternatively, one could select three convenient parameters and express the elements of S in terms of the chosen. The parameters should preferably be smooth functions of energy. Each choice leads to a parametrisation of the S matrix.

It is the our aim in this chapter to present various ways of parametrising the S matrix for nucleon-nucleon scattering at energies both below and above the inelastic threshold for pion production. We start with a general expression of an nxn matrix, and then consider the case when n =2. For the latter case, at energies below the inelastic threshold, the most commonly used parametrisations will be given. At energies above the threshold we shall first discuss the scattering matrix and later focus our attention on the elastic component of the scattering. In the elastic component, a matrix N responsible for the coupling between the elastic and other non-elastic components can be extracted out and parametrised. We shall discuss the various forms of parametrising N, and finally in the last section we shall compare these forms using numerical calculations.

5.2 A GENERAL FORM OF THE SCATTERING MATRIX

For a two body n-channel scattering process the S matrix is a symmetric and unitary nxn matrix containing $N = \frac{1}{2}n(n+1)$ independent parameters. The elements of the matrix are usually written as

$$S_{ii} = \eta_i \exp(2i\delta_i) \qquad i=1,2,\ldots,n$$

$$S_{ij} = N_{ij}\exp(i\phi_{ij}) \qquad i\neq j=1,2,\ldots,n \qquad (5.1)$$

where η_i and N_{ij} are the diagonal and off-diagonal amplitudes which are real and positive, δ_i and ϕ_{ij} are the diagonal and off-diagonal phase shifts respectively. By introducing a diagonal matrix U, where

$$U_{ij} = \delta_{ij}\exp(i\delta_i) \qquad i,j=1,2,\ldots,n \qquad (5.2)$$

and δ_{ij} is the standard Kronecker symbol, we can rewrite the S matrix as

$$S = U\hat{S}U. \qquad (5.3)$$

Defining $\phi_{ij} = \delta_i + \delta_j + \beta_{ij}$, gives

$$\hat{S}_{ii} = \eta_i \qquad i=1,2,\ldots,n$$
$$\hat{S}_{ij} = N_{ij}\exp(i\beta_{ij}) \qquad i\neq j=1,2,\ldots,n. \qquad (5.4)$$

The unitarity on S gives

$$\hat{S}\hat{S}^{+} = 1 \qquad (5.5)$$

since U is unitary. This form of expressing the S matrix allows us to choose δ_i as the first n independent parameters, thus leaving $\hat{n} = N - n = n(n-1)/2$ parameters in $\hat{S}$. For example, when n=2 we are left with only one parameter, while for n=3 we have $\hat{n}$=3 thus one could, in this case, choose either the η_i, β_{ij} or N_{ij} to define $\hat{S}$ completely. However for n>3 the choice is not all that simple.

5.3 TWO BODY ELASTIC SCATTERING WITH COUPLED STATES

This is the case where S is a 2x2 symmetric unitary matrix and three real parameters are required to specify the matrix. Writing the S matrix in terms of eq. (5.3), i.e.

$$S = U\hat{S}U,$$

we have in a more explicit form as

$$S = \exp(i\underline{\delta})\,\hat{S}\,\exp(i\underline{\delta}) \tag{5.6a}$$

where $\underline{\delta}$ is a diagonal matrix containing δ_1 and δ_2, the phase shifts. This form implies that we are left with only one parameter in $\hat{S}$. We may write $\hat{S}$ as

$$\hat{S} = \exp(2i\underline{\sigma}_x\varepsilon) \tag{5.6b}$$

where $\underline{\sigma}_x$ is the first Pauli spin matrix and ε is the mixing parameter which is real and $\hat{S}\hat{S}^{+} = 1$ is satisfied. This form of parametrisation is the well known "bar phase convention" of Stapp et al [Sta 57] (the SYM). A bar is normally written above the phase shifts to distinguish it from the "eigen phase convention" of Blatt and Biedenharn [Bla 52] (the BB) (we drop the bars in this thesis for convenience). The BB parametrisation of the channel S matrix is

$$S = \exp(-i\underline{\sigma}_y\varepsilon)\exp(2i\underline{\delta})\exp(i\underline{\sigma}_y\varepsilon) \tag{5.7}$$

where ε is the eigen mixing parameter, $\underline{\sigma}_y$ is the second Pauli spin matrix and $\underline{\delta}$ is a diagonal matrix containing the eigen phase shifts δ_1 and δ_2. The superscript "e" normally written on the parameters is dropped also.

In both the two forms of parametrisation, the two phase shifts can be thought as describing the direct channel to channel scattering while the mixing parameter describes the coupling between the two channels, as illustrated schematically in fig. 5.1. In the figure, the parame-

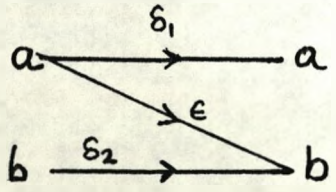

Fig. 5.1 A schematic representation of two coupled channel scattering (time reversal is not shown).

ters could be those of either the eigen or the bar phase convention. The channels are represented by a and b, e.g for n-p scattering they could be the $^3S_1$ and $^3D_1$ states respectively.

Recently Sprung [Spr 87] has shown that the set of parameters in the two conventions are related to one another through a "hidden" parameter θ. This parameter is a smoothly varying function of energy except at some points, for example when the bar mixing parameter is $\varepsilon=\pi/4$.

The parameters, in the two conventions are also smooth functions of energy. The phase shifts are mod π. For cases where the potential has bound states, the phase shifts are defined according to Levinson's theorem.

There are other forms of parametrising the two channel **S** matrix using matrices like the **M** and **K** (see [Ros 60], [Ker 67] and [Arn 82]), but we shall not discuss these in this thesis.

5.4 TWO BODY INELASTIC SCATTERING

At energies above the threshold, the 2x2 **S** matrix is no longer unitary but it is still symmetric and it requires six parameters, not three, to specify the elastic component of the scattering. In comparison with the uncoupled states, an obvious choice of parameters is to allow δ_1, δ_2 and ε to be complex. However, this leads to an awkward representation as pointed by Sprung and Kermode [Spr 82]. More convenient forms of choosing the required parameters has been suggested by various authors. It is the aim of this section to present some of these parameterisations.

5.4.1 THE SCATTERING MATRIX

The size of the **S** matrix depends on the number of channels present in the scattering process. For example, when only three channels are

involved in the scattering, the S-matrix is a 3x3 symmetric and unitary matrix. In this case, six independent parameters are required to specify the matrix and five out of the six parameters describe the elastic component of the scattering. This matrix contain some interesting properties that will be presented in the chapter 6. For one more extra channel present, S is a 4x4 unitary and symmetric matrix requiring ten parameters to specify. The elastic component requires six parameters out of the ten. One could visualise the parameters by a schematic representation of the scattering into four channels (a,b,c and d), as shown in fig. 5.2, where there are four direct phases δ_i and six mixing parameters.

In general, if the scattering involves n channels then the scattering matrix is a nxn symmetric unitary matrix and requires n(n+1)/2 parameters to specify. In this case the elastic component of the scattering is specified with only six independent parameters. Consequently, when one is interested in the elastic component of the scattering, it suffices to consider a four coupled channel scattering problem [Spr 82]. The parameters required to describe the submatrix is thus six, but one parameter is redundant when only three channels are involved. Bryan [Bry 81] studied the submatrix by considering a four coupled channel

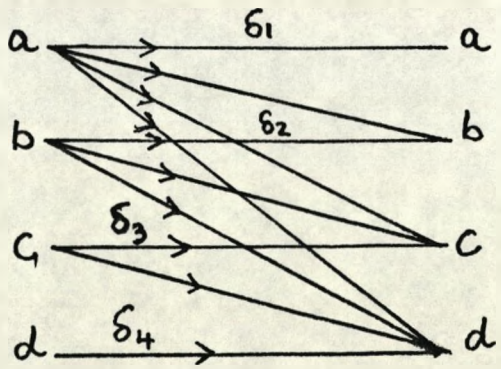

Fig. 5.2 A schematic representation of four coupled channels scattering. Time reversal part is not shown.

model in an elegant way. His model is a generalisation of the SYM form to a 4x4 matrix, where the matrix restores back to the SYM form when there is no inelasticity.

According to Bryan, the 4x4 scattering matrix can be parameterised as

$$S = \exp(i\underline{\Delta})\exp(\ iE\ )\cdot U\cdot\exp(\ iE\ )\exp(i\underline{\Delta}) \tag{5.8}$$

where $\underline{\Delta}$ is a diagonal matrix with elements δ_i $(i = 1,2,3,4)$, and $E = \begin{bmatrix} \sigma_x\varepsilon_1 & 0 \\ 0 & \sigma_x\varepsilon_2 \end{bmatrix}$. The matrix U is unitary and can be defined as

$$U = \Big[\prod_{i=1}^{4} \exp(i\theta_i\underline{\Gamma}_i)\Big]\cdot\Big[\prod_{i=1}^{4} \exp(i\theta_i\underline{\Gamma}_i)\Big]^T, \tag{5.9}$$

where θ_i are the remaining four parameters and $\underline{\Gamma}_i$ are 4x4 matrices. This form is consistent with the expression of S we had in eq. (5.3), where we now have $\hat{S} = \exp(iE\ )\cdot U\cdot\exp(iE\ )$. Equation (5.8) restores back to SYM form when $U = 1$ (eq. (5.6a)), i.e.

$$S_{2\times2} = \exp(i\underline{\Delta})\exp(2\cdot i\underline{E}\ )\ \exp(i\underline{\Delta}) \tag{5.10}$$

where we now have $\underline{\Delta} = \begin{bmatrix} \delta_1 & 0 \\ 0 & \delta_2 \end{bmatrix}$ and $E = \begin{bmatrix} 0 & \varepsilon_1 \\ \varepsilon_1 & 0 \end{bmatrix}$.

To extract the elastic component from the 4x4 matrix, the matrix is written in blocks of 2x2 matrices as follows:

$$S = \begin{bmatrix} S_e & S_{ie} \\ (S_{ie})^T & S_i \end{bmatrix}, \tag{5.11}$$

where S_e represents the elastic component, S_i is the inelastic component and S_{ie} accounts for the mixing of the two components. From eq. (5.8), the matrices $\underline{\Delta}$ and E can be written in two diagonal blocks with zero off-diagonal matrices and U as

$$U = \begin{bmatrix} N & iL \\ (iL)^T & M \end{bmatrix}. \qquad (5.12)$$

The matrices N, L and M are all real and symmetric, since U is symmetric and unitary. This matrix does not appear in the 2x2 elastic component of (5.10), thus it is responsible for the inelasticity of the scattering. Hence L=0 and N ,M are unit matrices in elastic scattering.

The elastic component of the 4x4 is [Bry 81]

$$S_e = \exp(i\underline{\Delta})\exp(i\underline{\sigma}_x\varepsilon)\ N\ \exp(i\underline{\sigma}_x\varepsilon)\exp(i\underline{\Delta}). \qquad (5.13)$$

This is a 2x2 symmetric but not unitary matrix, and it reverts to SYM form when N = 1. The subunitarity constraint on S_e implies that

$$1 \geq \det(1 - S_e^{+} S_e) = \det(1 - N^2) \geq 0. \qquad (5.14)$$

Also, the requirement that the cross section for the process should always be positive imposes [Kla 83]

$$\text{trace}(1 - S_e^{+} S_e) = \text{trace}(1 - N^2) > 0. \qquad (5.15)$$

The equality $\det(1 - N^2)=0$, holds when there is only one absorptive channel [Spr 82, Mel 83] and of course in the pure elastic case when N is the unit matrix. In this case S_e requires only five parameters, and two in N. We can now discuss the procedures on how to parametrise the matrix N, since other parameters in eq. (5.13) are well known.

5.4.2 PARAMETRISATION OF *N*

To parametrise N, we have to ensure that the two inequalities in eqs. (5.14) and (5.15) are satisfied and the matrix produced is symmetric. The chosen parameters have to be well defined and smoothly varying functions of energy. There has been various suggestions on how to select these parameters. In general, the approaches can be

grouped into two classes. The first takes the matrix **U**, containing **N**, and parametrise it by choosing the matrices Γ_i and θ_i as in eq. (5.9). The matrix **N**, containing only three parameters, is then extracted. This is the approach adopted by Bryan [Bry 81] and Sprung [Spr 85]. This procedure is consistent with the way the full **S** matrix is constructed, but one ends up with an **N** containing four parameters instead of three. The remedy to this is to "mechanically" put one of the parameters equal to zero, even though the choice is rather arbitrary. The other approach is to choose three variables and simply construct the **N** matrix in the most convenient way. This approach is much simpler but does not define the main matrix **U**. Writing the matrix **N** as

$$\mathbf{N} = \begin{bmatrix} N_{11} & N_{12} \\ N_{12} & N_{22} \end{bmatrix} . \qquad (5.16)$$

Kermode and Cooper [Ker 85] showed that the possible values of **N** can be represented by a geometrical model. Through a three dimensional space, with $N_{11}=x$, $N_{12}=z$ and $N_{22}=y$, they used eqs. (5.14) and (5.15) to construct a geometrical figure. A computer sketch of the figure is reproduced here in fig. 5.3 (see [Spr 85] also). In the figure a valid matrix **N** is represented by a point on or below the curved surface (or on and above its mirror image). The ridge in the figure is $x + y = 0$. The equality $\det(1-\mathbf{N}^2) = 0$ holds in the elastic case, when **N** is the unit matrix (points A and B on the figure), or if there is only one absorptive channel, where **N** requires two parameters and we have a point on the surface. For two or more inelastic channels, **N** requires three free parameters which could be any point on or below the curved surface.

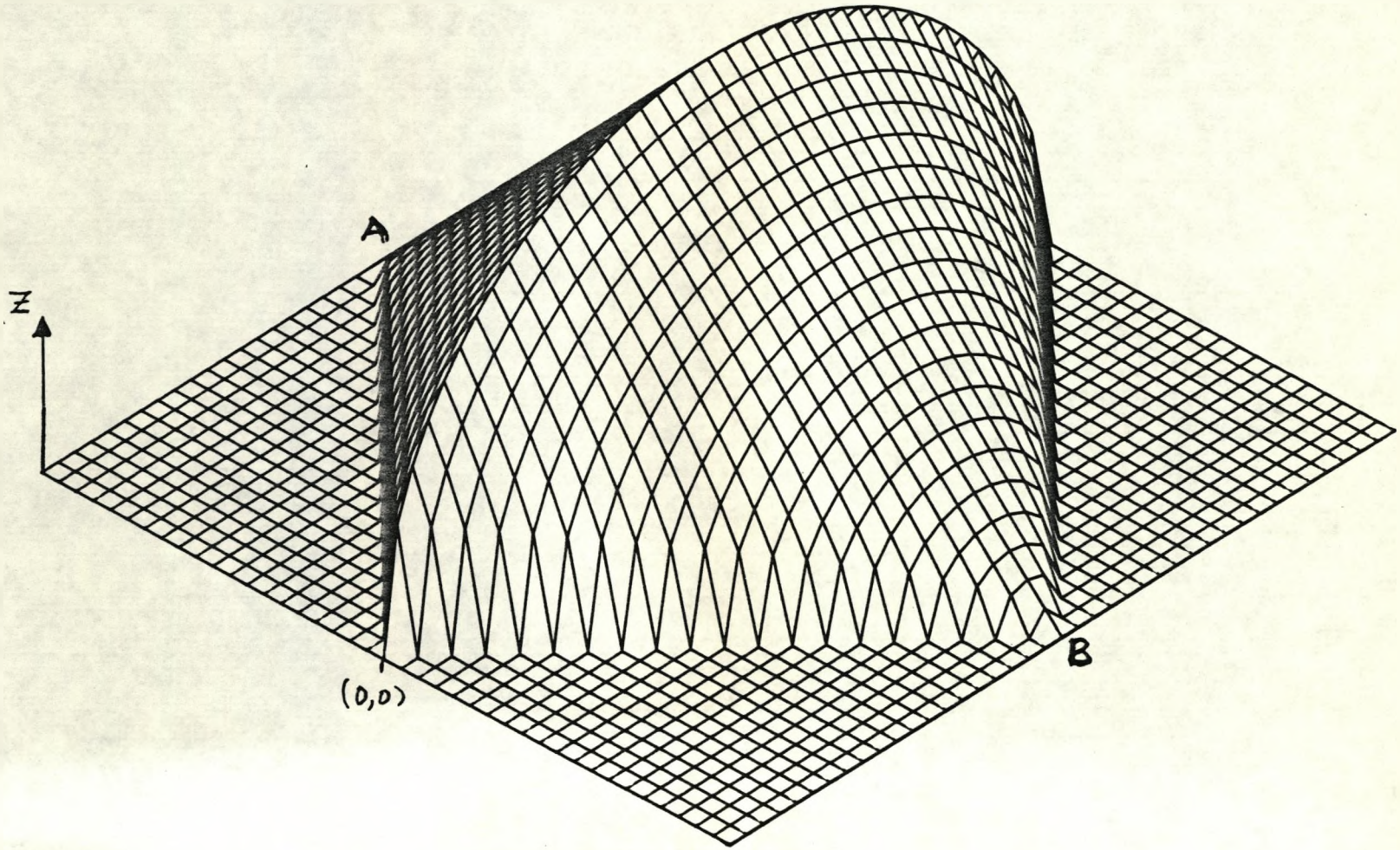

Fig. 5.3 The Kermode and Cooper geometrical model. Representing the possible values of **N** in (x,y,z) space.

We can now present the various parametrisations of **N** according to the following authors: Bryan [Bry 84], Klarsfeld [Kla 83], Melhem and Kermode [Mel 83] and Sprung [Spr 85]. Starting with the approach of expressing **U** and then extracting **N**, Bryan parametrised **U** in terms of the matrices Γ_i (see eq. (5.9)) which are defined as

$$\Gamma_1 = I_{13} + I_{31} \qquad \Gamma_2 = I_{14} + I_{41}$$
$$\Gamma_3 = I_{23} + I_{32} \qquad \Gamma_4 = I_{24} + I_{42}, \tag{5.17}$$

where I_{nm} is a 4x4 matrix whose sole entry is 1 at position nm, otherwise zero. The choice of these matrices was based on the coupling parameters of fig. 5.2, that is between the channels n and m (the exact meaning of the coupling is lost when **N** is considered, since one of the parameters is set to zero). Defining the matrices **A** and **B** as

$$\mathbf{A} = \exp(i\theta_2\Gamma_2)\exp(i\theta_3\Gamma_3) \text{ and } \mathbf{B} = \exp(i\theta_1\Gamma_1)\exp(i\theta_4\Gamma_4),$$

we have Bryan's **U** matrix as

$$\mathbf{U} = \mathbf{AB}\cdot\mathbf{BA}. \tag{5.18}$$

On expanding and extracting **N**, we have one too many parameters in **N**. Bryan remove this redundancy by putting $\theta_4 = 0$, ending with

$$\mathbf{N} = \begin{pmatrix} 2(\cos\alpha\cos\beta)^2 - 1 & -2(\sin\alpha\sin\gamma)(\cos\alpha\cos\beta) \\ -2(\sin\alpha\sin\gamma)(\cos\alpha\cos\beta) & \cos 2\gamma + 2(\sin\alpha\sin\gamma)^2 \end{pmatrix} \tag{5.19}$$

here $\theta_1=\alpha$, $\theta_2=\beta$ and $\theta_3=\gamma$. The parameters in terms of the elements of **N** are

$$\gamma = \pm\tfrac{1}{2}\cos^{-1}[N_{22} - N_{12}^2/(1 + N_{11})]$$
$$\beta = \pm\tfrac{1}{2}\cos^{-1}[N_{11} + N_{12}^2/(1 - N_{22})]$$
$$\alpha = \tan^{-1}\{-(\mathrm{sgn}\gamma)N_{12}/|[(1 + N_{11})(1 - N_{22})]^{\frac{1}{2}}|\}. \tag{5.20}$$

Sprung adopted the same procedure as Bryan, that is expressing **U** as in eq. (5.18) but argued that the expression for **N** is much simpler if $\theta_2=0$, i.e. leaving $\theta_1=\alpha$, $\theta_3=\mu$ and $\theta_4=\eta$. The matrix then becomes

$$\mathbf{N} = \begin{pmatrix} \cos 2\alpha & -\sin 2\alpha \sin\mu \\ -\sin 2\alpha \sin\mu & \cos^2\mu \cos 2\eta - \sin^2\mu \cos 2\alpha \end{pmatrix} \tag{5.21}$$

that is

$$\alpha = \pm\tfrac{1}{2}\cos^{-1}(N_{11}), \qquad \mu = \sin^{-1}[-N_{12}/(1 - N_{11}^2)^{\frac{1}{2}}],$$
$$\eta = \pm\tfrac{1}{2}\cos^{-1}[(N_{22} + \sin^2\mu\cos 2\alpha)/\cos^2\mu]. \tag{5.22}$$

Klarsfeld follows a closely related procedure to Bryan's, but using the variables ω, Γ and Γ' instead of the four parameters required in **U**, mainly because he was more concernedwith the matrix **N**. His parametrisation can be expressed in terms of the **U** matrix as (i.e. $\mathbf{U} = \mathbf{O}\mathbf{O}^{T}$)

$$\mathbf{O} = \exp(i\omega\underline{\sigma}_y)\exp[i\underline{\Gamma}_1(\Gamma' + \Gamma)]\exp[i\underline{\Gamma}_4(\Gamma' - \Gamma)], \tag{5.23}$$

where $\underline{\sigma}_y$ is the unsymmetric 4x4 Dirac matrix. The two parameters were further redefined as "eigen inelasticities" λ_1 and λ_2:

$$\lambda_1, \lambda_2 = \cos 2(\Gamma \pm \Gamma'), \tag{5.24}$$

thus producing an **N** matrix that looks like the form used in BB parametrisation, with ω acting like a mixing parameter, i.e.

$$\mathbf{N} = e^{-i\underline{\sigma}_y\omega} \cdot \begin{pmatrix} \lambda_1 & 0 \\ 0 & \lambda_2 \end{pmatrix} \cdot e^{i\underline{\sigma}_y\omega} \tag{5.25}$$

(here $\underline{\sigma}_y$ is the second Pauli spin matrix) giving

$$\omega = \tfrac{1}{2}\tan^{-1}[2N_{12}/(N_{11}-N_{22})]$$
$$\lambda_1 = \tfrac{1}{2}(N_{11} + N_{22} + 2N_{12}/\sin 2\omega)$$
$$\lambda_2 = \tfrac{1}{2}(N_{11} + N_{22} - 2N_{12}/\sin 2\omega). \tag{5.26}$$

The advantage of this form of parametrisation is that the trace and the determinant of $(1- S_e^+ S_e)$ depends on only two parameters. One can easily show that

$$\det(1- S_e^+ S_e) = (1- \lambda_1^2)(1- \lambda_2^2)$$
$$\text{trace}(1- S_e^+ S_e) = 2 - \lambda_1^2 - \lambda_2^2. \qquad (5.27)$$

The other much simpler approach to $\mathbf{N}$ is that of Melhem and Kermode, in which they parametrise the matrix in a much more convenient form as

$$\mathbf{N} = \begin{pmatrix} \cos\alpha & Q\sin\gamma \\ Q\sin\gamma & \cos\beta \end{pmatrix} \qquad (5.28)$$

where

$$Q = (1 - |N_{11} + N_{22}| + N_{11}N_{22})^{\frac{1}{2}} \qquad (5.29)$$

and

$$\alpha = \pm\cos^{-1}(N_{11}) \qquad \beta = \pm\cos^{-1}(N_{22}) \qquad \gamma = \sin^{-1}(N_{12}/Q). \qquad (5.30)$$

The most important advantage of this is form, is that it allows a much easier way of obtaining α, β and γ form the matrix $\mathbf{N}$. The expression for Q represents the curved surface in fig. 5.3. Note that the constrains on $\mathbf{N}$ in eq. (5.15) imposes a modulus on $N_{11} + N_{22}$ in the above expression.

One of the weaknesses of the above parametrisations in general, is that some parameters are undetermined for certain values of the elements of the $\mathbf{N}$ matrix. For example in some potentials, at the threshold of the fourth channel, where N_{22} takes the value of one while N_{12} becomes zero, β in Bryan's parametrisation is undetermined. In table 5.1, we show possible $\mathbf{N}$ matrices for which particular parameters are undetermined.

Table 5.1. **N** matrices for which previous parametrisations have an undetermined parameter.

Parametrisation	Condition	Undetermined parameter	Example[§]
Bryan	$N_{11} = -1$	γ	$\mathbf{N}_1$
	$N_{22} = 1$	β	$\mathbf{N}_2$
Klarsfeld	$N_{11} = N_{22}$ and $N_{12} = 0$	ω	$\mathbf{N}_3$
Melhem and Kermode	$Q = 0$	γ	$\mathbf{N}_2$
Sprung	$N_{11}^2 = 1$	μ	$\mathbf{N}_1$
	$N_{12}^2 = 1 - N_{11}^2$	η	$\mathbf{N}_4$

[§]Here:

$$\mathbf{N}_1 = \begin{pmatrix} -1 & 0 \\ 0 & p \end{pmatrix}; \quad \mathbf{N}_2 = \begin{pmatrix} p & 0 \\ 0 & 1 \end{pmatrix}; \quad \mathbf{N}_3 = \begin{pmatrix} p & 0 \\ 0 & p \end{pmatrix} \text{ and } \quad \mathbf{N}_4 = \begin{pmatrix} p & \sqrt{1-p^2} \\ \sqrt{1-p^2} & -|p| \end{pmatrix}$$

with $-1 \leq p \leq 1$.

In view of the problems associated with undetermined parameters, we propose an alternative parametrisation that determines all parameters for all possible values of the elements of the matrix **N**. In selecting these parameters we have to satisfy the following conditions:

1. Whenever there is only one absorptive channel, one of the parameters in **N** should always be zero. The off-diagonal element N_{12} should also be equal to Q (in eq. (5.28)), but it should have a definite sign unlike that of Melhem and Kermode where Q could either be ±ve.

2. The parameters should be well defined for what ever the values the elements of **N** take, unlike those in table 5.1.

3. The parameters should give us a feeling (measure) of what specific coupling they are accounting for.

Taking the above into consideration we (Kabir and Kermode [Kab 87a]) propose a parametrisation that is closely related to that of Melhem and Kermode in its simplicity and similar to those of Bryan and Sprung, in that one of the parameters is zero when only one absorptive channel is present. We propose that the N matrix should be parametrised as

$$\mathbf{N} = \begin{pmatrix} \cos 2\alpha & \sin(\phi + \xi) \\ \sin(\phi + \xi) & \cos 2\beta \end{pmatrix} \tag{5.31}$$

where

$$\xi = \sin^{-1}((\mathrm{sgn}N_{12})Q)$$

and

$$Q^2 = (1 - |N_{11} + N_{22}| + N_{11}N_{22})$$

giving

$$\alpha = \pm\tfrac{1}{2}\cos^{-1}(N_{11}) \qquad \beta = \pm\tfrac{1}{2}\cos^{-1}(N_{22})$$

$$\phi = \sin^{-1}(N_{12}) - (\mathrm{sgn}N_{12})\sin^{-1}Q. \tag{5.32}$$

The imposition of the sign of N_{12} on the parameter ξ allows the problem of Q being $\pm$ve to be overcome.

In the pure elastic case $\alpha = \beta = \phi = 0$, for one absorptive channel ϕ is zero and the off diagonal element of the **N** matrix is Q [Mel 83]. Compared with previous parametrisations, in the case of only one extra absorptive channel, our parametrisation is similar to those of Bryan and Sprung, in that one parameter associated with the coupling between the fourth (and higher) channel and the elastic channels is zero, unlike those of Klarsfeld, Melhem and Kermode where none of their parameters are zero to indicate no coupling to the fourth channel (except if Γ rather than λ is used for the Klarsfeld case).

For two or more absorptive channels our parametrisation is essentially an improvement on that of Melhem and Kermode and is simpler than all previous parametrisations, in addition to being well defined for all possible values of the **N** matrix. The parameter ϕ can be regarded as a direct measure of the coupling of the fourth (and higher) channel to the elastic channels and is obtained by the "subtraction" of Q from the off-diagonal element of **N**. The function Q accounts for the coupling of the third channel with the elastic channels. Therefore, for weak coupling to the fourth channel we expect ϕ to be very small.

5.5 APPLICATION OF THE PARAMETRISATIONS

One of the aims of parametrising the scattering matrix is to have parameters that would give us an insight into what is happening during the scattering process. Normally, we choose parameters that are smooth

functions of energy so that whenever a jump or discontinuity occurs at a particular energy, then such an event will signify a physical phenomena in the scattering. Having presented the various ways of expressing **S**, it is worthwhile to have a model that can be used to compare the various parameters as functions of energy. With this in mind, we consider a model and calculate the matrix $\mathbf{S}_e$. In particular, since the parameters δ_1, δ_2 and ε are well known parameters from the SYM form in the elastic case, the interest is on the matrix **N**. The model we choose for testing the parameters is a simple one. We assume a four channel scattering process in s-state.

To calculate the matrix $\mathbf{S}_e$, we solved a four coupled channel Schrodinger equation and calculated the **S** matrix at various energies. From $\mathbf{S}_e$ we can calculate the elements of **N** and apply the various forms of parametrisations discussed in the previous section.

The radial Schrodinger equation for a four coupled channel scattering in s-state is,

$$u_i''(r) - \sum_{j=1}^{4} V_{ij}(r)u_j(r) + \kappa_i^2 u_i(r) = 0 \qquad (5.33)$$

for i=1,2,3,4, here κ_i^2 is the energy for various channels defined as

$$\kappa_i^2 = \begin{cases} k_0^2 & \text{for the first channel} \\ k_0^2 - k_i^2 & \text{for other channels.} \end{cases}$$

where i represent the ith channel and k_i^2 is the threshold energy of the ith channel. The potential $V_{ij}(r)$ represent the coupling between the ith and jth channel. Since our aim is to investigate the energy dependence of the parameters in **N**, the particular shape of the potential is not important provided the elements of **N** are smooth. Therefore, we shall use the simplest potential —a square potential, defined as

$$V_{ij}(r) = V_{ji}(r) = \begin{cases} -V_{ij} & \text{for } r<a \\ 0 & \text{for } r>a \end{cases}$$

where a is the range of the potential. A similar calculation was made using a gaussian potential, but no difference in the results was obtained, we shall therefore not present the calculations here. We shall be using three potentials to investigate the energy dependences of the parameters.

In table 5.2, the numerical values of the three potentials are given. The three potentials were chosen such that the effect (if any) of bound states on the parameters can be investigated. We have chosen the first potential to have no bound states, while the second and the third potentials have one and two bound states respectively. The existence of bound states in the potentials was determined numerically using the procedure given in appendix A.

The first step towards calculating the scattering matrix is to solve the Schrodinger equation above (eq. (5.33)) using numerical methods. A numerical method for solving differential equations containing only second order derivative is the Cowell-Numerov method [Fro 70]. This method requires two initial conditions, the first being $u_i(0)=0$. For the second, there are four possibilities; $u_i(h) = h\delta_{ij}$ for $j=1,2,3,4$ where h is the step length of integration. Each one of these initial condition leads to a solution $u_i(r)$, when integrated from r=0 to r=a. Thus the wave function for each channel is a linear combination of the four solutions, which we may write as $u_{ij}(r)$ for $i,j=1,2,3,4$. At r>a, the solutions to $u_i(r)$ are the asymptotic functions. At r=a, we can match the four solutions with the asymptotic functions, four sets of equations were obtained as

$$\sum_{m=1}^{4} A_{ni} u_{jn}(a) = \delta_{ij} \cos(\kappa_i a) + M_{ij} \sin(\kappa_i a)/\kappa_i \quad \text{for } k_0^2 > k_i^2$$

$$\sum_{m=1}^{4} A_{ni} u_{jn}(a) = \delta_{ij} \cosh(\kappa_i a) + M_{ij} \sinh(\kappa_i a)/\kappa_i \quad \text{for } k_0^2 < k_i^2$$

Table 5.2. Coefficients, V_{ij}, for the square well potentials used. Threshold energies are: $k_2^2 = 0.0202$ fm^{-2}, $k_3^2 = 0.2002$ fm^{-2} and $k_4^2 = 0.8802$ fm^{-2}.

Potential (1)	1.50	0.45	0.85	1.35
(no bound state)	0.45	1.55	0.35	0.25
	0.85	0.35	1.60	0.15
	1.35	0.25	0.15	1.65
Range of the potential	a = 2.0 fm			
Potential (2)	1.50	0.65	0.75	0.95
(one bound state)	0.65	1.55	0.65	0.65
	0.75	0.65	1.60	0.65
	0.95	0.65	0.65	1.65
Range of the potential	a = 2.0 fm			
Potential (3)	1.60	0.35	0.25	0.25
(two bound states)	0.35	1.25	0.35	0.25
	0.25	0.35	1.70	0.35
	0.25	0.25	0.35	1.75
Range of the potential	a = 3.0 fm			

where M_{ij} are the elements of the **M** matrix (see [Ker 67]). There is another set of four equations for the derivatives. For i,j = 1,2,3,4 we have four sets of eight equations with 32 unknowns, i.e. the M_{ij} and A_{ij}. The **M** matrix is obtained by solving these equations, and the **S** matrix determined from

$$S = 1 + 2ik^{\frac{1}{2}} \cdot (M - ik)^{-1} \cdot k^{\frac{1}{2}} \qquad (5.34)$$

where **k** is a 4x4 diagonal matrix with elements κ_i.

The submatrix S_e is the first 2x2 block of **S**. From S_e the **N** matrix along with δ_1 ,δ_2 and ε were obtained using Bryan's [Bry 84] method of extracting the phases from S_e. From the elements of the **N** matrix each set of parameters are calculated. The energy dependence of these parameters for the different potentials is shown in figs. 5.4 to 5.6.

The graphs show that at energies below the third channel threshold the parameters behave as expected. Above the third channel threshold the new parametrisation and those of Bryan and Sprung behave satisfactorily by having one of the parameters equal to zero except when **N** takes any of the values given in table 5.1. However, λ_1 in Klarsfeld's parameters is unity not zero (but Γ is zero). Also, changes in the sign of N_{12} makes the Melhem and Kermode parameter γ fluctuate between $\pm\frac{1}{2}\pi$ because $Q = |N_{12}|$ and whenever Q=0, γ is undetermined.

When the fourth channel is open all parametrisations have their parameters describing the scattering varying reasonably smoothly with energy except when **N** is one of the special cases given in table 5.1. Klarsfeld's "inelastic mixing parameter" ω was allowed to vary smoothly by adding $\pm n\pi$, where n is an integer.

Near the threshold of the fourth channel N_{12} tends to zero while N_{11} or N_{22} tends to unity (at the threshold N_{12} is zero and N_{11} or

N_{22} is unity). We notice that, since interchanging the diagonal elements of $\mathbf{N}$ does not change $\det(1-\mathbf{N}^2)$ or $\mathrm{trace}(1-\mathbf{N}^2)$, the values of N_{11} could be those of N_{22} and vice versa, this results in some ambiguities at the threshold of the fourth channel. The values of the parameters α (Bryan), ω (Klarsfeld), γ (Melhem and Kermode) and μ (Sprung) are not well defined at the threshold (for example α (Bryan) could be either zero or $\frac{1}{2}\pi$ depending on N_{22}). However our parameters are well defined at threshold.

One of the advantages of our parametrisation is that ϕ, as a direct measure of the coupling between the fourth and the elastic channels, is very small for potentials (2) and (3) even beyond the threshold of the fourth channel, and for potential (1) it is not small. This is because of the weak coupling to the fourth channel in the first two cases whereas for potential (1) there is a strong coupling to the fourth channel (i.e., $V_{14}(=1.35)$ is greater than V_{13} or V_{23}). When the energy dependence of $\mathrm{trace}(1-\mathbf{N}^2)$, a measure of the absorption cross section, is compared with the trace when the threshold of the fourth channel is large, for example $k_4^2 = 5.8\ \mathrm{fm}^{-2}$ (i.e. the case of only one absorptive channel), the difference for the potentials (2) and (3) was less than 10% whereas in potential (1) it was about 50%. This suggests that ϕ is a measure of the amount of flux lost to the fourth channel.

In plotting the graphs it was assumed that whenever a parameter was undetermined a value was taken so as to make the curves continuous, thus giving the smooth energy dependence shown in the graphs. Also, Melhem and Kermode's parameter γ was assumed to be constant ($\frac{1}{2}\pi$ in fig. 5.4 and 5.5, and $-\frac{1}{2}\pi$ in fig. 5.6) below the threshold of the fourth channel to avoid any fluctuation.

From the figures, the elements of the $\mathbf{N}$ matrix are clearly smooth functions of energy for all the three potential despite the fact that

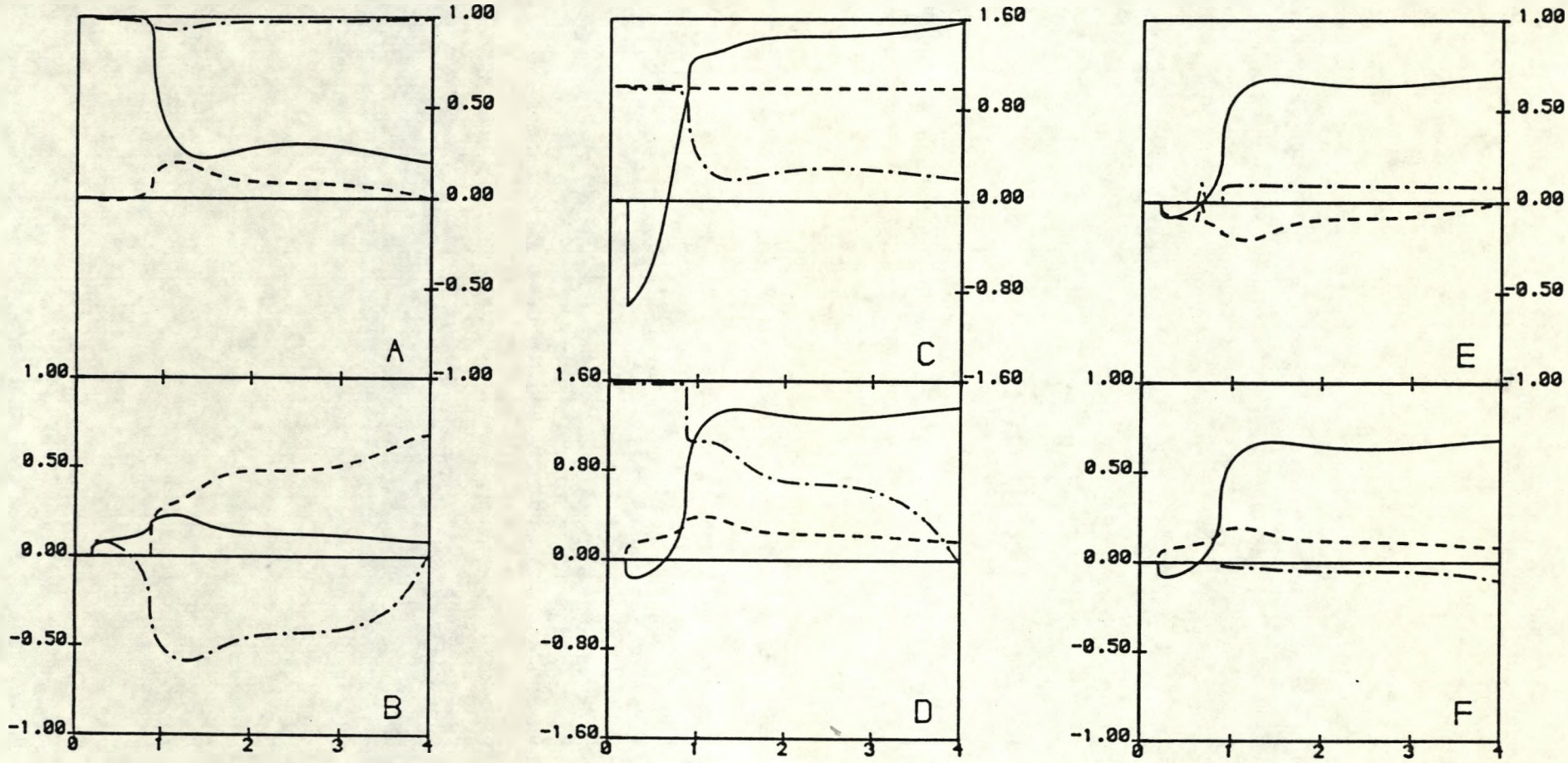

Fig. 5.4 The energy dependence (in fm^{-2}) of various parametrisations of the N matrix for square potential (1), which supports no bound state (see table 5.2). Graph (A) shows the elements of N matrix (N_{11} ; full curve: N_{12} ; broken curve: N_{22} ; chain curve), (B) shows Bryan's parameters (γ ; full curve: β ; broken curve: α ; chain curve), (C) shows those of Klarsfeld (ω ; full curve: ρ_1 ; broken curve: ρ_2 ; chain curve), (D) shows those of Melhem and Kermode (α ; full curve: β ; broken curve: γ ; chain curve), (E) shows those of Sprung (α ; full curve: μ ; broken curve: η ; chain curve) and (F) shows our new parameters (α ; full curve: β ; broken curve: ϕ ; chain curve). All angles are given in radians.

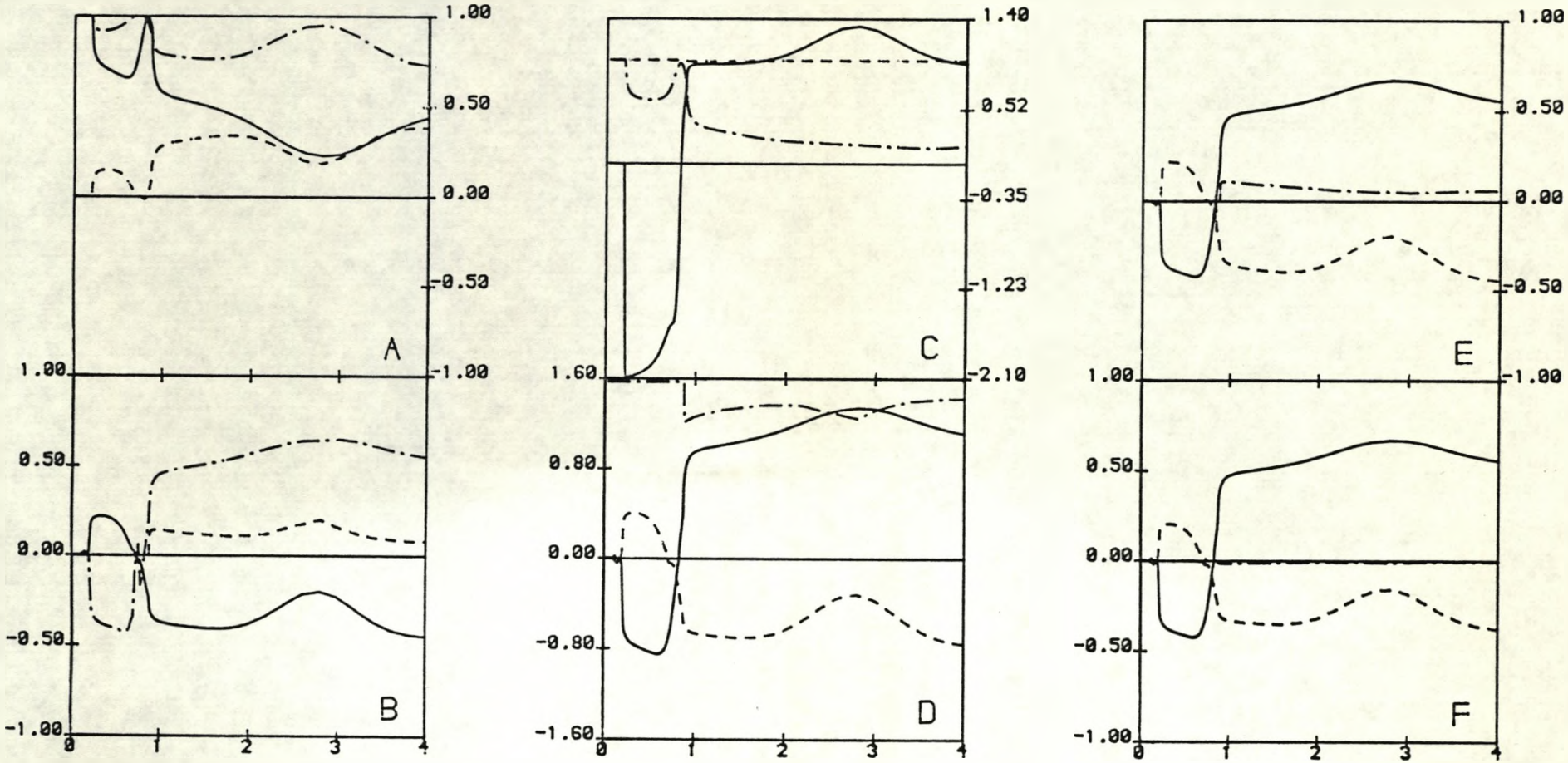

Fig. 5.5 As in fig. 5.4 but with potential (2) which supports one bound state.

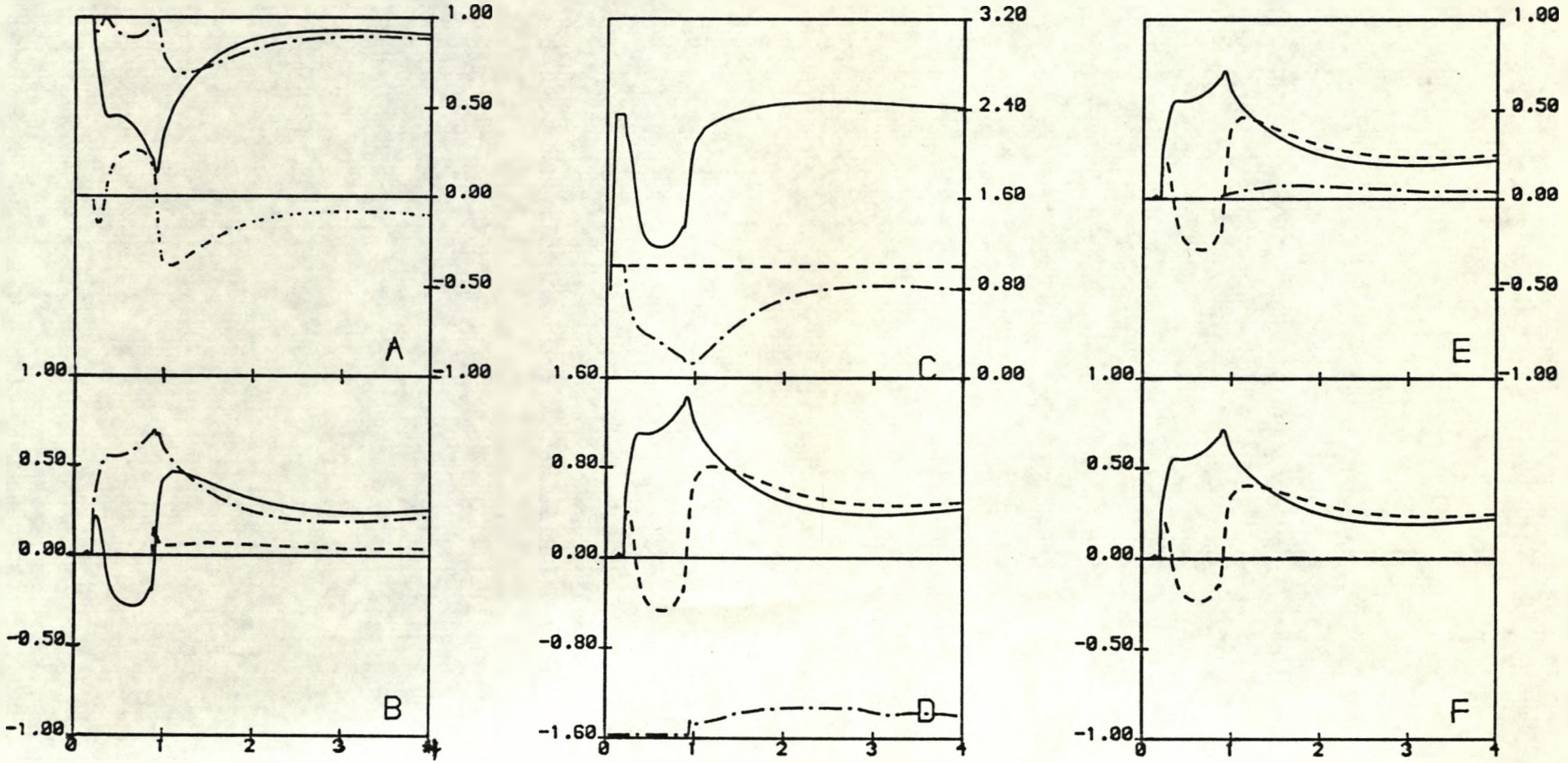

Fig. 5.6 As in fig. 5.4 but with potential (3) which supports two bound states.

the potentials contain different number of bound states. Therefore, we conclude that there is no clear bound state effect on the elements of $\mathbf{N}$ and the variables in all the parametrisations considered. It should also be noted that the behaviour of the parameters is not dependent on the type of potential.

Another problem we encountered with previous parametrisations is that when applied to the set of data given by Arndt et al [Arn 83] for nucleon-nucleon scattering up to 1 GeV, it was observed that in some instances the modulus of the arguments of the inverse of sine or cosine was slightly greater than 1. This, of course, was due to experimental errors. For our parametrisation, ϕ is determinable but its error bars would be reduced by the constraint $\det(1-\mathbf{N}^2) \geq 0$.

5.6 SUMMARY

To summarise the chapter, we have seen that the elastic component of the nucleon-nucleon scattering matrix can be written in a parametrised form in eq. (5.13). It is a symmetric matrix, and also unitary at energies below the inelastic threshold (with $\mathbf{N}$ being the unit matrix). At energies above the threshold, the matrix is not unitary but satisfies the inequalities of eqs. (5.14) and (5.15). In this case the matrix $\mathbf{N}$ accounts for the inelasticity of scattering. This matrix is real and symmetric, it requires three parameters to define for two or more extra channels present but two when there is only one additional channel. There have been many suggestions on how to describe this matrix. In this chapter, we have considered them and their weaknesses. We have also presented a new form of parametrising the matrix which overcomes these weaknesses. Finally, a model comparison for all the parametrisations was made in which the energy dependence of each parametrisation was investigated.

CHAPTER 6

THE THREE CHANNEL SCATTERING MATRIX.

6.1 INTRODUCTION

In the previous chapter the scattering matrix for a general n-channel scattering process was discussed. The matrix $\mathbf{S}$ is symmetric and unitary requiring $N=n(n+1)/2$ independent real parameters to define it uniquely. There are two ways of writing the matrix in terms of the required parameters. The one we have presented in the previous chapter is parametrising the matrix by selecting N parameters and then expressing the elements of $\mathbf{S}$ in terms of these parameters. The other alternative way is to write the matrix in its usual complex form, containing 2N variables, and then use the unitary condition on $\mathbf{S}$ to find the relationships between the N variables. That is, since we require N independent parameters to specify $\mathbf{S}$, we can express the other N variables in terms of the chosen parameters. The procedure of expressing these variables is more tedious than merely choosing N independent parameters (as in the previous chapter). However, in section 5.2, we have given a procedure that would reduce some of this difficulties, by extracting the set of diagonal phases $\{\delta_i\}$, thus leaving $\hat{n}=n(n-1)/2$ parameters in $\hat{\mathbf{S}}$. That is, by writing the scattering matrix as

$$\mathbf{S} = \mathbf{U}\hat{\mathbf{S}}\mathbf{U}, \tag{6.1}$$

where the δ_i are contained in the unitary diagonal matrix $\mathbf{U}$. With this, one simply use the unitarity condition on the matrix $\hat{\mathbf{S}}$ to obtain the relationships between the elements of the matrix.

For example for n=2, the solution is quite trivial. Writing the matrix as

$$S = \begin{pmatrix} e^{i\delta_1} & 0 \\ 0 & e^{i\delta_2} \end{pmatrix} \begin{pmatrix} \eta_1 & N_{12}e^{i\beta_{12}} \\ N_{12}e^{i\beta_{12}} & \eta_2 \end{pmatrix} \begin{pmatrix} e^{i\delta_1} & 0 \\ 0 & e^{i\delta_2} \end{pmatrix}$$

we obtain from $SS^{+} = 1$, $\beta_{12} = \pi/2$ and

$$\eta = \eta_1 = \eta_2 = \sqrt{1 - N_{12}^2}. \qquad (6.2)$$

Thus the matrix may be specified by δ_1, δ_2 and N_{12}. This is similar to the SYM form by letting $\eta = \cos\varepsilon$.

According to Horn's theorem [Hor 54], for an nxn unitary matrix ($n \geq 2$) if the diagonal elements are written as $S_{ii} = \eta_i \exp(2i\delta_i)$, i.e. $|S_{ii}| = \eta_i$ then

$$0 \leq \eta_i \leq 1 \quad \text{and} \quad \sum_{i}^{n} \eta_i - 2\eta_j \leq n-2$$

for i,j=1,2,3,...,n. This puts bounds on the amplitudes. Thus the substitution $\eta = \cos\varepsilon$ above is within the bounds.

For n=3, Waldenstrom [Wal 74 & 81] presented some of the relationships between the elements of the matrix, and used Horn's theorem to put bounds on the elements of the matrix. The aim of this chapter is to derive the relationships between the elements of the matrix, in a similar fashion to that of Waldenstrom, but it will be shown [Kab 87b] that they lead to some interesting relationships not obtained by Waldenstrom. We shall also add more boundary conditions on the parameters (elements), this is borne out of our numerical application of the problem [Kab 87c].

For the 3x3 S matrix, the matrix $\hat{S}$ (eq. (6.1)), contains three sets of variables, each set has three parameters, thus there is a one to one mapping of the elements in the sets $\{\eta_i\}$, $\{\beta_{ij}\}$, and $\{N_{ij}\}$. Since $\hat{n}=3$, then we can select any set to represent the N=6 independent pa-

rameters required to specify S. Hence the diagonal elements in the 3x3 matrix alone are sufficient to specify the matrix.

For $n \geq 4$, the choice of the parameters in S are limited compared to the n=3 case, we have to select either the set $\{\beta_{ij}\}$ or $\{N_{ij}\}$. Thus the diagonal elements alone are not sufficient to specify the S matrix. Of course one can always choose a mixture of the all the parameters to obtain the required N=n(n+1)/2 parameters. However, this procedure involves quite tedious algebraic manipulations that may not necessarily be worth it, since there is a much easier way of specifying the scattering matrix by choosing the required number of parameters and write the matrix in terms of those parameters (eg Bryan's parametrisation of the 4x4 matrix [Bry 81]). Therefore, we shall not attempt to do this.

6.2 THE RELATIONSHIPS BETWEEN THE ELEMENTS OF THE 3X3 MATRIX.

The symmetric matrix can be written in the same form of eq. (6.1) that is,

$$S = \begin{pmatrix} e^{i\delta_1} & 0 & 0 \\ 0 & e^{i\delta_2} & 0 \\ 0 & 0 & e^{i\delta_3} \end{pmatrix} \begin{pmatrix} \eta_1 & \gamma_{12} & \gamma_{13} \\ \gamma_{12} & \eta_2 & \gamma_{23} \\ \gamma_{13} & \gamma_{23} & \eta_3 \end{pmatrix} \begin{pmatrix} e^{i\delta_1} & 0 & 0 \\ 0 & e^{i\delta_2} & 0 \\ 0 & 0 & e^{i\delta_3} \end{pmatrix}$$

where $\gamma_{ij} = N_{ij}\exp(i\beta_{ij})$ and η_i is a real parameter.

Thus,

$$S_{ii} = \eta_i \exp(2i\delta_i) \tag{6.3a}$$

and

$$S_{ij} = N_{ij} \exp[i(\delta_i+\delta_j+\beta_{ij})] \quad i \neq j. \tag{6.3b}$$

Note that due to the symmetry of the matrix the subscripts ij and ji are the same, we shall sometimes use both notations.

The unitarity condition $S^{+}S = 1$ gives, for the diagonal equations,

$$\sum_{j \neq i} N_{ij}^{2} + \eta_i^{2} = 1 \qquad i=1,2,3 \tag{6.4}$$

and for the off-diagonal equations

$$N_{12}[\eta_1 \exp(i\beta_{12}) + \eta_2 \exp(-i\beta_{12})] = N_{13}N_{23}\exp[i(\pi+\beta_{23}-\beta_{13})] \qquad (6.5)$$

and cyclic (1→2→3→1) and complex conjugate. Squaring and adding the real and the imaginary parts of eq. (6.5), we have

$$N_{12}^2(\eta_1+\eta_2)^2\cos^2\beta_{12} + N_{12}^2(\eta_1-\eta_2)^2\sin^2\beta_{12} = N_{13}^2N_{23}^2$$

$$= N_{13}^2N_{23}^2(\cos^2\beta_{12} + \sin^2\beta_{12}).$$

Thus

$$\tan^2\beta_{12} = \frac{[N_{12}^2(\eta_1+\eta_2)^2 - N_{13}^2N_{23}^2]}{[N_{13}^2N_{23}^2 - N_{12}^2(\eta_1-\eta_2)^2]}. \qquad (6.6a)$$

Similarly for the β_{13} and β_{23}, from the cyclic relationships we have

$$\tan^2\beta_{13} = \frac{[N_{13}^2(\eta_1+\eta_3)^2 - N_{12}^2N_{23}^2]}{[N_{12}^2N_{23}^2 - N_{13}^2(\eta_1-\eta_3)^2]}, \qquad (6.6b)$$

and

$$\tan^2\beta_{23} = \frac{[N_{23}^2(\eta_2+\eta_3)^2 - N_{12}^2N_{13}^2]}{[N_{12}^2N_{13}^2 - N_{23}^2(\eta_2-\eta_3)^2]}. \qquad (6.6c)$$

To eliminate the N_{ij} in the above equations, i.e. expressing the β_{ij} in terms of the η_i, we substitute the solution to eq. (6.4) namely,

$$2N_{ij}^2 = (1-\eta_i^2-\eta_j^2-\eta_3^2) + 2\eta_k^2, \qquad (i,j,k)=(1,2,3) \qquad (6.7)$$

into the equations above. Note that (i,j,k)=(1,2,3) represents a cyclic mapping, i.e. for (i,j,k) the allowed values are only (1,2,3), (2,3,1) and (3,1,2). We have, after much algebra, in a compact form

$$\tan^2\beta_{ij} = AB_i/B_jB_k \qquad (i,j,k)=(1,2,3) \qquad (6.8)$$

where

$$A = (\eta_1+\eta_2+\eta_3)^2-1, \qquad (6.9)$$

$$B_i = 1-(\eta_i+\eta_j-\eta_k)^2 \qquad (i,j,k)=(1,2,3). \tag{6.10}$$

The eqs. (6.8) to (6.10) allow us to express the $\{\beta_{ij}\}$ in terms of the $\{\eta_i\}$. We shall now consider the inverse relationships. From the expressions of A and the B_i, we can write the η_i as

$$2\eta_1 = (1-B_1)^{\frac{1}{2}} + (1-B_3)^{\frac{1}{2}} \tag{6.11}$$

$$2\eta_2 = (1-B_2)^{\frac{1}{2}} + (1-B_1)^{\frac{1}{2}} \tag{6.12}$$

$$2\eta_3 = (1-B_3)^{\frac{1}{2}} + (1-B_2)^{\frac{1}{2}} \tag{6.13}$$

$$(A+1)^{\frac{1}{2}} = (1-B_1)^{\frac{1}{2}} + (1-B_2)^{\frac{1}{2}} + (1-B_3)^{\frac{1}{2}}. \tag{6.14}$$

The latter expression can be written in a more convenient form, by dividing by $A^{\frac{1}{2}}$, and writing t for 1/A,

$$(1+t)^{\frac{1}{2}} = (t-b_i)^{\frac{1}{2}} + (t-b_j)^{\frac{1}{2}} + (t-b_k)^{\frac{1}{2}} \tag{6.15}$$

where (from eq (6.8))

$$b_i = B_i/A = |\cot\beta_{ik}\cot\beta_{jk}| \qquad (i,j,k)=(1,2,3) \tag{6.16}$$

Note that b_i has to be positive, thus necessitating the introduction of a modulus in the right hand side of the equation. We can also define

$$\mu_i = 1 - b_i + b_j + b_k = 8\eta_i\eta_j/A \qquad (i,j,k)=(1,2,3) \tag{6.17}$$

which are obtained by expanding eqs. (6.9) and (6.10). We can now write the expression for η_i in terms of the β_{ij} from the above equation as,

$$\eta_i^2 = A\mu_i\mu_k/8\mu_j \qquad (i,j,k)=(1,2,3) \tag{6.18}$$

where A can be obtained from

$$t = 1/A = (\mu_1\mu_2 + \mu_1\mu_3 + \mu_2\mu_3)/8\mu_1\mu_2\mu_3 - 1 \tag{6.19}$$

Therefore, the above expressions allow us to express $\{\eta_i\}$ in terms of $\{\beta_{ij}\}$. The equations we obtained are indeed quite interesting particularly their cyclic nature i.e. (i,j,k)=(1,2,3).

6.2.1 BOUNDS ON THE PARAMETERS.

According to Horn's theorem, the bound on $\{\eta_i\}$ are

$$0 \leq \eta_i \leq 1 \text{ and } \quad \eta_1 + \eta_2 + \eta_3 - 2\eta_i \leq 1. \tag{6.20}$$

for i=1,2,3. The lower bound on the last expression is not zero but -1. For example consider the case $\eta_1=1$ and $\eta_2=\eta_3=0$. Thus in a more explicitly form we have

$$-1 \leq (\eta_1 + \eta_2 + \eta_3) - 2\eta_i \leq 1. \tag{6.21}$$

Similarly from eq. (6.4), it follows that

$$0 \leq N_{ij} \leq 1 \tag{6.22}$$

Also, the following cases can be obtained from eqs. (6.4), (6.5) and the other cyclic set of eq. (6.5) (not shown), i.e. when:

$\eta_3 = 0$ then $\eta_1 + \eta_2 = 1$;

$\eta_2 = 0$ then $\eta_1 + \eta_3 = 1$;

$\eta_1 = 0$ then $\eta_2 + \eta_3 = 1$;

in a compact form we have, when

$$\eta_i = 0 \text{ then } \eta_j + \eta_k = 1 \qquad (i,j,k)=(1,2,3). \tag{6.23}$$

Similarly, when

$$\eta_i = 1 \text{ then } \eta_j = \eta_k \qquad (i,j,k)=(1,2,3). \tag{6.24}$$

The eq. (6.24) corresponds to a complete decoupling of one of the channels. For example, if the third channel is not present, then $\eta_3=1$ and implies that $N_{13}= N_{23}= 0$, which also leads to eq. (6.2), i.e. $\eta_1 = \eta_2 = \sqrt{1- N_{12}^2}$.

These equations give six lines in a (η_1, η_2, η_3) plane, which represent the set of bounds that form the Waldenstrom pyramid with the vertex at (1,1,1) as shown in fig. 6.1. This point represent the elastic limit, where all the off diagonal elements vanish i.e. $N_{ij} = 0$. The equation for the three planes of the pyramid are the equality in Horn's inequalities (eq. (6.20)), i.e.

$$(\eta_1 + \eta_2 + \eta_3) - 2\eta_i = 1 \qquad \text{for } i=1,2,3. \tag{6.25}$$

and the bottom surface (hidden in the figure) is

$$\eta_1 + \eta_2 + \eta_3 = 1. \tag{6.26}$$

Thus points inside the pyramid are bounded by

$$(\eta_1 + \eta_2 + \eta_3) - 2\eta_i \leq 1 \qquad \text{for } i=1,2,3,$$

and

$$\eta_1 + \eta_2 + \eta_3 \geq 1.$$

Thus, the values of η_i cannot have arbitrary values but bounded by a pyramid of fig. 6.1.

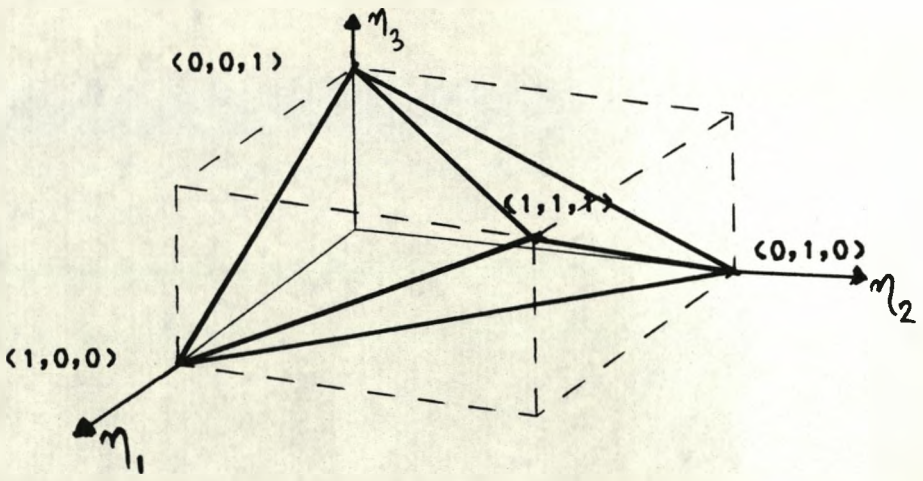

Fig. 6.1 The Waldenstrom pyrmaid in (η_1,η_2,η_3) space.

From these relationships, we can now consider the possible ways of parametrising the scattering matrix. For the full 3x3 matrix, six real parameters are required to specify the matrix uniquely. If three of those are taken to be the phases of the diagonal elements (i.e. twice the real phase shifts), the other three can be taken from the set of: (a) diagonal amplitudes (η_i); (b) off-diagonal phases (β_{ij}); (c) off-diagonal amplitudes (N_{ij}) or (d) η_1, η_2 and N_{12}.

The procedure for obtaining the complete **S** matrix for each of these cases is as follows:

Case (a). Calculate the amplitudes N_{ij} from the solutions to eq. (6.4), i.e.

$$N_{12}^2 = (1 - \eta_1^2 - \eta_2^2 + \eta_3^2)/2 \qquad (6.27)$$

and cyclic. Calculate the phases β_{ij} from eq. (6.8)-(6.10).

Case (b). Calculate the amplitudes η_j from eqs. (6.16)-(6.19) and the amplitudes N_{ij} from eq. (6.27)

Case (c). Calculate the amplitudes η_i from

$$\eta_1^2 = 1 - N_{12}^2 - N_{13}^2 \qquad (6.28)$$

and cyclic, which is eq. (6.4). The phases β_{ij} follow from eqs. (6.8)-(6.10).

Case (d). Calculate

$$N_{13}^2 = 1 - \eta_1^2 - N_{12}^2 \qquad (6.29a)$$

$$N_{23}^2 = 1 - \eta_2^2 - N_{12}^2 \qquad (6.29b)$$

$$\eta_3^2 = \eta_1^2 + \eta_2^2 + 2N_{12}^2 - 1 \qquad (6.29c)$$

and then the phases β_{ij} as above.

This may be particularly useful when the inelastic 2x2 submatrix S_e is considered. The five parameters that specify S_e are δ_1, δ_2, η_1, η_2 and N_{12}. However, we note that the phase shifts δ_1 and δ_2 are

not the two (bar) phase shifts in the usual expression for S_e. Without a consideration of the 4x4 matrix, it is not possible to see how the sixth parameter in the general parametrisation of S_e is not free in the three-channel case. We shall now investigate the energy dependence of these parameters.

6.4 NUMERICAL APPLICATIONS

To investigate the energy dependence of the parameters $\{\eta_i\}$, $\{\beta_{ij}\}$ and $\{N_{ij}\}$, we use a numerical method similar to the one used in the previous chapter to calculate the scattering matrix. Here only three channels are coupled, so the Schrodinger equation is a set of three coupled differential equations. We calculated the scattering matrix by solving the Schrodinger equation of eq. (5.33) but with $V_{4i} = 0$ (i=1,2,3,4) and k_4 set to a large number, which means that there is no coupling to the fourth channel. Thus we are effectively solving a three channel problem. With these values, the solution to the Schrodinger equation gives $u_4(r)=0$, $S_{4i}=S_{i4}=0$ for i=1,2,3, and $S_{44}=1$ at all energies. We also set the threshold of the third channel to be small, so that at all energies all the three channels are opened. For this case, a rigorous test of the parameters in S is not needed, because the equations are valid for three channels only. Therefore, the scattering matrices are calculated when $\kappa_i > k_3$ in eq. (5.33).

After calculating the S matrix, we used eqs. (6.3a) and (6.3b) to calculate the diagonal amplitudes and the off-diagonal phases. These values were used in the eqs. (6.8)-(6.10) to calculate β_{ij} and eq. (6.18) to calculate the η_i. The values we obtained were all found to be correct. In fig. 6.2 we show the energy dependence of these parameters for a square potential with one bound state. The existence of a bound state in the potential was determined using the procedure given

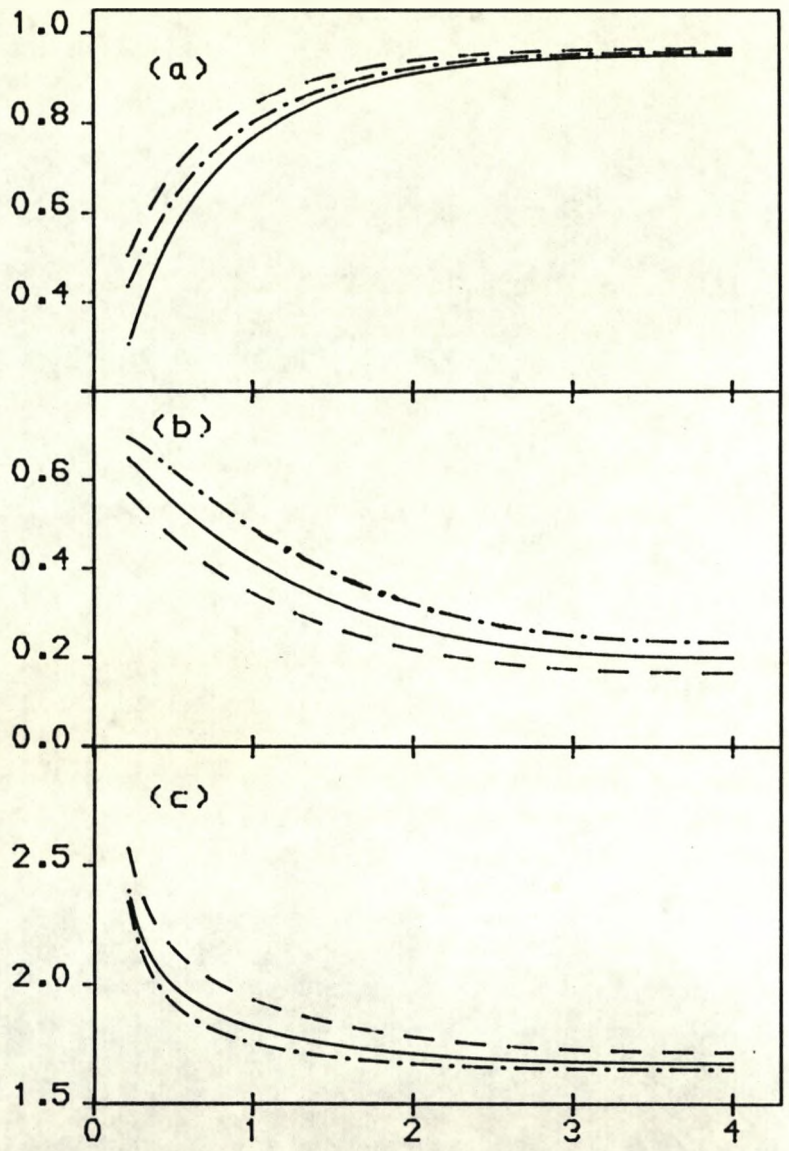

Fig. 6.2 The energy dependence (in fm^{-2}) of: (a) η_i, the diagonal amplitudes. (b) N_{ij}, the off-diagonal amplitudes. (c) β_{ij}, the off-diagonal phases. The full curves represent i = 1 and j = 2. The dashed curves reperesent i = 2 and j = 3 The dot-dashed curves represent i = 3 and j = 2. For a three coupled channel square well potential V_{ij} (fm^{-2}) where;

$$V_{ij} = \begin{pmatrix} 0.33 & 0.23 & 0.27 \\ 0.23 & 0.30 & 0.19 \\ 0.27 & 0.19 & 0.28 \end{pmatrix};$$

and a= 2 fm, which supports a bound state.

in appendix A. As shown in the figure, the parameters are all smooth functions of energy, thus any of them can be used to specify the scattering matrix. They are also not affected by the existence of a bound state in the potential, like those in the previous chapter.

6.5 CONCLUSION

The relationships between the elements of a 3x3 symmetric matrix, we derived here, are indeed interesting and unique for only a three channel matrix. The parameters, as was shown, do not take arbitrary values, rather they are bounded. In particular, the diagonal amplitudes are bound by the Waldenstrom pyramid. This is not the first time we have seen the unique properties of the three channel scattering matrix. In the previous chapter, it is shown that the elastic component $\mathbf{S}_e$ of an nxn scattering matrix contains a real matrix $\mathbf{N}$ which describes the coupling to the inelastic channels. This matrix requires three independent real parameters to specify when the scattering involves more than three channels. However, it requires only two parameters for a three channel process and in this case the off diagonal element becomes $N_{12} = Q = (1-|N_{11}+ N_{22}|+ N_{11}N_{22}|)^{\frac{1}{2}}$. The matrix also satisfies $\det(1-\mathbf{N}^2) = 0$ for the three channel process and its possible values are points only on the surface of the Kermode and Cooper geometrical figure (see fig. 5.3).

In conclusion, the relations that we have presented in this chapter will prove useful in checking the numerical solutions of the Schrodinger equation in the case of three open channels. Also, in the construction of the $\mathbf{S}$ matrix from experimental data, the formulae

(6.8)-(6.10) and (6.18) and (6.19) will provide information as to whether the physical process involves three channels (the formulae are valid) or four or more channels (the formulae are not valid).

CHAPTER 7

CONCLUDING REMARKS AND SUMMARY

Section I.

In this thesis we have presented a satisfactory explanation to the mechanism responsible for the oscillatory structure observed in the fusion excitation function of light heavy-ions (below the f-shell). These ions were classified into two groups, the symmetric and nonsymmetric systems, and a further subdivision in terms of spinless and non-zero spin systems was made.

For the symmetric spin zero systems, experimental measurements reveal that the oscillations appeared in systems with reduced mass not greater than that of $^{20}Ne + ^{20}Ne$ system. In these systems, because of the symmetrisation of the system, the odd partial waves do not contribute. The oscillations appear because of the difference in the barrier heights of two successive even partial waves. For the lighter ions, this difference is large (for the lower-ℓ), but for the heavier ions the difference is small. That is why the excitation functions for the symmetric heavier ions possess no oscillations. It was demonstrated [Pof 83] that the curvature of the Coulomb barrier is important in determining the sharpness of the cut-off of the transmission coefficient as a function of the angular momentum of the system; a sharp transmission coefficient is essential in reproducing the oscillations. Nuclear potential with large surface diffuseness produce such transmission coefficients.

For the symmetric non-zero spin systems, for which apart from the $^{14}N + ^{14}N$ system no experimental measurements have been made to date, we have demonstrated that using the symmetrisation of the system both the even and odd partial waves contribute to the fusion reaction, but

not in equal weight. Using a simple approximation to the transmission coefficient, we showed that oscillations are likely to appear in a system of two light spin-$\frac{1}{2}$ nuclei. Oscillations may also appear in spin-1 bosons, if the reduced mass of the system is less than that for the $^{14}N + ^{14}N$ system. For other systems, no oscillations are expected. These deductions are quite interesting and would require experiments to confirm.

For the nonsymmetric ions, we have shown that for systems in which the interacting nuclei differ by one or few nucleons, the oscillations appear because of elastic transfer of a valence particle between two identical cores. This transfer, observed in the elastic scattering, is evident at large angles where anomalously large scattering cross sections were observed. The large angle scattering cross sections were reproduced using a parity dependent potential that describes the elastic transfer mechanism. The same potential was used in reproducing the fusion oscillations. Without this elastic transfer, there would be no oscillations in the fusion excitation function. That is why some other nonsymmetric systems that differ by few nucleons, but with no evidence of elastic transfer process, possess no oscillations. It was argued that the binding energy and the spin of the valence particle are important. This explains why the $^{12}C + ^{16}O$ and $^{12}C + ^{11}B$ systems have pronounced oscillations in the excitation functions, whereas $^{12}C + ^{13}C$ has very little structures. For this reason also, oscillations may be observed in the fusion excitation function of $^{24}Mg + ^{23}Na$ system, even though the reduced mass is quite large and oscillations were neither observed in $^{24}Mg + ^{24}Mg$ nor do we expect any in the $^{23}Na + ^{23}Na$ system (because $I = 3/2$).

In fitting the fusion cross section data, we showed that it is essential for the transmission coefficient to have a sharp cut-off in

ℓ-space. This is realised by using a large surface diffuseness for the real potential. For other systems that do not possess oscillations in the excitation function, the use of a large surface diffuseness is still justifiable, as we illustrated in the fit to σ_f for $^{14}N + ^{14}N$ system. The use of large a_r is also appropriate in the elastic scattering of many heavy-ions like $^{28}Si + ^{28}Si$, where the the SCO model is a good description of the scattering. We have also illustrated that to reproduce oscillations in other nonsymmetric ions, a mechanism is required that would shift the barrier heights of odd-even partial waves. It is this shift in the barrier heights that brings the oscillations. An example of this was the fit we made for $\alpha + ^{40}Ca$ system.

The fits to the fusion excitation functions, we made, have illustrated that, fusion reaction could provide valuable information on the radial dependence of the nucleus-nucleus interaction potential, particularly it can be used to verify some theoretical potentials commonly used. For example in the fits to the cross sections for: $^{12}C + ^{16}O$; $^{12}C + ^{24}Mg$; $\alpha + ^{40}Ca$ and $^{14}N + ^{14}N$ systems, we have shown that the conventional Woods-Saxon potentials do not adequately describe the nuclear potentials of these systems. We solved the problem by using the sum of two Woods-Saxon terms for some of these systems and for other using a Woods-Saxon squared. The potential described by the sum of the two Woods-Saxon terms requires more parameters compared with a conventional Woods-Saxon potential. Therefore, it is not the most convenient form of describing the nuclear potential. However the use of such a potential stress that a slight generalisation of the standard Woods-Saxon appears necessary. Further work can be directed into investigating the most convenient form of describing the nuclear potential.

In this thesis, it has also been shown that it is possible to reproduce the oscillations in fusion excitation function while at the same time obtaining a satisfactory fits to the elastic scattering cross sections. We demonstrated that the real potential is the same in both processes, but the imaginary potentials are different. The imaginary potential required for the fusion is confined to the interior of the real interacting barrier and it is part of a larger imaginary potential required to for the elastic scattering. An important result we showed is that the parity dependence required in fitting the anomalous large angle scattering cross sections is consistent with that required to fit the fusion oscillations. This was demonstrated in the $^{12}C + ^{16}O$ and $^{12}C + ^{13}C$ systems, where the large angle scattering cross section were reproduced satisfactorily.

In the final analysis, this thesis has successfully explained the mechanism that brings fusion oscillations in some light heavy-ions. The model presented was also used in predicting oscillations in some other systems.

Section II

In this section we have shown that the parametrisation of the various scattering matrices reveals some interesting relationship between the elements of the matrices. We showed that, the unitary 3x3 S matrix is particularly special because it requires six independent real parameters which can be constructed from appropriate combinations of the three real amplitudes and the three real phases of the three diagonal or three off-diagonal elements. Additionally, if this matrix is written in a form similar to that of Waldenstrom, then the diagonal amplitude, the off-diagonal amplitude and phases have interesting cy-

clic relationships. The diagonal amplitudes were bounded by the Waldenstrom pyramid as shown in fig. 6.1.

The 4x4 **S** matrix, which requires ten parameters to specify, has four real amplitudes (phases) for the diagonal elements and six real amplitudes (phases) for the off-diagonal elements. It was shown that the choice of the free parameters for the 4x4 case is not as wide as that for the 3x3 case. This matrix, was parametrised by Bryan [Bry 81] and the elastic component of matrix was parametrised in a form similar to the "bar phase shift convention" of Stapp et al [Sta 57]. But the elastic component now contains a matrix **N** that describes the coupling between the two elastic and the inelastic channels. The matrix **N**, which is real and symmetric, requires three parameters if there are more than one inelastic channel present, but two for one inelastic channel. The possible values of the matrix were represented by the Kermode and Cooper geometrical model (see fig. 5.3). This matrix has been parametrised in various ways. We have presented the parametrisations suggested in recent years and we have applied them to a four coupled channel potential wells. We showed that when only one inelastic channel is present some of these parametrisations are not completely satisfactory. An improved form of parameterising the matrix was suggested, which is suitable for any number of channels.

The results in this section have illustrated some of the interesting relationships between the elements of the scattering matrices and they apply to any complex symmetric unitary matrix. The parameterisations are useful in phase shift analysis and other non-nuclear physics applications (such as circuit theory as pointed out by Waldenstrom [Wal 81]). The new form parametrising the matrix **N** could provide useful information on the coupling between the elastic and inelastic channels.

APPENDIX A

DETERMINATION OF BOUND STATES

For n coupled channel problem, the Schrodinger equation is a coupled differential equation and the potentials form a symmetric nxn matrix. The potentials may support a bound state(s), this appendix is a formulation on how to determine the bound state(s). The formulations are similar to the one used in determining the bound state of a deuteron (n=2). The Schrodinger equation may be written as

$$u''_{ia} - \sum_{j}^{n} V_{ij} u_{ia} = -(E - Q_i)u_{ia} \tag{A.1}$$

for i=1,2,3,...,n, where E is the energy and Q_i is the threshold energy of the ith channel. If one were to determine the solution of the above equation numerically, then an inexact equation can be written as

$$u''_{ib} - \sum_{j}^{n} V_{ij} u_{ib} = -(E - Q_i - \delta E)u_{ib} \tag{A.2}$$

where δE is a deviation from the exact energy. Multiplying eq. (A.1) with u_{ib} and eq. (A.2) with u_{ia}, and then subtracting the two equations we have

$$[u''_{ia}u_{ib} - u''_{ib}u_{ia}] - \sum_{j}^{n} V_{ij}[u_{ia}u_{ib} - u_{ib}u_{ia}] = -\delta E\, u_{ia}u_{ib}. \tag{A.3}$$

Summation over all the channels, we have,

$$\sum_{i}[u''_{ia}u_{ib} - u''_{ib}u_{ia}] - \sum_{ij} V_{ij}[u_{ia}u_{ib} - u_{ib}u_{ia}] = -\sum_{i}\delta E\, u_{ia}u_{ib}. \tag{A.4}$$

The second term in the above equation is zero. Thus

$$\sum_{i}[u''_{ia}u_{ib} - u''_{ib}u_{ia}] = -\sum_{i}\delta E\, u_{ia}u_{ib}. \tag{A.5}$$

Integrating between zero and infinite gives,

$$\sum_{i}\int_{0}^{\infty}\frac{d}{dr}(u'_{ia}u_{ib} - u'_{ib}u_{ia})dr = -\delta E\sum_{i}\int_{0}^{\infty} u_{ia}u_{ib}dr. \tag{A.6}$$

Splitting the limits into 0 to $R^{(-)}$ and $R^{(+)}$ to ∞ (where $R^{(-)}$ is almost the same point as $R^{(+)}$ or they could differ by the step length of integration), we have

$$\text{L.H.S.} = \sum_i [(u_{ia}u_{ib} - u_{ib}u_{ia})\Big|_0^{R^{(-)}} + (u_{ia}u_{ib} - u_{ib}u_{ia})\Big|_{R^{(+)}}^{\infty}]. \qquad (A.7)$$

If a bound state exist at energy E, then $u_{ia}(\infty)=0$ and $u_{ia}(0)=0$. The above equation becomes

$$\text{L.H.S.} = \sum_i \{[u'_{ia}(R^{(-)})u_{ib}(R^{(-)}) - u'_{ib}(R^{(-)})u_{ia}(R^{(-)})] - [u'_{ia}(R^{(+)})u_{ib}(R^{(+)}) - u'_{ib}(R^{(+)})u_{ia}(R^{(+)})]\}.$$

If R is the cut-off radius of the potential, then $u_{ia}(R^{(-)})=u_{ia}(R^{(+)})$ and $u'_{ia}(R^{(-)})=u'_{ia}(R^{(+)})$. Similarly u_{ib} has to be continuous, thus $u_{ib}(R^{(-)})=u_{ib}(R^{(+)})$. Therefore, the above expression becomes

$$\text{L.H.S.} = -\sum_i u_{ia}(R)[u'_{ib}(R^{(-)}) - u'_{ib}(R^{(+)})].$$

The asymptotic wave function is then $u_i \sim \exp(-\alpha_i r)$ (here $\alpha_i^2 = E-Q_i$) and the R.H.S of eq. (A.6) becomes, assuming $u_{ia} = u_{ib} = u_i$,

$$\text{R.H.S.} = -\delta E \sum_i [\int_0^{R^{(-)}} u^2{}_i dr + \frac{N_i^2}{2\alpha_i}\exp(-2\alpha_i R)]$$

where N_i is a normalisation constant. Thus we can write δE as

$$\delta E = \frac{\sum_i u_i(R)[u'_{ib}(R^{(-)}) - u'_{ib}(R^{(+)})]}{\sum_i [\int_0^{R^{(-)}} u_i^2 dr + N_i^2 \exp(-2\alpha_i R)/2\alpha_i]}.$$

Since the wave functions u_{ib} are not the exact solutions of the Schrodinger equation, all but one (say i=n) could have continuous first derivatives, i.e. $[u'_{ib}(R^{(-)}) - u'_{ib}(R^{(+)})] = 0$ for i=1,2,...,(n-1) and the

equation above becomes

$$\delta E = \frac{u_{na}(R)[u'_{nb}(R^{(-)}) - u'_{nb}(R^{(+)})]}{\sum_i [\int_0^R u_i^2 dr + N_i^2 \exp(-2\alpha_i R)/2\alpha_i]}. \qquad (A.8)$$

To determine the energy of the bound state, δE is iterated as a function of E until it converges to zero, i.e. $u'_{nb}(R^{(-)}) - u'_{nb}(R^{(+)}) = 0$, and thus eqs. (A.1) and (A.2) are the same. To iterate δE, the wave functions u_i at various energies E have to be determined. A numerical method similar to the one presented in chapter 5 can be used. The method leads to $u_{ij}(r)$ solutions. At the cut off radius, we have

$$\sum_j^n A_j u_{ij}(R) = N_i \exp(-\alpha_i R) \qquad (A.9)$$

for i=1,2,..,n and for the derivatives;

$$\sum_j^n A_j u'_{ij}(R) = -\alpha_i N_i \exp(-\alpha_i R) \qquad (A.10)$$

for i=1,2,..,n-1 (since for i=n the derivative is not continuous). Assuming that $N_1 = 1$, then one ends up with 2n-1 equations containing 2n-1 unknowns. Thus A_i and N_i can all be determined. Using the two equations above, we may write

$$u'_n(R^{(-)}) - u'_n(R^{(+)}) = -\alpha_n N_n \exp(-\alpha_n R) - \sum_j^n A_j u_{nj}(R). \qquad (A.11)$$

With this, eq. (A.8) can then iterated at various energies until it converges to zero. If the potentials do not support a bound state then δE diverges. Thus $u'_n(R^-) \neq u'_n(R^+)$ at the cut off radius.

A square potential

If the potential is a square potential, i.e.

$$V_{ij}(r) = V_{ji}(r) = \begin{cases} -V_{ij} & \text{for } r<R \\ 0 & \text{for } r>R \end{cases}$$

then an easier method of determining the wave functions (and the S-matrix) is presented here. Suppose the solution to eq. (A.1) is

$$u_i = A_i \sin K_i r \qquad \text{for } r<R. \tag{A.12}$$

Substituting into eq. (A.1) for i=1,2,3,....,n, we have, in a matrix form,

$$\mathbf{D}\,\mathbf{A} = \mathbf{K}\,\mathbf{A} \tag{A.13}$$

where $D_{ii} = -V_{ii} + k_i^2$ (here $k_i^2 = E-Q_i$) and $D_{ij} = -V_{ij}$ for $i \neq j$. The matrix **A** is a column vector containing the wave functions. The matrix **K** is diagonal containing K_i^2. The above equation is an eigen problem with the eigenvalues in **K** and n eigenvectors. That is K_i can be determined from det(**D** - **K**)=0. This leads to an nxn matrix **B** containing all the possible eigenvectors, and the wave functions are now

$$u_i = \sum_j^n B_{ij} \sin K_j r \tag{A.14}$$

for i=1,2,3,..,n. From the above wave function the bound state can be determined.

REFERENCES

[Abr 65] M.Abramowitz and I.A.Stegun ed. *Handbook of Mathematical functions* (Dover Publ. Inc.: New York) 1965

[Arn 82] R.A.Arndt and L.D.Roper *Phys. Rev.* **D25** (1982) 2011

[Arn 83] R.A.Arndt, L.D.Roper, R.A.Bryan, R.B.Clark, B.J.VerWest and P.Signell *Phys. Rev.* **D28** (1983) 97

[Bas 77] R.Bass *Phys. Rev. Lett.* **39** (1977) 265.

[Bay 77] D.Baye, J.Deenen and Y.Salmon *Nucl. Phys.* **A289** (1977) 511

[Bay 86] D.Baye *Nucl. Phys.* **A460** (1986) 581

[Bla 52] J.M.Blatt and L.C.Biedenharn *Phys. Rev.* **86** (1952) 399

[Bla 54] J.S.Blair *Phys. Rev.* **95** (1954) 1218.

[Boh 71] H.G.Bohlen and W.Von Oertzen *Phys. Lett.* **37B** (1971) 451.

[Boh 74] W.Bohne, C.K.Gelbke, P.Branun-Munzinger, W.Grochulski, H.L.Harney and H.Oeschler *Nucl. Phys.* **A222** (1974) 117

[Bri 62] D.M.Brink and G.R.Satchler *Angular momentum* (Oxford Univeristy Press, Oxford 1962).

[Bri 77] D.M.Brink and N.Takigawa *Nucl. Phys.* **A279** (1977) 159

[Bry 81] R.Bryan *Phys. Rev.* **C24** (1981) 2659

[Bry 84] R.Bryan *Phys. Rev.* **C30** (1984) 305

[Cen 81] S.B.Di Cenzo, J.F.Peterson and R.R.Betts *Phys. Rev.* **C23** (1981) 2561.

[Cha 70] R.A.Chatwin, J.S.Eck, D.Robson and A.Richter *Phys. Rev.* **C1** (1970) 795.

[Cha 76] P.Charles, F.Auger, I.Badaway, B.Berthier, M.Dost, J.Gastebois, B.Fernandez, S.M.Lee and E.Plagnol *Phys. Lett.* **62B** (1976) 289

[Cla 85] N.M.Clarke Computer program unpublished. (Kings College London.)

[Cuj 76] B.Cujec and C.A.Barnes *Nucl. Phys.* **A266** (1976) 461

[Dan 82] K.Daneshvar, D.G.Kavor, S.J.Krieger and K.T.R.Davies *Phys. Rev.* **C25** (1982) 1342

[DeY 82] P.A.DeYoung, J.J.Kolata, L.J.Satkowiak and M.A.Xapsos *Phys. Rev.* **C26** (1982) 1482

[Ebe 79] K.A.Eberhard, Ch.Appel, R.Bangert, L.Cleemann, J.Eberth, and V.Zobel *Phys. Rev. Lett.* **43** (1979) 107

[Ebe 82] K.A.Eberhard Ed. *Resonances in Heavy Ions reactions* Proceedings, Bad Honnef Germany 1981. (Springer-Verlag Berlin 1982).

[Eck 75] J.S.Eck et al *Nucl. Phys.* **A255** (1975) 157

[For 76] H.Frohlich, P.Duck, W.Galster, W.Treu, H.Voit, H.Witt, W.Kuhn and S.M.Lee *Phys. Lett.* **64B** (1976) 408

[Fra 63] W.E.Frahn and R.H.Venter *Ann. of Phys.* **24** (1963) 243.

[Fre 81] R.M.Freeman et al *Phys. Rev.* **C24** (1981) 2390.

[Fro 70] C-E.Froberg *Introduction to Numerical Analysis* (1970) 2nd ed. (London: Addision-Wesley)

[Gla 74] D.Glas and U.Mosel *Phys. Rev.* **C10** (1974) 2620.

[Gla 76] D.Glas and U.Mosel *Nucl. Phys.* **A264** (1976) 268.

[Gob 73] A.Gobbi, R.Wieland, L.Chua, D.Shapira and D.A.Bromley *Phys. Rev.* **C7** (1973) 30.

[Gut 73] H.H.Gutbrod, R.Bock, W.Von Oertzen and U.C.Schlotthauer-Voos *Z. Physik.* **262** (1973) 377

[Hil 53] D.L.Hill and J.A.Wheeler *Phys. Rev.* **89** (1953) 1102.

[Hor 54] A.Horn *Am. J of Maths* **76** (1954) 620.

[Hos 68] N.Hoshizaki *Prog. Theor. Phys. Suppl.* **42** (1968) 1

[Jac 81] C.M.Jachcinski, D.G.Kavor, R.R.Betts, C.N.Davids, D.F.Geesamann, C.Olmer, M.Paul, S.J.Sanders and J.L.Yntemma *Phys. Rev.* **C24** (1981) 2070.

[Kab 87a] A.Kabir and M.W.Kermode *J. of Phys.* **G13** (1987) 501

[Kab 87b] A.Kabir and M.W.Kermode *J. of Phys.* **A20** (1987) 5199

[Kab 87c] A.Kabir and M.W.Kermode *J. of Phys.* **A20** (1987) 6635

[Kab 87d] A.Kabir Institute of Physics, Nuclear & Particle Physics Conference, (Birmingham April 1987), Contribution No. P17

[Kab 88] A.Kabir, M.W.Kermode and N.Rowley *Nucl. Phys.* **A481** (1988) 94

[Kab 88b] A.Kabir, M.W.Kermode and N.Rowley Institute of Physics, Nuclear Physics Conference, (Manchester March 1988), Contribution No. TB5

[Ker 67] M.W.Kermode *Nucl. Phys.* **A99** (1967) 605

[Ker 85] M.W.Kermode and S.G.Cooper *J. of Phys.* **G11** (1985) 821

[Kla 83] S.Klarsfeld *Phys. Lett.* **126B** (1983) 148

[Kon 80] Y.Kondo, D.A.Bromley and Y.Abe *Phys. Rev.* **C22** (1980) 1068

[Kov 79] D.G.Kovar, D.F.Geesaman, T.H.Briad, Y.Eisen, W.Henning, T.R.Ophel, M.Paul, K.E.Rehm, S.J.Sanders, P.Sperr, J.P.Schiffer, S.L.Tabor, S.Vigdor, B.Zeidman and F.W.Prosser *Phys. Rev.* **C20** (1979) 1305

[Kue 69] J.A.Kuehner and E.Almquist *Phys. Rev.* **134** (1964) 1229.

[Lin 84] R.Lindsay and N.Rowley *J. of Phys.* **G10** (1984) 805.

[Mac 68] M.H.MacGregor, R.A.Arndt and R.M.Wright *Phys. Rev.* **169** (1968) 1149

[Mai 73] P.Mailandt, J.S.Lilley and G.W.Greenless *Phys. Rev.* **C8** (1973) 2189.

[Mal 72] R.E.Malmin, R.H.Siemssen, D.A.Sink and P.P.Singh *Phys. Rev. Lett.* **28** (1972) 1590.

[Mat 82] J.F.Mateja, A.D.Frawley, L.C.Dennis, K.Abdo and K.W.Kemper *Phys. Rev.* **C25** (1982) 2963

[Mel 83] Z.Melhem and M.W.Kermode *J. of Phys.* **G9** (1983) L267

[Nag 86] M.A.Nagarajan, N.Rowley and R.Lindsay *J. of Phys.* **G12** (1986) 529

[Nag 86a] M.A.Nagarajan and G.R.Satchler *Phys. Lett.* **B173** (1986) 29.

[Ohk 87] S.Ohkubo and D.M.Brink *Phys. Rev.* **C36** (1987) 966

[Ohk 87a] S.Ohkubo and D.M.Brink *Phys. Rev.* **C36** (1987) 1375

[Pap 86] C.T.Papadopoulos et al *Phys. Rev.* **C34** (1986) 196

[Pat 71] J.R.Patterson, B.N.Nagorcka, G.D.Symons and W.M.Zuk *Nucl. Phys.* **A165** (1971) 545

[Pof 83] N.Poffe, N.Rowley and R.Lindsay *Nucl. Phys.* **A410** (1983) 498

[Ros 60] M.H.Ross and G.L.Shaw *Ann. of Phys.*, NY **9** (1960) 391

[Row 77] N.Rowley, H.Doubre and C.Marty *Phys. Lett.* **69B** (1977) 147

[Row 80] N.Rowley *J. of Phys.* **G6** (1980) 697

[Row 80a] N.Rowley, C.Marty and E.Plagnol *Phys. Lett.* **93B** (1980) 16

[Sat 83] G.R.Satchler *Direct Nuclear Reaction* (Oxford Univeristy Press: New York, 1983)

[Sat 87] G.R.Satchler, M.A.Nagarajan, J.S.Lilley and I.J.Thomspon *Anns. of Phys.* **178** (1987) 110.

[Sha 85] M.S.Shalaby and G.R.Satchler *Nucl. Phys.* **A442** (1985) 469.

[Spe 76] P.Sperr, S.Vigdor, Y.Eisen, W.Henning, D.G.Kovar, T.R.Ophel and B.Zeidman *Phys. Rev. Lett.* **36** (1976) 405

[Spe 76a] P.Sperr et al *Phys. Rev. Lett.* **37** (1976) 321

[Spr 82] D.W.L.Sprung, M.W.Kermode and S.Klarsfeld *J. of Phys.* **G8** (1982) 923

[Spr 85] D.W.L.Sprung *Phys. Rev.* **C32** (1985) 699

[Spr 87] D.W.L.Sprung *Phys. Rev.* **C35** (1987) 869

[Sta 57] H.P.Stapp, T.Ypsilantis and N.Metropolis *Phys. Rev.* **105** (1957) 302

[Tab 78] S.L.Tabor, D.F.Geesaman, W.Henning, D.G.Kavor, K.E.Rehm and F.W.Prosser Jr. *Phys. Rev.* **C17** (1978) 2136.

[Tan 80] O.Tanimura *Phys. Lett.* **90B** (1980) 204

[Uda 85] T.Udagawa, B.T.Kim and T.Tamura *Phys. Rev.* **C32** (1985) 124

[Voi 88] H.Voit, N.Bischof, W.Tiereth, I.Weitzenfelder, W.Von Oertzen and B.Imanishi *Nucl. Phys.* **A476** (1988) 491.

[Von 69] W.Von Oertzen, H.H.Gutbrod, U.C.Voos and R.Bock *Nucl. Phys.* **A133** (1969) 101

[Von 73] W.Von Oertzen and W.Norenberg *Nucl. Phys.* **A207** (1973) 113

[Von 75] W.Von Oertzen and H.G.Bohlen *Phys. Rep.* **19** (1975) 1.

[Wal 74] S.Waldenstrom *Nucl. Phys.* **B77** (1974) 479

[Wal 81] S.Waldenstrom *Arkiv for Det Fysiske Seminar Trondheim* **no 2** (1981).